Development of an Image-based Multi-Scale Finite Element Approach to Predict Fatigue Damage in Asphalt Mixtures

By:
Amir Arshadi

A Dissertation Submitted in Partial
Fulfillment of the Requirement for the Degree
of

Doctor of Philosophy
(Civil and Environmental Engineering)

At

The University of Wisconsin-Madison

2015

Date of final oral examination: 5/8/2015

The dissertation is approved by the following members of the Final Oral Committee:

Hussain U. Bahia (Advisor), Professor, Civil and Environmental Engineering

Jose Pincheira, Associate Professor, Civil and Environmental Engineering

Gustavo Parra-Montesinos, Professor, Civil and Environmental Engineering

William J. Likos, Associate Professor, Civil and Environmental Engineering

Robert E. Rowlands, Professor, Mechanical Engineering

Dedication

To my lovely wife and lifelong friend, Elika

Your love, encouragement, and patience gave me the support needed in this journey.

Acknowledgements

I would like to express my regards to my advisor, Professor Hussain Bahia, for all of the supports, encouragements, and counseling he provided during my Ph.D. program at University of Wisconsin-Madison. A sincere thank you is offered to my committee members, Professor Robert Rowlands, Professor Jose Pincheira, Professor William Likos, and Professor Gustavo Parra-Montesinos for their help and input in completing this thesis.

I appreciate the supports and helps from my colleagues at Modified Asphalt Research Center of University of Wisconsin-Madison. I also wish to thank my friends Mr. Adel Ardalan, Dr. Hassan Tabatabaee, and Dr. Nima Roohi, for all their supports.

Finally, I like to thank my family, Marjan, Mina, Hossein, Mansour, Ali, Sahar, Masoud, and Mahbod, for their ever-present love and support in my life.

Table of Contents

List of Figures

List of Tables

CHAPTER 1: OVERVIEW AND OBJECTIVE

Abstract

Image-based simulation of complex materials is a very important tool for understanding their mechanical behavior and an effective tool for successful design of composite materials. Asphalt concrete as one of these multi-phase complex materials is a composite of asphalt binder, air voids, and mineral aggregate particles. Simulation of asphalt concrete with numerical methods is not a new topic but is faced with many challenges. In addition to requiring tremendous computational cost, it is not clear yet how to effectively model the aggregate-to-aggregate contact behavior during loading and deformation. In this thesis an image-based Multi-scale modeling is developed to reduce the computational cost significantly by reducing the amount of elements in the numerical model. In this approach the "up-scaling" and homogenization of each scale to the next is critically designed to improve accuracy. In addition to this multi-scale efficiency, this study introduces an approach for consideration of particle contacts at each of the scales in which mineral particles exist. The Finite Element (FE) analysis is performed in the study at four scales, asphalt binder, mastic, mortar, and asphalt mixture scale.

One of the most important pavement distresses which seriously affects the pavement performance is fatigue cracking. As this cracking generally takes place in the binder phase of the asphalt mixture, the binder fatigue behavior is assumed to be one of the main factors influencing the overall pavement fatigue performance. It is also known that aggregate gradation, mixture volumetric properties, and filler type and concentration can affect damage initiation and progression in the asphalt mixtures. This study was conducted to develop a tool to characterize the damage properties of the asphalt mixtures at all scales.

The linear amplitude sweep (LAS) test is currently considered as a surrogate to time sweep (TS) test for specification of asphalt binder fatigue resistance. Although the TS test consists of repeated cyclic loading at constant amplitude; the LAS test uses increasing loading amplitudes to accelerate the rate of damage accumulation in the material. Viscoelastic continuum damage (VECD) mechanics can be utilized to model the fatigue behavior of asphalt binders from a single LAS test. In the present study the VECD model is implemented into the well-known finite element (FE) software ABAQUS via the user material subroutine (UMAT) in order to simulate the state of damage in the binder phase under the repeated uniaxial sinusoidal loading. ABAQUS is used to conduct FE simulations at all scales. The inputs are based on the experimentally derived measurements for the binder viscoelastic properties and fatigue parameters. For the scales of mastic and mortar, the artificially 2-Dimensional (2D) images of mastic and mortar scales were generated and used to characterize the properties of those scales. Finally, the 2D scanned images of asphalt mixtures after elimination of fine aggregate particles is used to study the asphalt mixture failure behavior under loading.

In order to validate the proposed model, the experimental test results and the FE simulation results were compared at two scales: mastic scale and asphalt mixture scale. The FE model was used for simulation of the asphalt mastics with varying filler volume fractions (FVF). Comparisons between mastic LAS test results and FE simulation results indicated that the model coupled with the VECD mechanics is capable of predicting the damage response of mastics produced from various FVFs with an acceptable accuracy. Indirect tensile (IDT) fatigue tests were also conducted on asphalt mixture samples with two levels of aggregate gradation and four levels of binder type. A comparison between experimental results and the results from stress-controlled FE simulation shows that the model developed in this study is capable of predicting

the effect of asphalt binder properties and aggregate micro-structure on mechanical behavior of asphalt concrete under loading. A strain-controlled analysis was conducted on the asphalt mixtures to obtain the fatigue life of the asphalt mixtures.

Background and Problem Statement

The physical properties of asphalt mixture are governed by the characteristics of its constituents such as aggregate properties (gradation, shape, structure, modulus, etc.) and binder properties (complex modulus, relaxation characteristic, etc.). Although experimental testing can provide the researchers with the macro-mechanical behavior of asphalt concrete, it is time consuming and costly to investigate the micro-mechanical response of the asphalt mixture in a laboratory due to difficulties in controlling the micro-structural features such as: aggregate shape, size, distribution, gradation, and volume fraction.

Many researchers developed constitutive models in order to predict the physical properties of asphalt concrete and eliminate the costly and time consuming tests on asphalt mixtures for the design of asphalt pavements (Hirsch, 1962; Hashin, et al., 1963; Mori, et al., 1973; Christensen, et al., 2003). Although these models use the binder and aggregate properties to estimate the asphalt concrete properties; there are some issues with the accuracy of the models and furthermore, they are unable to determine the effect of micro-structure on asphalt mixture behavior.

In order to study the effect of micro-structure of asphalt concrete, a number of researchers applied image analysis and micro-mechanical finite element methods (FEM) for modeling complex behavior of asphalt mixture (Sepehr, et al., 1994; Kose, et al., 2000; Sadd, et al., 2004; Dai, et al., 2006; Dai, et al., 2007; Abu Al-Rub R.K., et al., 2011; Roohi, et al., 2012;

Arshadi, et al., 2015). These methods provide information that cannot be directly obtained from experimental data, such as local stress and strain distribution in asphalt mixture components and the evolution of mixture micro-structure and micro-mechanical response under loading. Dai et al. used a mixed FEM to study the behavior of asphalt mixtures by using rigid elements and continuum elements for aggregates and asphalt mastics, respectively. The properties of the asphalt mastic elements were specified through a user material (UMAT) subroutine within the ABAQUS code to incorporate the linear and damage-coupled viscoelastic constitutive behavior of continuum phase (Dai, et al., 2006). Dai et al. (2007) presented a micromechanical FE model to predict the viscoelastic creep stiffness of asphalt mixtures. The creep stiffness of the sand mastic of the asphalt mixture was used as the input viscoelastic properties of the model. They showed that the model gives reasonable prediction of the mixture creep stiffness across the reduced loading time. Abu Al-Rub et al. (2011) indicated that the effects of aggregate shape, aggregate distribution, and aggregate volume fraction should be considered in modeling the behavior of asphalt mixtures. Although these studies show the importance of micro-structure of asphalt mixture; lacking of an appropriate approach for consideration of the contact between the fine aggregate particles in FE framework makes them dependent to costly and time consuming tests at the mortar scale level (mixture of the fine aggregates with binder).

A number of research works have been done on micro-mechanical modeling of asphalt mixtures using Discrete Element Modeling (DEM) (Dai, et al., 2007; Chang, et al., 1999; Luo, et al., 2010). In DEM, aggregates are represented as discrete elastic particles and their interactions are controlled by the response of an asphalt thin film. Some of the most important benefits of the discrete element modeling are the ability to handle complex and changing contact geometries

and large displacements. The disadvantage of this method is the huge computational cost and power which is needed for this type of modeling.

The asphalt mixture damage behavior is generally complicated. In order to meet the design requirements, understanding the damage-induced behavior of asphalt mixture is essential. Due to heterogeneity and time dependent behavior of asphalt mixtures, the damage constitutive modeling of asphalt mixtures is extremely intricate. There are numerous combinations in mix designs and loading conditions; therefore, identifying the damage-induced behavior of asphalt mixtures only by performing the laboratory tests is costly and time consuming. Recently, some of the researchers tried to develop analytical and computational models in order to overcome this issue (Sadd, et al., 2004; Park, et al., 1996; Lee, et al., 2000; Guddat, et al., 2002; Kim, et al., 2005). Although the developed continuum-damage models by Park et al. and Lee et al. are capable of predicting the structural degradation, they have significant challenges such as their dependency to laboratory tests at the mixture scale level and the assumption of the asphalt mixture as a statistically homogeneous continuum (Park, et al., 1996; Lee, et al., 2000).

Considering the aforementioned challenges regarding the micro-mechanical and damage-induced modeling of asphalt mixture, there is a need to improve the numerical procedures in order to capture the impact of micro-structural change on binder (mastic) response and consequently on initiation and propagation of damage within binder (mastic) phase.

Hypotheses

To address the aforementioned challenges regarding the micro-mechanical modeling of asphalt mixture, the following hypotheses are proposed:

- Using an improved micro-mechanical model, asphalt mixture physical properties can be obtained directly from the constituents (i.e. the viscoelastic properties of the binder and characteristics of the aggregates such as shape, size, distribution, modulus, etc.).
- Binder damage behavior obtained from Linear Amplitude Sweep (LAS) test, using the continuum damage analysis, can be coupled with the micromechanical model in a finite element framework, leading to a better understanding of the damage initiation and propagation within the asphalt mixture.

Objectives

This dissertation focuses on achieving the following objectives:

- Development of an image-based methodology capable of considering the whole aggregate particles ranging from 1 μm up to 30 mm in the modeling.
- Development of a multi-scale methodology coupled with a finite element frame work to mode the contact between cemented particles at all scales.
- Implement the damage behavior of asphalt binder obtained from experimental tests into the finite element software.
- Study the impact of aggregate skeleton on binder response and consequently its effect on damage initiation and propagation within the binder phase.

Research Methodology and Scope

A comprehensive literature review is conducted to achieve the current state of knowledge on mathematical modeling of complex behavior of asphalt binder. Binder damage properties are characterized using the LAS test and using the most reliable mathematical model, the

characteristics of the asphalt binder is implemented in the finite element software through UMAT.

Artificial images of mastic and mortar scales are generated based on the particle shapes, gradation, and volume fraction and the properties of each scale are obtained by performing the FE simulation analysis. The obtained properties of the mortar scale are material input values for the continuous matrix of asphalt mixture scale. The asphalt mixture performance under repeated cyclic loading is studied trough FE simulation.

Laboratory experiments are carried out at mastic and asphalt mixture level to validate the developed model. Linear amplitude sweep test is performed on mastic samples and Indirect Tensile (IDT) test is performed on asphalt mixtures at the force controlled mode and the results are compared with the FE simulation results.

Outline

This study is separated into six chapters:

Chapter 1: Introduction

The introduction includes background information on numerical simulation of asphalt mixtures, a problem statement, hypothesis, and objectives of this research.

Chapter 2: Literature Review

This chapter is divided into seven separate sections: asphalt binder rheological modeling, digital imaging techniques of asphalt mixtures, finite element analysis of asphalt mixtures, multi-scale analysis of asphalt mixtures, micro-mechanical modeling of particle interaction, asphalt pavement fatigue, and asphalt binder fatigue testing.

Chapter 3: Development of an Image-based Multi-Scale Finite Element Approach

In this chapter the image-based multi-scale model is developed and validated with the experimental data.

Chapter 4: Coupling of Viscoelastic Continuum Damage Mechanics and Finite Element Modeling

The mathematical interpretation of binder damage test is studied and the model used to implement the binder damage test into FE framework is explained and developed in this chapter. The developed model is validated trough experimental testing at binder and mastic scales.

Chapter 5: FE Simulation of Fatigue Damage in Asphalt Mixtures and Validation

In this chapter the laboratory testing at the asphalt mixtures is explained. The experimental results are used to validate the multi-scale model in prediction of fatigue behavior of asphalt mixtures.

Chapter 6: Summary of Findings

The findings gathered from the study are summarized in this section.

CHAPTER 2: LITERATURE REVIEW

Asphalt Binder Rheological Modeling

Asphalt binder is a product of crude petroleum refining, used for road paving, roofing, adhesives, coatings and construction. It is the only fraction of crude petroleum which does not volatilize during the distillation process. Having a material which satisfies standard specifications for paving is the final goal in production of asphalt binder from crude petroleum refining (Roberts, et al., 1996).

Asphalt binder has a colloidal structure, consisting of insoluble asphaltene molecules distributed in the maltene phase. Aromatics and saturates are the components of the maltene phase. The asphaltene is responsible for time dependency behavior of asphalt binder while the maltene phase gives its temperature sensitivity.

The asphalt binders are classified as rheological materials; that is, their behavior is dependent to rate (or time) of loading and temperature. It is shown by researchers that the style and propagation of distresses in asphalt mixtures correlate with the time-dependent (i.e., viscoelastic) properties of asphalt binder (Souza, et al., 2004; Wen, et al., 2009). Therefore, it is indispensable to characterize the viscoelastic properties of the binder. The interest in understanding the rheological behavior of asphalt binders dates back to 1888 when H. C. Bowen designed the Bowen Penetration Machine to measure the depth of penetration of a truncated No. 2 sewing needle in an asphalt binder sample under specified conditions of load, time, and temperature. This measurement method became highly popular and the ASTM standardized the procedure in 1915 (Halstead, et al., 1974). Later, researchers developed procedures to determine

some other rheological properties of the asphalt binder such as softening point and viscosity (Romberg, et al., 1947). In the end of the 20th century a research program sponsored by US congress was conducted to improve the performance of American roads and highways. Superior Performing Asphalt Pavements (Superpave) standard specification was recommended as a result of the study (Harrgan, et al., 1994). The use of Dynamic Shear Rheometer (DSR) was recommended by the Superpave specification to characterize the viscoelastic properties of asphalt binder. There are many testing methods to characterize the time-dependent behavior of viscoelastic materials however, cyclic and creep test techniques are two of the best to represent the properties of this class of materials.

Many researchers have attempted to use spring-dashpot models to describe the viscoelastic behavior of the asphalt binder. Saal et al. proposed the use of Maxwell model and Voigt model and Lethersich suggested the Burger's model (Saal, et al., 1958; Lethersich, 1942). In these models, the response of a spring represents the elastic part and the response of a dashpot represents the viscous part. The Maxwell model is a combination of dashpot and spring in series (Figure 1) and the Voigt model is their combination in parallel (Figure 2). The Burger's model is a combination of these two units in series (Figure 3).

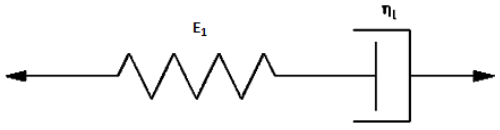

Figure 1: Maxwell model

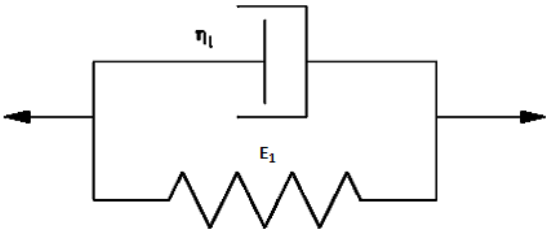

Figure 2: Voigt model

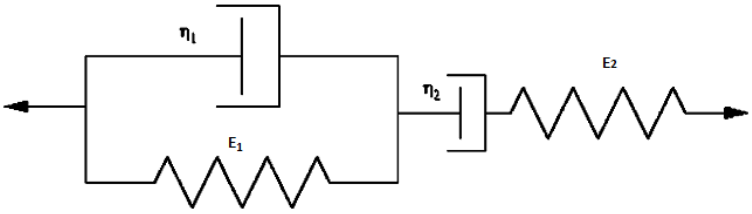

Figure 3: Burger's model

Grabowski et al. (2002) showed that although Maxwell, Voigt, and Burger's models seem to be appropriate for description of the asphalt binder viscoelastic behavior, especially the Burger's model; they exhibit significant limitations (GRABOWSKI, et al., 2002). They indicated that the generalized Maxwell model which consists of $\boldsymbol{M}$ Maxwell elements (Figure 4) is the most adequate one. In the generalized Maxwell model the same strain is shared across all the elements. The relaxation modulus of the generalized Maxwell model can be determined by the following equation:

$$\boldsymbol{E(t) = E_{\infty} + \sum_{m=1}^{M} E_m . e^{\frac{-t}{\tau_m}}} .$$ **Equation 1**

In which:

- E_{∞} is the long term modulus
- E_m is the Prony series relaxation modulus
- t is loading time, and
- τ_m is relaxation time

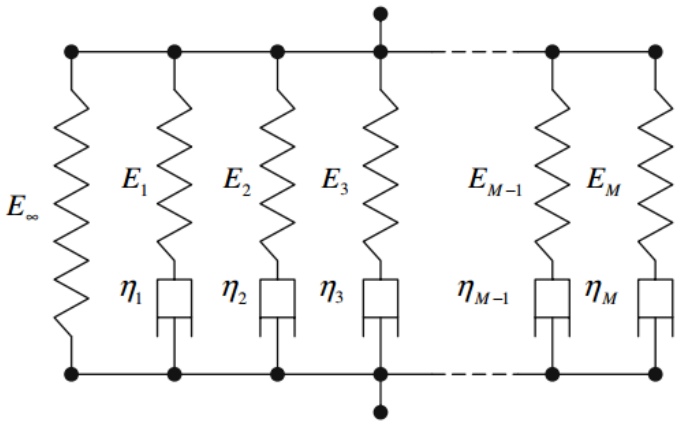

Figure 4: The generalized Maxwell viscoelastic model for the asphalt binder

The Prony series representations has been preferred by researchers to many other curve-fitting techniques due to its precise fit to data and efficiency for use in mathematical operations. Papagiannakis et al. (2002) used a generalized Maxwell model with three Maxwell units to represent the viscoelastic behavior of asphalt binder and implemented it in the FE software. It was indicated that the asphalt concrete FEM model shows promise in simulating Superpave shear tester measurements of the asphalt concrete dynamic modulus (Papagiannakis, et al., 2002). Dai et al. (2006) used a generalized Maxwell model to represent the mastic creep stiffness. The model includes one spring and four Maxwell units. The results indicated that the complex modulus predictions of the FE simulation have good correlations with laboratory data (Dai, et al., 2008).

In this study the binder phase is assumed to be describable by the principals of linear viscoelasticity. The generalized Maxwell model with one spring and four Maxwell units is used to represent the viscoelastic behavior of the asphalt binder. The implementation of the binder properties in FE framework is explained in detail in the following chapter.

Digital Imaging Techniques of Asphalt Mixtures

Visualization of components is a process that has helped many industries understand components they produce or utilize and has brought tremendous benefits to many fields, especially in the medical field. In the field of asphalt paving there has been significant attempts to utilize this technique to better understand HMA behavior, especially for modeling the material response and behavior.

In recent years, the application of image analysis technique in studying the microstructure of asphalt mixtures has been increased extremely. In these studies the image analysis is used to capture the internal structure of asphalt mixtures and distribution of air voids in the asphalt mixture. The images can be captured using destructive or non-destructive methods. In the destructive method the sample should be cut in horizontal or vertical directions to provide a smooth surface for flatbed scanners (Figure 5). X-ray computed tomography (XRT) is a non-destructive imaging method, capable of capturing 2D or 3D image of the internal structure of an asphalt mixture sample (Figure 6). The planar x-rays from different directions pass through the material and are captured by a detector. Attenuations of x-rays may be recorded to identify different components of the asphalt mixture and their spatial location. After finishing the collection of x-ray attenuations for a full rotation, the sample is moved downward for scanning the next level (Ying, 2010).

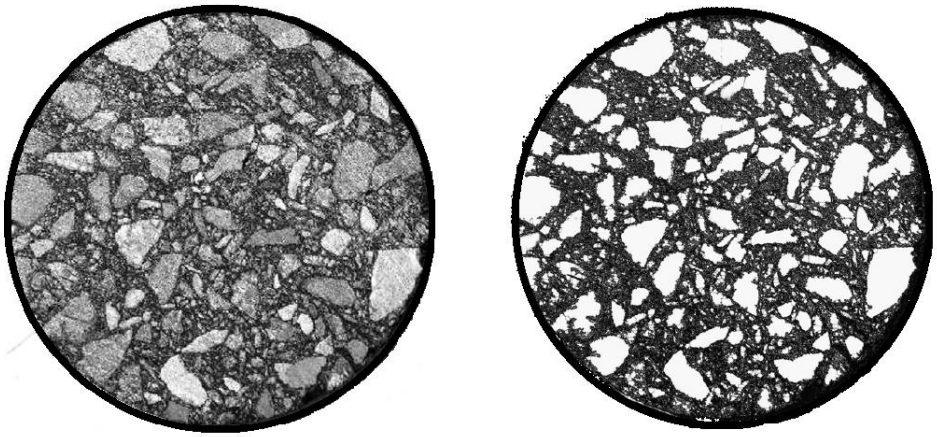

(a) (b)

Figure 5: (a) A horizontal plane section taken from a pavement core (b) Resulting binary image

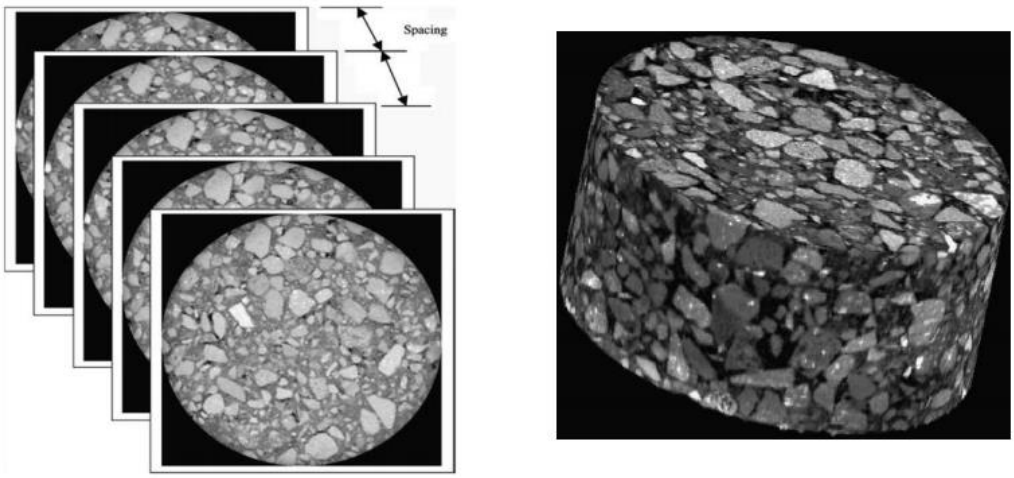

(a) (b)

Figure 6: (a) Cross-sectional images produced by XRT imaging (b) Visualization in 3D of an asphalt concrete specimen

Masad et al. (2002) studied the air void distribution in the asphalt mixtures using an x-ray computed tomography system along with image analysis techniques. It was concluded that air void distribution of gyratory compacted samples follows a bathtub shape distribution (Masad, et al., 2002). Recently, the image analysis techniques have been used to quantify the aggregate shape characteristics (Al-Rousan, et al., 2007) and study the effect of compaction equipment on

degree of compaction of the mixtures (Gopalakrishnan, et al., 2006). Many researchers tried to quantify internal structure properties of asphalt mixtures for modeling and simulation purposes (Adhikari, et al., 2008; Coenen, et al., 2011; Roohi, et al., 2012). Adhikari et al. (2008) used the x-ray CT techniques to analyze and model the aggregate orientation, aggregate gradation, sand mastic distribution, and air void distribution in the asphalt mixture. Coenen et al. (2011) improved the image filtering procedure by matching actual measured volumetrics. They indicated that the presented digital image analysis method can be used to quantify gradation, volumetrics, and contact points. The 2D image processing software named IPAS (i.e., Image Processing and Analysis System) was developed in this study. Later, Roohi et al. (2012) successfully showed that the internal aggregate structure properties of asphalt mixture can be quantified using a newly developed image analysis indices defined for both the total aggregates and for the effective load bearing aggregate structure, namely: number of aggregate-to-aggregate contact zones, aggregate contact (proximity) length, and contact plane orientation. This study demonstrated that there is a correlation between the internal structure indices and the mixture rutting performance. The results of this study was used for development of IPAS2 which is a significantly improvement of previous version of IPAS.

IPAS2 was used in a more recent study to investigate the effect of particle mobility on formation of aggregate structure in asphalt mixtures (Roohi, et al., 2013). In this study the aggregate structure of asphalt mixtures with two different gradations and four different binder levels were studied using the image analysis software at various compaction temperatures and compaction levels. It was concluded that in order to obtain the maximum packing, the mixture compaction temperature has to be selected based on the mastic viscosity.

X-Ray Tomography and 2D scanning has become very common in research, but challenges regarding how much one can visualize and the tremendous cost of x-ray tomography are still being phased. Thus currently researchers have been attempting to enhance accuracy of images in represent HMA components and thus make 2D visualization a more effective tool. In the current study a flatbed scanner was used to capture color images at a resolution of 20 μm/pixel of HMA cross sections and the 2D digital image processing software IPAS2 was used to convert the color images to binary images.

Finite Element Analysis of Asphalt Mixtures

Composite materials are heterogeneous materials including two or more different phases. Particulate composite materials usually consist of a polymer matrix reinforced by stiff inclusions (Ahmed, et al., 1990). It is well known that asphalt concrete (AC) is a particulate, porous composite of mineral aggregates, asphalt binder, and air voids. Aggregate particles used in pavements typically have irregular shapes, random orientations, and varying sizes, ranging from less than 1μm up to 30 mm (Lanceley, et al., 1966). Lakes et al. showed that for particle volume fraction of 40 percent and less, the Hashin-Shtrikman lower bound formula is capable of predicting the stiffness of particulate composite materials with an acceptable accuracy, however; for larger volume fractions the model predicted stiffness is higher than the composite stiffness (Hashin, et al., 1963; Lakes, et al., 2002). Since the asphalt mixture is a composite with a large volume fraction of particles with irregular and angular shapes, therefore; dilute approximations are inadequate for the full range. Finite element analysis is a qualified and efficient tool for predicting the behavior of such a material (Lakes, et al., 2002).

The first comprehensive presentation of Finite Element Method (FEM) is attributed to Turner et al. (1956). Since its beginning, many researchers used this method and the literature on this topic has increased exponentially (Zienkiewicz, et al., 1988; Reddy, 1993). Finite element analysis is based on discretizing the domain of the problem to smaller subdomains (elements). Based on the nodal displacements of an element, one can obtain the displacements, strains, and stresses over the area or volume of that element. The strain and nodal displacement relation is given in **Equation 2**:

$$\{\boldsymbol{\epsilon}\} = [\boldsymbol{B}]\{\boldsymbol{U}\} \qquad \textbf{Equation 2}$$

where, ε is the strain vector; B is a matrix of linear operators (derivatives of shape functions) and U is nodal displacement vector. The element stiffness matrices are calculated using:

$$\boldsymbol{K}^e = \int \boldsymbol{B}^T \boldsymbol{D}\boldsymbol{B} dv \qquad \textbf{Equation 3}$$

where D is the constitutive matrix. The element stiffness matrices should be assembled into the overall stiffness matrix. The resulting system of equations (**Equation 4**) should be solved for unknown nodal displacements.

$$\boldsymbol{K}\boldsymbol{U}^q = \boldsymbol{F} \qquad \textbf{Equation 4}$$

where K is the overall stiffness matrix; Uq is the nodal displacement vector; and F is the equivalent nodal force element. One can recover the stresses and strains from the nodal displacements.

Although experimental testing can obtain the macro-mechanical behavior of asphalt concrete, it is time consuming and costly to investigate the micro-mechanical response of the asphalt mixture in a laboratory due to difficulties in controlling the micro-structural features such

as: aggregate shape, gradation, and volume fraction. It has been proven that finite element method (FEM) is a suitable technique for application to complex constitutive behaviors and microstructure geometries pavement problems (Kose, et al., 2000; Sepehr, et al., 1994; Sadd, et al., 2004).

Over the past twenty years many researchers tried to use FE method to simulate and study the microstructure effect on asphalt mixture behavior (Stankowski, 1990; Sepehr, et al., 1994; Guddati, et al., 2002; Kose, et al., 2000; Darabi, et al., 2011; Lakes, et al., 2002). Chen et al. (1990) used the FE analysis software, ABAQUS, to study the effect of heavy axil load on performance of asphalt mixtures (Chen, et al., 1990; 2009). They showed that the asphalt layers show larger tensile strain under the uniform pressure than under non-uniform pressure. In another study, Helwany et al. (1998) used 3D FE analysis and indicated that the tensile strains at the bottom of Asphalt Concrete (AC) layer are highly sensitive to load speed and only longitudinal strains at top and bottom of AC layer were sensitive to tire pressure (Helwany, et al., 1998).

Three dimensional (3D) finite element can solve all of the problems solved with the two dimensional (2D) finite element. However, using 3D finite element is expensive in terms of computational time and data preparation. Asphalt pavement has a large dimension in comparison with to the other dimensions; therefore, one can use 2D plane strain condition instead of 3D modeling for this problem. Hua (2000) compared 2D and 3D finite element results of pavement rutting (Hau, 2000). Figure 7 shows the surface profile obtained from 2D and 3D FE modeling. As it can be seen the difference between 2D and 3D results is not significant. The maximum difference of rut depth between the two models is less than 2%.

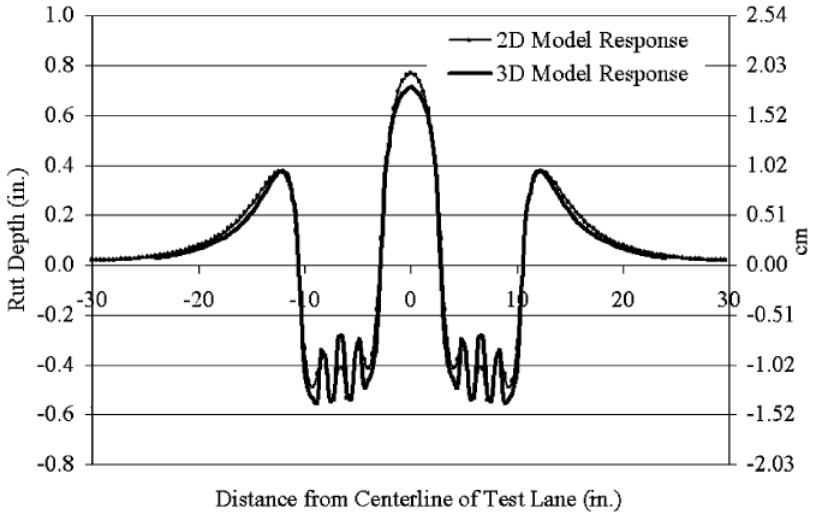

Figure 7: Comparison of 2D and 3D model responses (Hau, 2000)

Kose et al. analyzed 2D digitized images using finite element methodology to determine the strain distribution within the binder domains by considering elastic properties for the binder and the aggregate phases (Kose, et al., 2000). A 2D micromechanical FE model was developed by Papagiannakis et al. to predict the shear modulus and phase angle of the gyratory compacted asphalt mixtures (Papagiannakis, et al., 2002).

Recently, researchers have tried to define the complex behavior of asphalt binder (mastic) with constitutive models and incorporated it within the ABAQUS software through user material (UMAT) subroutine to improve the accuracy of the FE simulation results. Dai et al. (2006) used a mixed FE approach to study the behavior of asphalt mixtures by using rigid elements and continuum elements for aggregates and asphalt mastics, respectively (Dai, et al., 2006). By using Schapery's nonlinear viscoelastic model, a unified approach for the rate-dependent and rate-independent damage behavior was developed. To incorporate the linear and damage-coupled viscoelastic constitutive behavior of asphalt mastic, the properties of the continuum elements were specified through a UMAT subroutine within the ABAQUS code. Abu Al-Rub et al. (2011)

indicated that the effects of aggregate shape, aggregate distribution, and aggregate volume fraction should be considered in modeling the behavior of asphalt mixtures. They also concluded that the proposed constitutive model can provide the macroscopic behavior of asphalt concrete based on the distribution and properties of the constituents (Abu Al-Rub R.K., et al., 2011). A thermodynamic-based constitutive model which couples nonlinear thermo viscoelasticity, thermo-viscoplasticity, and thermo-viscodamage behavior of asphalt mixtures was used in the study (Darabi, et al., 2011) and the model was implemented in commercial FE software via UMAT.

Based on the literature review of finite element analysis of asphalt mixtures, it was decided to use 2D plane strain FE modeling in this thesis. The constitutive models used in this study are all incorporated within the ABAQUS code through UMAT. The details are presented in the following chapter.

Multi-scale Analysis of Asphalt Mixtures

Aggregate particles used in pavements typically have irregular shapes and varying sizes, ranging from 1 μm up to 30 mm (Lanceley, et al., 1966). Simulation of such a material with numerical methods requires tremendous computational cost (Lutif, et al., 2009). The search for an accurate analysis method which can account for the micro-structure of the mixture at a reasonable computational cost has led researchers to the multi-scale modeling approach.

The main goal of multi-scaling is to determine the averaged global behavior of a composite by considering the phenomena that occur on the smaller scales (Lutif, 2011; Aigner, et al., 2009). In the multi-scale approach the behavior of global structure can be obtained by analyzing each smaller scale heterogeneously to determine the bulk material response properties

at the desired scale. Different length scales are linked by applying homogenization principles (Figure 8). Therefore, the multi-scale modeling reduces the cost of analysis, however; it takes into account the properties of each of the composite's constituents.

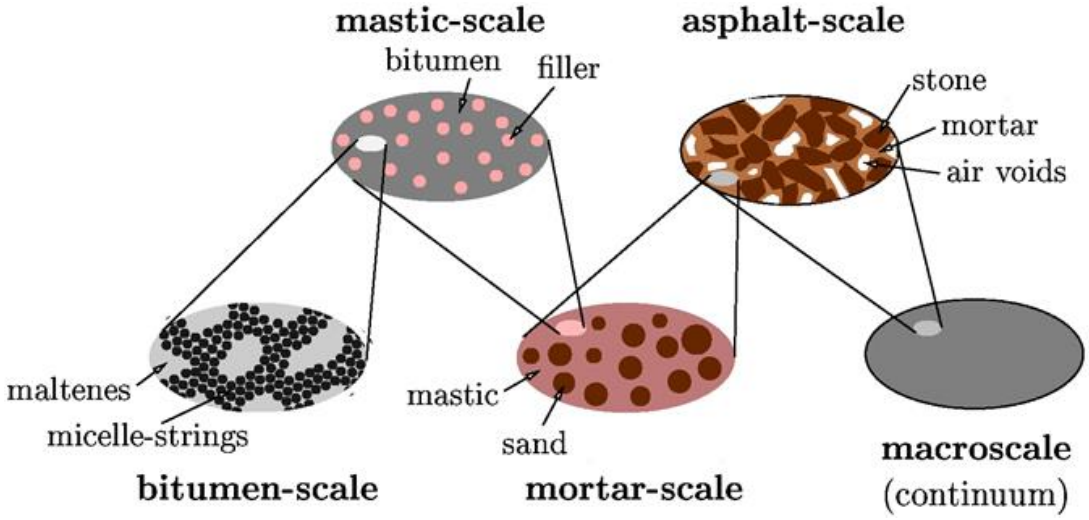

Figure 8: Multi-scale model with four additional observation scales below the macro-scale (Aigner, et al., 2009)

Multi-scaling has gained considerable popularity in recent years (Lutif, et al., 2009; Aigner, et al., 2009; Valenta, et al., 2010; Yin, et al., 2011). Lutif et al. (2009) used an efficient scale-linking technique to simulate the mechanical response of asphalt mixtures. The global scale was homogenized from local scale responses and the model was implemented in a finite element platform. The researchers concluded that the effect of material heterogeneity, inelasticity, and anisotropic damage accumulation in the micro-scale on the macro-scale behavior of structures can be taken into account by use of multi-scaling and finite element technique. It was also shown that this approach can significantly reduce the computational effort compared to single scale modeling which requires an impractical number of degrees of freedom. In another study, Aigner et al. (2009) proposed a multi-scale model to explain the complex behavior of asphalt mixture. The elastic-viscoelastic "correspondence-principle" was employed to determine the viscoelastic

properties of the mastic, mortar, and asphalt concrete from rheological properties of the asphalt binder. They showed that good agreement can be achieved between the creep properties of asphalt concrete resulted from presented multi-scale model and experimental results by means of cyclic tests and static uniaxial creep tests. Valenta et al. (2010) conducted a two-step homogenization to determine the material properties of the asphalt mixture. In that study the properties of the asphalt mastic were derived from experiment then the effective properties were found for a mortar phase, a composite of mastic matrix and fine aggregates. These properties were used to estimate the model parameters on macro-scale (Figure 9). Comparison of the results with Mori-Tanaka predictions indicated the limitations of the classical micro-mechanical models. Yin et al. (2011) proposed a multi-scale model by combining macro-scale and meso-scale so that the heterogeneity of asphalt mixture can be involved in the analysis. The proposed model was used to simulate the three-point bending fracture test. The results showed that multi-scale modeling reduces the cost of the computation by reducing the amount of elements in the numerical model and at the same time the modeling results are feasible and reasonable by comparing with experimental results.

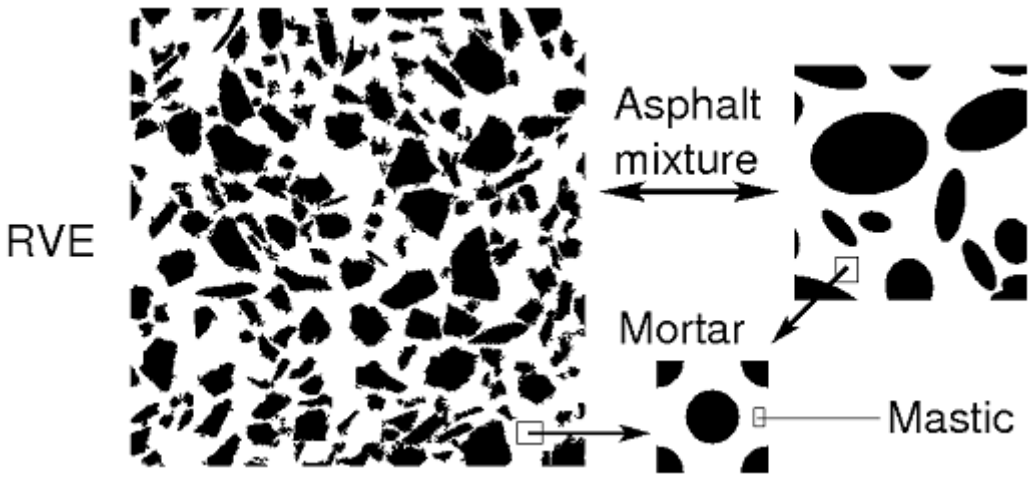

Figure 9: Three distinct scales of Mastic Asphalt mixture (Valenta, et al., 2010)

The up-scaling approach is presented in this study to relate the macro-scale behavior of asphalt mixture to rheological properties of asphalt binder. In the multi-scale approach, each scale is modeled heterogeneously to determine the bulk material response properties at the analyzed scale. If statistical homogeneity at the analyzed scale has been satisfied, the properties calculated at that scale are then inputted into a homogeneous matrix at the next-higher level. The multi-scale model developed in this study is presented elsewhere (Arshadi, et al., 2015).

Micro-mechanical Modeling of Particle Interactions

About a hundred years ago researchers started to work on micro-mechanical models of multi-phase media with non-interacting particles (Voigt, 1889; Reuss, 1929). However; research studies on micro-mechanical behavior of particulate materials with interacting particles, started less than three decades ago with remarkable improvements in numerical calculation method and computer hardware.

Studies conducted on cemented particulate materials provide information on load transfer mechanism between interacted particles (Dvorkin, et al., 1995; Zhu, et al., 1996). Dvorkin et al. solved the contact problem between two circular elastic grains with an elastic cement layer between them by considering some simplifying assumptions. They showed that the cement layer can be considered as an elastic foundation under normal compression which reduces the interaction problem to a linear integral equation (Dvorkin, et al., 1991). Latter Dvorkin and Yin solved the contact problem between two cemented particles with arbitrary-shaped surfaces (Figure 10). They showed that their solution is valid as long as the cement layer is thin and small in comparison with grains and contacting grain surfaces are smooth (Dvorkin, et al., 1995). It should be noted that this method is not efficient when the particle surfaces are not smooth or the

cement layer is thick. Zhu et al. (1996) presented the details on normal and tangential load transfer of a system of two elastic particles with a thin visco-elastic binder layer in between. Later, the work by Zhu et al. was used to derive the macro-rheological behavior of granular materials assuming a Maxwell type visco-elastic binder layer between particles, as show in Figure 11 (Chang, et al., 1997).

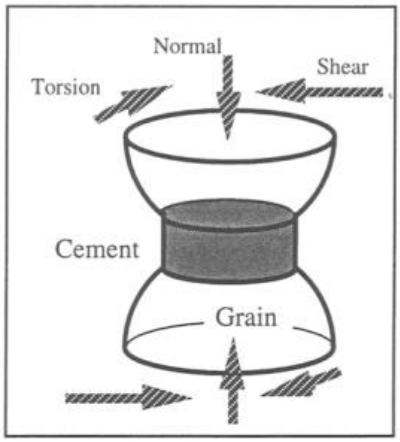

Figure 10: Cemented grains with smooth grain surfaces (Dvorkin, et al., 1995)

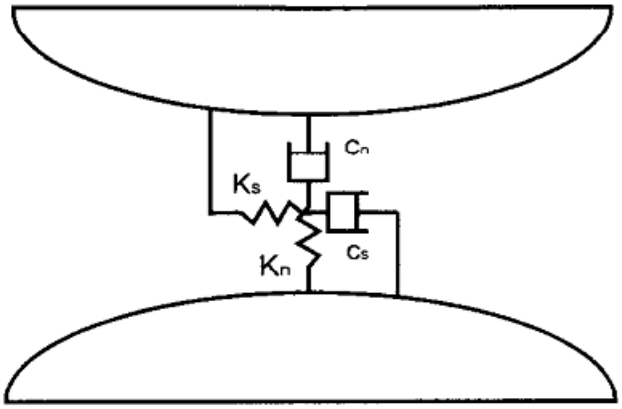

Figure 11: Schematic plot for the inter-particle model of a system consisting of two particles with a binder (Chang, et al., 1997)

Asphalt mixture is a multi-phase material containing aggregate, binder, and air voids. There are two identified load carrying mechanisms for asphalt mixtures: through the mastic

stiffness and through the aggregate to aggregate contact (Cheung, et al., 1999). Aggregate particles used in asphalt mixtures typically have irregular shapes, different orientations and surface texture, and varying sizes, ranging from less 1μm up to 30mm which make the aggregate particle contacts more complicated. Many studies reported the use of contact-based micro-mechanical models to predict the behavior of asphalt mixtures (Chang, et al., 1997; Cheung, et al., 1999; Zhu, et al., 2000; Buttlar, et al., 2000). Cheung et al. (1999) applied the isolated contact modeling approach, developed for powder compaction analysis, to model the behavior of an idealized asphalt mixture. In the isolated contact modeling it is assumed that the binder displaced by each contact deformation flows into an air void rather than into other contacts in the vicinity. Zhu et al. (2000) used the previously developed contact model (Zhu, et al., 1996) to study the effect of aggregate angularity on stress-strain relationship of Maxwell binder coated aggregates. The results of the study indicated that the higher percentage of angular aggregates in asphalt pavement leads to a higher overall stiffness. Furthermore, it is shown that higher aggregate angularity enhances the aggregate interlock mechanism which makes a more rut resistant asphalt mixture.

Recently, researchers have started to incorporate the developed contact models into numerical analysis methods, such as DEM and FEM (Buttlar, et al., 2000; Papagiannakis, et al., 2002; Sadd, et al., 2004; Dai, et al., 2006). Buttlar et al. (2000) presented a DEM approach for modeling asphalt concrete considering the changing contact geometries. In this study a linear force-displacement behavior was considered for the particles and simple bonding model was employed as shown in Figure 12. A number of research works are done on micro-mechanical modeling of asphalt mixtures using DEM (Dai, et al., 2007; Chang, et al., 1999; Luo, et al., 2010). In DEM, aggregates are represented as discrete elastic particles and their interactions are

controlled by the response of an asphalt thin film. Some of the most important benefits of the discrete element modeling are the ability to handle complex and changing contact geometries and large displacements. The disadvantage of this method is the huge computational cost and power which in needed for this type of modeling.

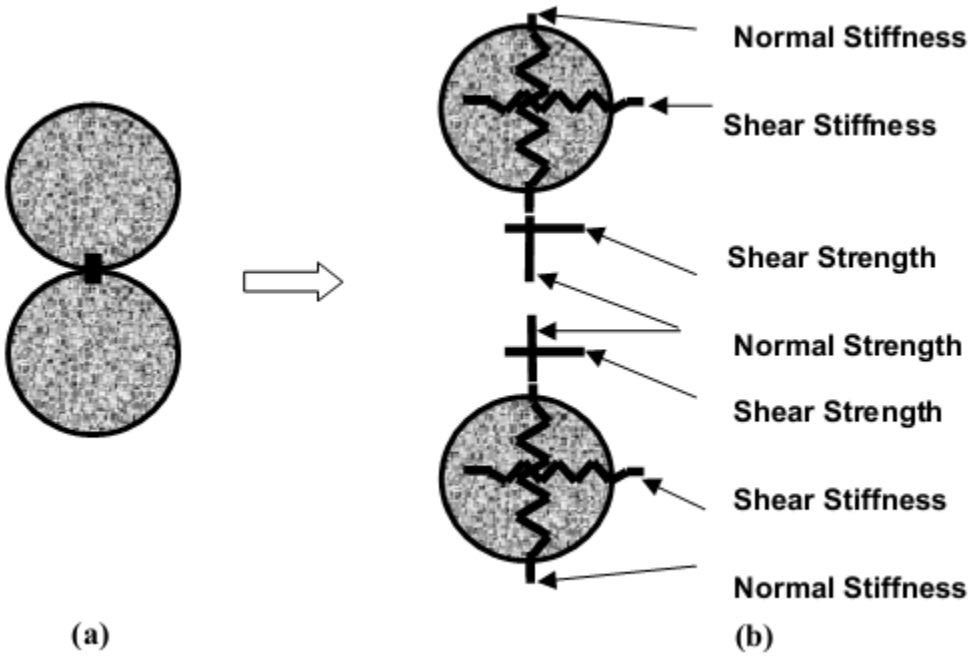

Figure 12: Schematic of contact models: (a) bonded discs and (b) detail of contact models (Buttlar, et al., 2000)

Papagiannakis et al. (2002) incorporated the contact model developed by Zhu et al. (2000) into FE software, ABAQUS, to relate the microstructure of asphalt concretes to their viscoelastic behavior. Sadd et al. implemented the contact law presented by Dvorkin et al. (1995) in ABAQUS using nonlinear user defined element (UEL) subroutine to simulate the indirect tension test (IDT) and investigate the effect of micro-structure on sample response considering idealized aggregate geometries (Figure 13). They derived a formulation for the stiffness matrix of the cement layer between two adjacent particles and showed that the layer stiffness increases

as the particles get closer to each other (Sadd, et al., 2004). Dai et al. (2006) used the same contact modeling technique to simulate the 2D linear and damage-coupled viscoelastic behavior of asphalt mixtures. They verified the model by comparing the FE simulated mixture creep stiffness with the test data.

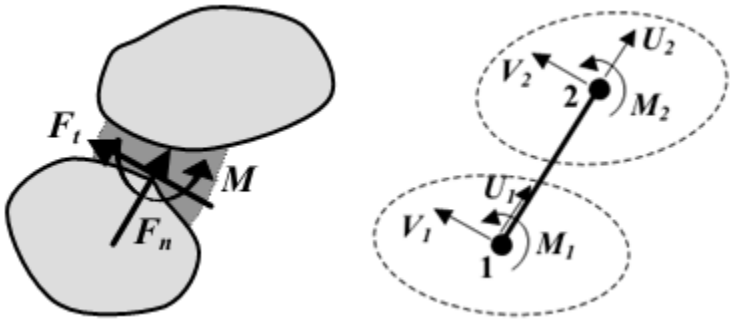

Figure 13: Resultant load transfer between actual aggregate pairs and idealized aggregate pairs (Sadd, et al., 2004)

Most current asphalt mixture multi-scale models face challenges with regards to accurate implementation of aggregate geometry, by either utilizing artificially generated geometric aggregate, or if scanned aggregate geometries are used, it is only at the coarsest scale of analysis due to limitation in imaging precision. Furthermore, as mentioned above there are still some critical problems regarding particle interactions in FE micro-mechanical modeling of asphalt mixtures. In the present study the developed multi-scale aggregate geometries are significantly advanced for the finer scales through use of real particle shapes and gradations. Besides, a simple aggregates contact rule is defined and implemented through UMAT (Appendix C) in the FE software to simulate the particle-to-particle contact behavior at all scales (Arshadi, et al., 2015).

Asphalt Pavement Fatigue

Classical fatigue cracking or bottom-up cracking usually happens in thin pavements. In these pavements the formation of the cracks happens at the bottom of the pavement where the tensile strain (or stress) is the maximum and then the cracks propagate to the surface as inter-connected network of cracks, often referred to as alligator cracking. Bottom-up cracking is known as the most common type of fatigue cracking (Figure 14). Top-down cracking usually initiates at the surface of the pavement where the localized stress is high due to interaction of tire and pavement. Top-down cracks propagate downward and lead to longitudinal cracking in the wheel path (Figure 15).

Figure 14: Alligator fatigue cracking in asphalt pavement

Figure 15: Longitudinal fatigue cracking in asphalt pavement

Fatigue cracking usually happens as a result of decrease in pavement load supporting characteristics due to saturation of pavement layers during thawing in spring which reduces their load carrying capacity (Huang, 2004). Hence, the fatigue cracking experiments are performed at the intermediate temperatures corresponding to spring conditions.

Characterization of the pavement damage is complicated due to unpredictable distresses that asphalt pavement experiences during its service life. Fatigue cracking in asphalt pavements often occurs when it is subjected to excessive loads during its design life or has been stressed to the limit of its fatigue life by repetitive loading (Kingery, 2004).

Laboratory testing on fatigue of asphalt mixture consists of two different test approaches: constant applied stress amplitude and constant applied strain amplitude (Hahtala, et al., 1997). In these tests the cyclic loading is applied to the sample until the failure happens in it. In the controlled stress mode of test the stress amplitude is maintained constant during the test and an increase happens in the tensile strain of the specimen due to decrease in material stiffness (Figure 16). In the strain controlled mode of fatigue test the behavior is different. In this test the needed load to generate a certain strain amplitude decreases during the test (Figure 17).

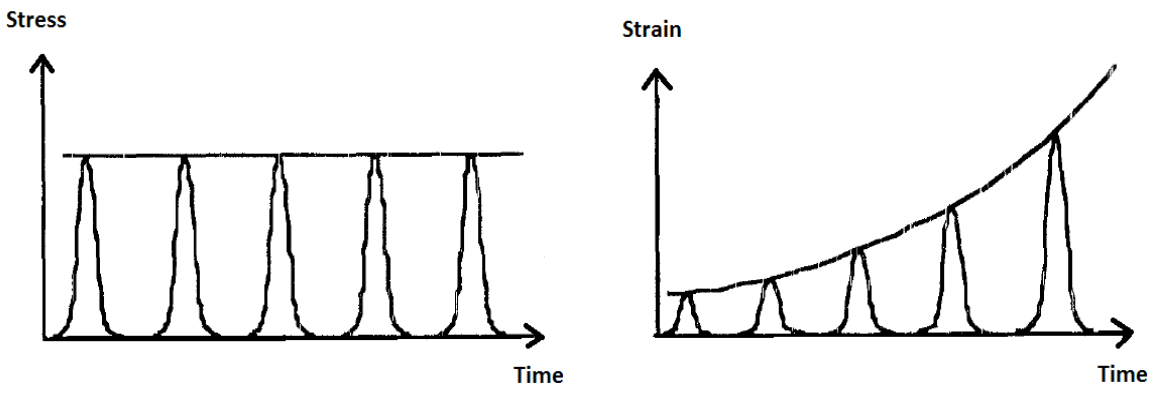

Figure 16: Schematic stress and strain in constant stress amplitude mode of fatigue test (Hahtala, et al., 1997)

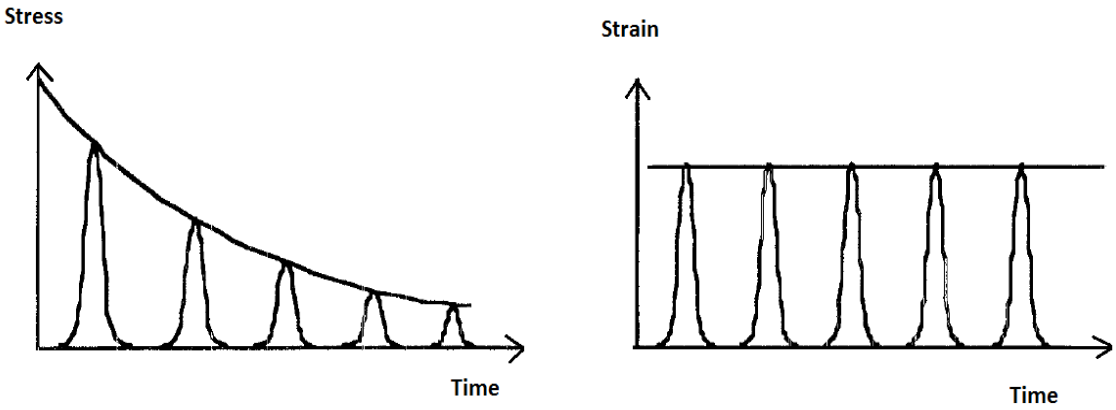

Figure 17: Schematic stress and strain in constant strain amplitude mode of fatigue test (Hahtala, et al., 1997)

Indirect Tensile (IDT) test is one of the most common test procedures for measuring the fatigue response of asphalt mixtures. Researchers have used the IDT test for over 30 years to characterize the fracture resistance properties of HMA mixes (Walubita, et al., 2002). In this test the specimen is typically loaded diametrically in compression and this induces horizontal tensile stresses at the middle of sample which ultimately causes the failure of the specimen (Figure 18).

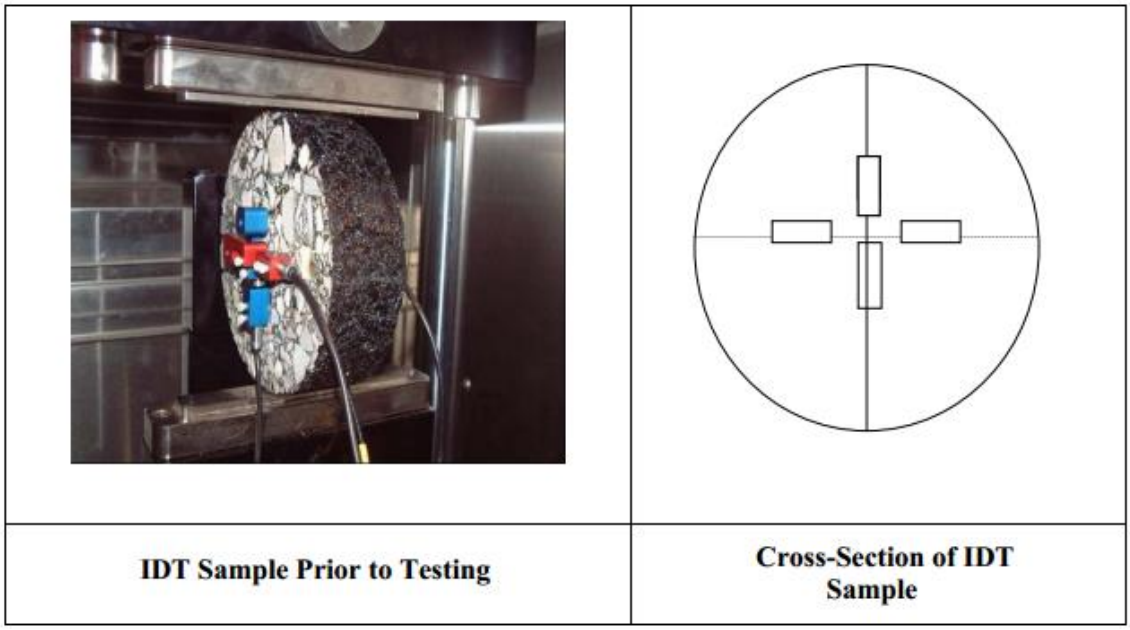

Figure 18: IDT Test Setup

The indirect tensile test procedure is standardized in ASTM D 6931 and AASHTO T 322 specifications (ASTM-D6931, 2012; AASHTO-T322, 2012). The loading device used for both of the specification is similar, but the rate of applying the load for strength determination in AASHTO standard is slower (13.5 mm/min instead of 50 mm/min). The AASHTO TP9-96 explains the standardized test procedure for fatigue cracking analysis.

The test method determines D(t), St, and ν of asphalt mixture which are creep compliance, tensile strength, and Poisson's ratio, respectively. The creep compliance is defined as the time-dependent strain divided by the applied stress and the tensile strength is defined as the strength of the specimen corresponded to the peak load.

The specimens can be gyratory compacted samples in accordance with AASHTO T 312 or specimens obtained by coring from pavements in accordance with ASTM D 5361. The

specimens are typically 150 mm in diameter and 38 to 50 mm in height and both sides have to be smooth and parallel.

The advantage of the IDT test over the other tests is its simple and easy specimen preparation. The short time duration of the test is another advantage of the test. Witczak et al. (2002) showed a fair correlation between IDT horizontal tensile strain at failure with the amount of observed cracking. Kim et al. (2002) developed a procedure by combination of the indirect tensile creep test and strength test and application of Viscoelastic Continuum Damage (VECD) to measure a mixture response parameter, fracture energy. They indicated that the measured fracture energy is highly correlated to the occurrence of pavement fatigue cracking. Mehta et al. conducted an extensive literature review to provide the Wisconsin Department of Transportation (WisDOT) with the asphalt mixture test methods that can be used to evaluate asphalt concrete mixtures (Mehta, et al., 2005). They reported that the IDT test can be used to characterize the pavements structures. The resilient modulus (under repeated loadings), indirect tensile strength, and failure strain measured by the IDT test can be used to evaluate the fracture related distresses of asphalt mixtures. It is also reported that the creep compliance from the IDT test shows high correlation with thermal cracking data.

There are also some issues regarding the IDT test. One of them is the gauge length of the Linear Variable Displacement Transducers (LVDTs). In the coarse graded mixtures, the existence of the large aggregates at the center of the specimen can affect the displacement measurements. Another disadvantage of the IDT test is the existence of a biaxial stress state (Matthews, et al., 1993). The complexity of the stress field in the IDT specimen makes the failure mode of the specimen a mixture of tension, compression, and shear (Molenaar, et al., 2002). Also, the high stress concentrations at the upper and lower supports may cause the local

and thus total specimen failure (Walubita, et al., 2002). The combined effect of these stress complexities makes the IDT results subjective and reduces the accuracy of the test in prediction of pavement fatigue resistance. Table 1 summarizes the pros and cons of the IDT test.

Table 1 : Advantages and Disadvantages of IDT (Huang, et al., 2005)

Advantages	Disadvantages
Simple to conduct	Permanent deformation under the loading strip is undesirable
Specimens can be easily obtained from Superpave gyratory compactor or field cores	Only controlled stress testing may be performed
Existing equipment, such as Marshall testing system, can be utilized	Strain distribution in the middle of the specimen is quite non-uniform
Failure is not seriously affected by sample surface conditions	The stress state during the diametrical test on a specimen under loading is complicated and not a realistic representation of the stress state in the whole pavement structure
The stress state in the vicinity of the center is similar to that at the bottom of the asphalt layer	If the compressive strength of the material under loading is lower than three times the tensile strength, specimen fracture will be initiated by compressive failure
	High stresses at the supports in IDT may cause local failure at these points

Mathematical modeling of fatigue performance of asphalt mixture is a very challenging problem due to viscoelastic hereditary effect of the material and complex nature of damage evolution. A considerable amount of research work has been conducted on development of asphalt mixture fatigue performance models (Tayebali, et al., 1992; Deacon, et al., 1994). Due to the empirical nature of the most of these models, they are dependent to a large amount of laboratory testing. Recently, Kim et al. were successful in development of a mechanistic constitutive model of asphalt concrete (Kim, et al., 1997). They developed the viscoelastic

continuum damage (VECD) model based on the research work on crack growth in viscoelastic media performed by Schapery (Schapery, 1984). The most important benefit of VECD analysis is that it allows for prediction of fatigue characteristics from a single test. It has been shown that VECD model can predict the damage resistance of asphalt mixtures with an acceptable accuracy (Park, et al., 1996; Lee, et al., 2000; Daniel, et al., 2002). A few researchers have tried to use the VECD model to predict the fatigue behavior of asphalt mixtures. Mun et al. conducted a research on implementation of VECD model of asphalt concrete in the commercially available FE program, ABAQUS. They verified the accuracy of the FE model and showed that the damage model is accurate for strain rates greater than 0.00002/sec. However, for lower strain rates the viscoplasticity of the material has a significant role and has to be considered in the modeling (Mun, et al., 2005). Kim et al. used the VECD model implemented in the FE program to evaluate the cracking performance of asphalt pavements with different layer thickness and material strength. Their research demonstrated that the Equivalent Axle Load Factor of different load levels can be directly determined from the damage level computed by the VECD model (Kim, et al., 2006). In a more recent study conducted by Yun et al. the viscoelastoplastic continuum damage modeling is used to study the stress-strain behavior of asphalt mixture under compression. A corrective measure was used to account for the effect of aggregate locking. It was shown in the study that the mechanistic model predicts the rutting performance and under compression behavior of asphalt mixture accurately (Yun, et al., 2013).

In the current study an image-based multi-scale FE model coupled with VECD model is developed to estimate the fatigue resistance of asphalt mixtures based on their constituents' properties. The IDT fatigue test was used to validate the developed multi-scale model. The

details of the test conditions and model validation are presented in following chapters of the thesis.

Asphalt Binder Fatigue Testing

One of the most important pavement distresses which seriously affects the pavement performance is fatigue cracking. As this cracking generally takes place in the binder phase of the asphalt mixture, the binder fatigue behavior is assumed to be one of the main factors influencing the overall pavement fatigue performance. As it is mentioned earlier, the asphalt binder exhibits a very complex behavior. At low temperatures or high loading frequencies it behaves like an elastic material; however, at high temperatures or low loading frequencies the asphalt binder exhibits a more viscous behavior. Dynamic Shear Rheometer (DSR) is a widely used device to evaluate asphalt binder properties such as dynamic shear modulus (G^*) and phase angle (δ) at different temperatures and loading frequencies. DSR is also a common device to evaluate fatigue resistance of asphalt binders.

In DSR testing, a cylindrical sample of asphalt binder is placed between a rotating plate and a fixed one and the torsion is effectively applied to the specimen as depicted in Figure 19. This device is able to directly apply and measure the applied torque (T) and the deflection angle of the specimen (φ). The instrument also reports the maximum shear stress and shear strain of the sample which happens at the edge of the sample.

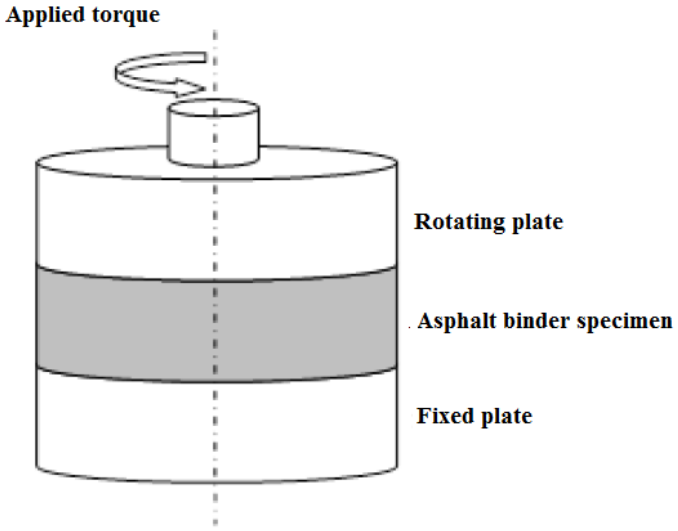

Figure 19: Schematic of dynamic shear rheometer (DSR)

Extensive research on fatigue cracking of asphalt pavements has shown that the mechanical properties of binder and mastic phases largely influence the overall pavement fatigue performance (Bahia, et al., 2001). The current fatigue specification was developed by Superpave (SUperior PERforming Asphalt PAVEments) based on the assumption that a softer, more elastic binder increases the fatigue resistance. In this specification a maximum limit of 5 MPa is placed for the $|G^*|.\sin\delta$ of the asphalt binder, (where G^* is the asphalt binder complex shear modulus and δ is the binder phase angle), measured at frequency of 10 rad/sec and strain amplitude of 1% in the DSR. However, recent researches on asphalt mixture fatigue resistance showed that the Superpave approach lacks the ability to characterize actual damage resistance (Bahia, et al., 2001; Bahia, et al., 2002; Tsai, et al., 2005). Another weakness of this specification is that it does not account for the traffic loading and the pavement structure and the measurement is made at one, low strain level over a few cycles of loading.

In order to solve the abovementioned shortcomings of the current specification, National Cooperative Highway Research Program (NCHRP) Project 9-10 proposed the time sweep test

procedure (Bahia, et al., 2001). In the time sweep test a repeated sinusoidal loading is applied to the binder specimen in the DSR (Figure 20). The changes in complex shear modulus and phase angle with number of loading cycles are used to determine the fatigue life. The loading amplitude in this procedure can be selected based on the pavement structure and traffic loading. Bahia et al, showed that the results of this test correlate with the mixture fatigue test results (R^2= 0.84), showing the binder contribution in fatigue resistance of asphalt mixture.

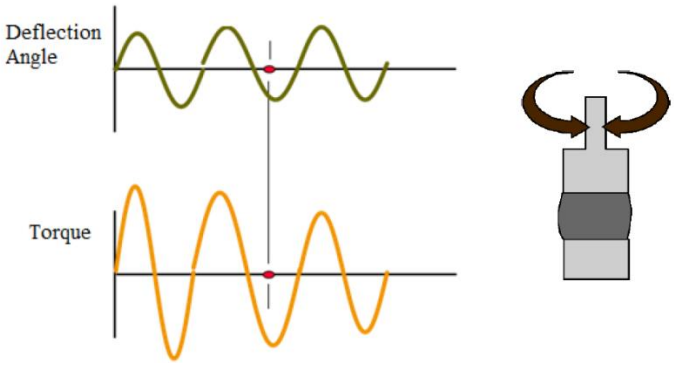

Figure 20: Schematic of time sweep loading and response

Time sweep test is a time consuming experiment which can take long for several hours. In order to decrease the test time the Linear Amplitude Sweep (LAS) test has been proposed by Johnson (Johnson, 2010). This test is similar to the time sweep test; however, the strain amplitudes are systematically increased up to 30% to accelerate damage, as shown in Figure 21. Recently Hintz modified the LAS test to eliminate the effect of crack tip conditioning due to abrupt changes in loading amplitudes by increasing the strain amplitude with a very small amount at each successive loading cycle (Figure 22). In addition to amplitude sweep loading, the LAS test includes a frequency sweep test prior to the amplitude sweep to obtain an undamaged material response used in VECD modeling. The frequency sweep is conducted at small load amplitude of 0.1% strain to avoid inducing damage. Use of VECD mechanics allows for prediction of fatigue life at any strain amplitude from a single 30 minute test, thus allowing for consideration of pavement

structure (i.e., strain) and traffic (i.e., number of cycles to failure). The LAS procedure received the FHWA Binder ETG's approval in 2011 and designated a provisional AASHTO standard procedure under AASHTO TP101 in 2012.

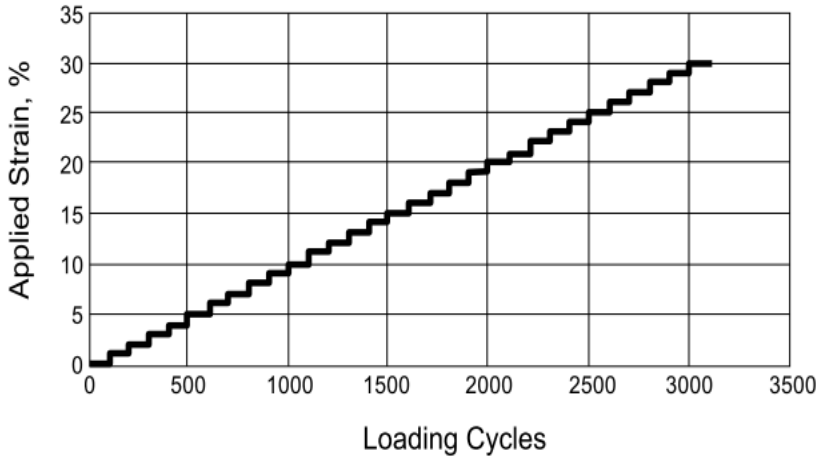

Figure 21: Schematic of LAS loading proposed by Johnson (Johnson, 2010)

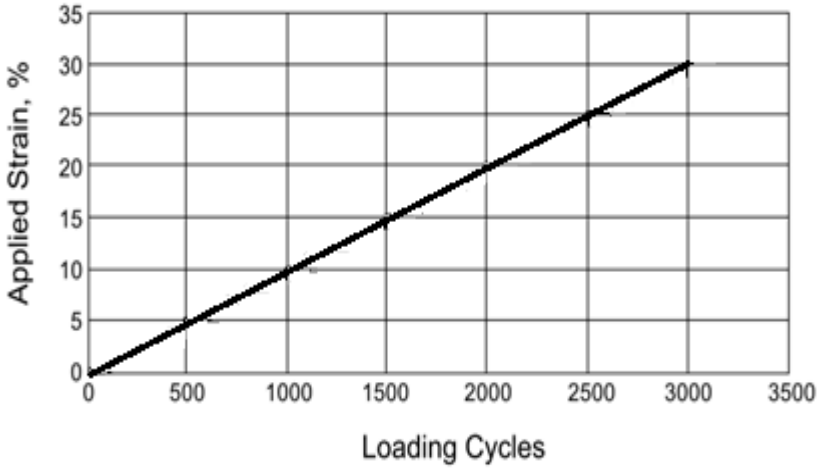

Figure 22: Schematic of LAS loading proposed by Hintz (Hintz, 2012)

In a recent study by UWM as a part of the Wisconsin Highway Research Program project the cracking behavior of the several field sections in Wisconsin has been successfully characterized by LAS binder fatigue performance indices and compared to $|G^*|.\sin\delta$ parameter (Tabatabaee et al., 2013). As shown in Figure Figure 23 there is a much better relationship

between LAS data and field performance in comparison with |G*|.sinδ parameter and the field performance.

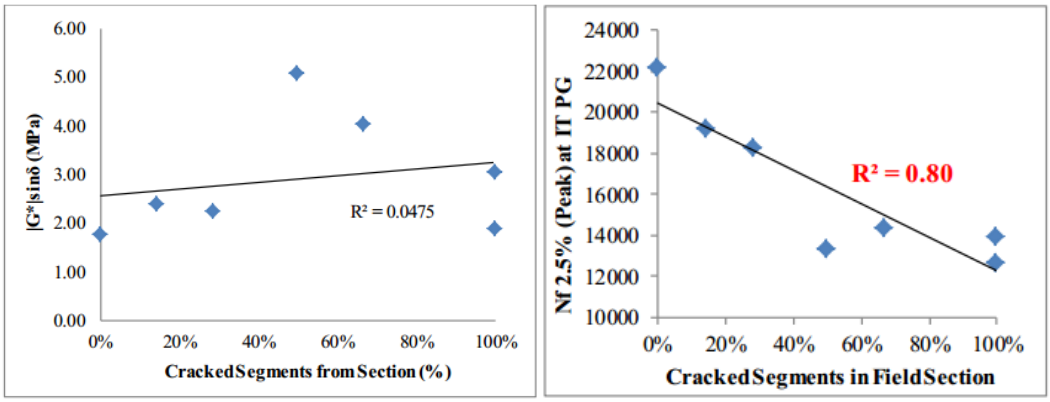

(a) field vs. |G*|sinδ. (b) field vs. LAS parameter

Figure 23: Relationship between field performance and binder laboratory test results

Although using the VECD model eliminates the need of numerous experimental tests to predict the fatigue characteristics of asphalt mixtures; it still requires the costly and time consuming tests on asphalt mixture scale. In the present study the VECD mechanics is utilized to model the fatigue behavior of asphalt binder from a single LAS test. The VECD model is implemented into the well-known FE software ABAQUS via the user material subroutine (UMAT) in order to simulate the state of damage within the binder phase under the cyclic sinusoidal loading. The FE simulation is then conducted through a multi-scale framework to obtain the damage response of asphalt mixtures with different aggregate gradations and binder modifications.

CHAPTER 3: DEVELOPMENT OF AN IMAGE-BASED MULTI-SCALE FINITE ELEMENT APPROACH

Multi-scale Analysis Approach

Early in this study it was recognized that even the highest resolution 2D scanning and filtering techniques can only accurately detect a certain range of aggregate sizes. This is mainly due to obscuring of fine particles during the cutting process through smearing of the binder, and loss of a portion of very fine imaged particle after application of filters during image analysis. Thus it was understood that such particles should be included in analysis of finer scales if a realistic simulation of mixture mechanical behavior is desired. Asphalt mixtures in this study were therefore considered at four interconnected scales: the binder scale, for which mechanical response is directly measured through use of a Dynamic Shear Rheometer, the "mastic-scale" which contains fillers ranging from 1μm up to 75μm in a binder matrix; the "mortar-scale" containing fine aggregates ranging from 75μm to 1.18mm in a mastic matrix, and the "asphalt mixture-scale" which contains all larger aggregates (those detected using simple 2D scanners and binary imaging filters) in a continuous mortar matrix.

In order to specify the asphalt mixture properties at each scale, the FE analysis software ABAQUS v6.12 (2012) was used to conduct the simulations. For the mastic and mortar scales the artificially generated images were used to model the scales. For the asphalt mixture scale a flatbed scanner was used to capture color images and the image processing software IPAS2 was used to convert the color images to binary images following a filtering procedure described by Coenen et al. (2012). In the multi-scale approach, each scale is modeled heterogeneously to

determine the bulk material response properties at the analyzed scale. The properties calculated at each scale are then inputted into a homogeneous matrix at the next-higher level (Figure 24). The multi-scale procedure developed in this study as well as a summarization of the model calibration protocol and required input properties is shown in a flowchart in Figure 25. In the following sub-sections the homogenization and up-scaling process of the developed multi-scale model is described in detail.

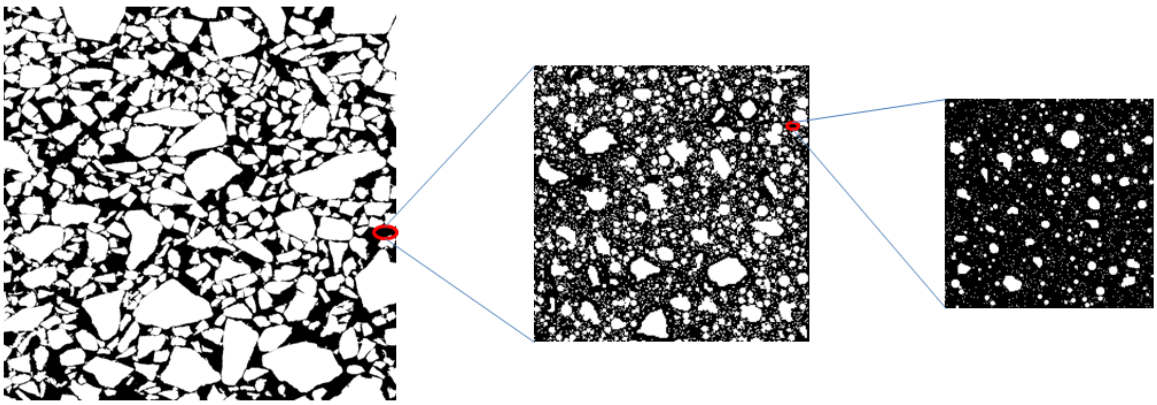

(a) (b) (c)

Figure 24: Multi-scale analysis scheme: (a) Asphalt mixture-scale (large aggregates in mortar matrix) (b) Mortar-scale (fine aggregates in mastic matrix) (c) Mastic-scale (fillers in binder matrix)

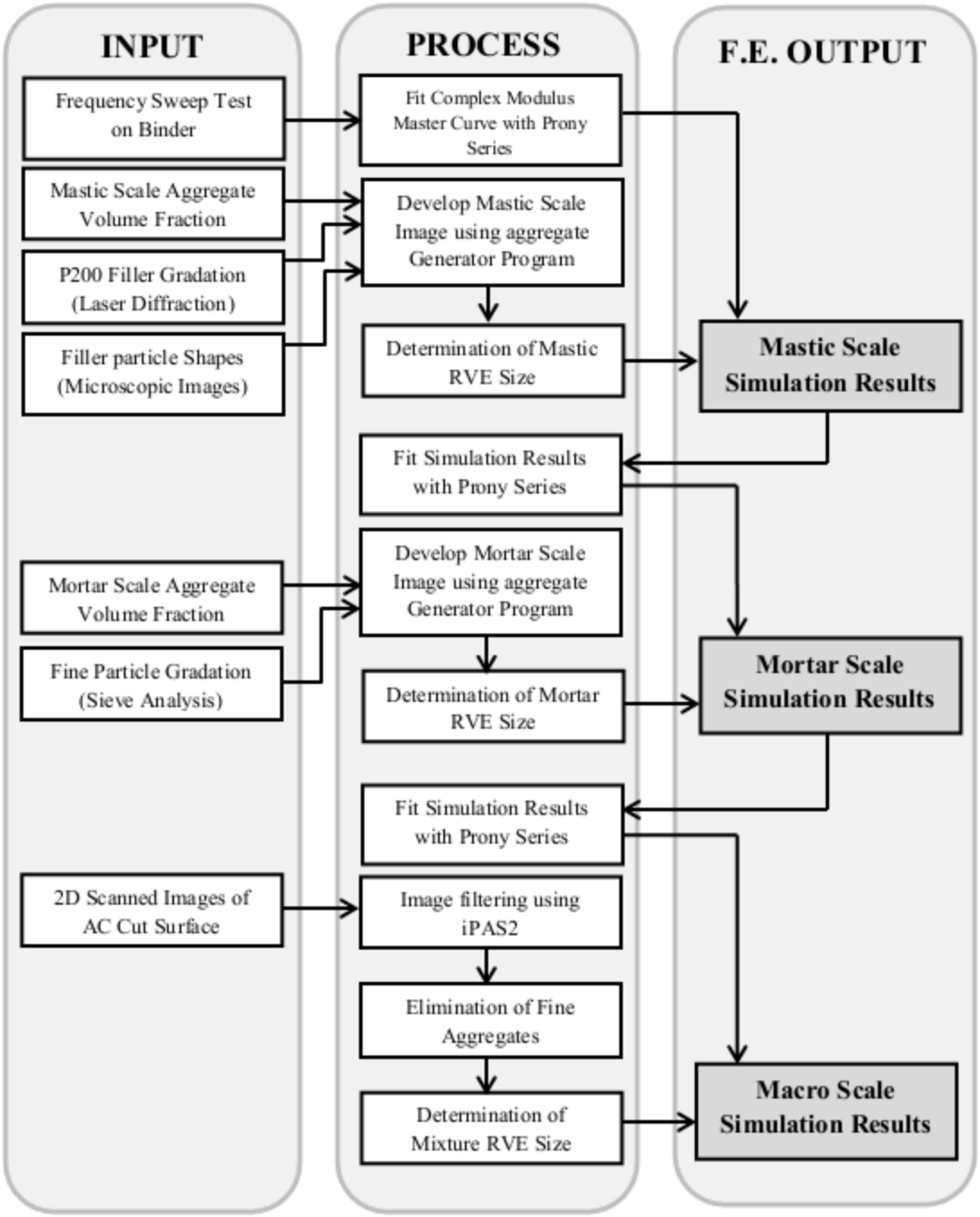

Figure 25: Flowchart of calibration and utilization of the multi-scale model developed in this study

Numerical Implementation of Binder Constitutive Model

The one-dimensional linear constitutive behavior of the asphalt binder can be expressed by Boltzmann superposition integral as shown in Equation 5.

$$\boldsymbol{\sigma(t) = \int_0^t E(t-\tau)\frac{d\epsilon(\tau)}{d\tau}d\tau,}$$ **Equation 5**

The relaxation modulus is described using a Prony series form as shown in Equation 6. The initial parameters of the Prony series were determined by fitting a curve to the binder master curve resulted from frequency sweep test results.

$$\boldsymbol{E(t) = E_\infty + \sum_{m=1}^{M} E_m . e^{\frac{-t}{\tau_m}}}.$$ **Equation 6**

In which:

- E_∞ is the long term modulus
- E_m is the Prony series relaxation modulus
- t is loading time, and
- τ_m is relaxation time

The incremental finite-element modeling scheme with constant strain rate over each time increment, presented by Zocher and Groves (Zocher, et al., 1997), was used to formulate the three-dimensional behavior of asphalt binder by uncoupling the stress tensor to volumetric and deviatoric components, such that:

$$\boldsymbol{\sigma_{ij} = (\frac{\sigma_{kk}}{3}\delta_{ij}) + \hat{\sigma}_{ij},}$$ **Equation 7**

where σ_{ij} and $\hat{\sigma}_{ij}$ are volumetric and deviatoric stress tensors, respectively. For an isotropic material it can be obtained that $\sigma_{kk} = 3K\epsilon_{kk}$, where $K = \frac{E}{3(1-2\upsilon)}$. Therefore, the volumetric constitutive relationship can be expressed as

$$\boldsymbol{\sigma_{kk}(t) = 3K_{\infty}\epsilon_{kk}(t) + \int_0^t 3K(t-\tau)\frac{d\epsilon_{kk}(\tau)}{d\tau}d\tau.}$$ **Equation 8**

By assuming a constant volumetric strain rate at each time increment, the incremental formulation of the volumetric behavior is obtained as

$$\boldsymbol{\Delta\sigma_{kk} = 3K_{\infty}\Delta\epsilon_{kk} + \frac{3\Delta\epsilon_{kk}}{\Delta t}\sum_{m=1}^{M} K_m\tau_m(1-e^{\frac{-\Delta t}{\tau_m}})}$$ **Equation 9**

$$\boldsymbol{- 3\sum_{m=1}^{M}\left(1-e^{\frac{-\Delta t}{\tau_m}}\right)H_m(t_n),}$$

and

$$\boldsymbol{H_m(t_n) = \frac{\Delta\epsilon_{kk}}{\Delta t}K_m\tau_m(1-e^{\frac{-\Delta t}{\tau_m}}) + e^{\frac{-\Delta t}{\tau_m}}H_m(t_{n-1})}$$ **Equation 10**

For the deviatoric stress-strain relationship it can be obtained that $\hat{\sigma}_{ij} = \sigma_{ij} - \frac{\sigma_{kk}}{3}\delta_{ij} = 2G(\epsilon_{ij} - \frac{\epsilon_{kk}}{3}\delta_{ij}) = 2G\hat{\varepsilon}_{ij}$, where $G = \frac{E}{2(1+\upsilon)}$. The deviatoric constitutive behavior can be expressed as

$$\boldsymbol{\hat{\sigma}_{ij}(t) = 2G_{\infty}\hat{\epsilon}_{ij}(t) + \int_0^t 2G(t-\tau)\frac{d\hat{\epsilon}_{ij}(\tau)}{d\tau}d\tau.}$$ **Equation 11**

The incremental formulation can be expressed as

$$\boldsymbol{\Delta\hat{\sigma}_{ij} = 2G_{\infty}\Delta\hat{\epsilon}_{ij} + \frac{2\Delta\hat{\epsilon}_{ij}}{\Delta t}\sum_{m=1}^{M} G_m\tau_m(1-e^{\frac{-\Delta t}{\tau_m}})}$$ **Equation 12**

$$\boldsymbol{- 2\sum_{m=1}^{M}\left(1-e^{\frac{-\Delta t}{\tau_m}}\right)R_m(t_n),}$$

and

$$R_m(t_n) = \frac{\Delta \hat{\epsilon}_{ij}}{\Delta t} G_m \tau_m \left(1 - e^{\frac{-\Delta t}{\tau_m}}\right) + e^{\frac{-\Delta t}{\tau_m}} R_m(t_{n-1}).$$ **Equation 13**

The procedure described above is implemented in the well-known FE analysis software ABAQUS through a user-defined subroutine, UMAT, and is used to conduct multi-scale FE simulations. The accuracy of the written code was verified by comparing the deformation of a simple column under pressure resulted from UMAT with the exact deformation available for an elastic material and a linear viscoelastic material represented by the Burger's Model. Figure 26 shows the flowchart of the computational process in ABAQUS.

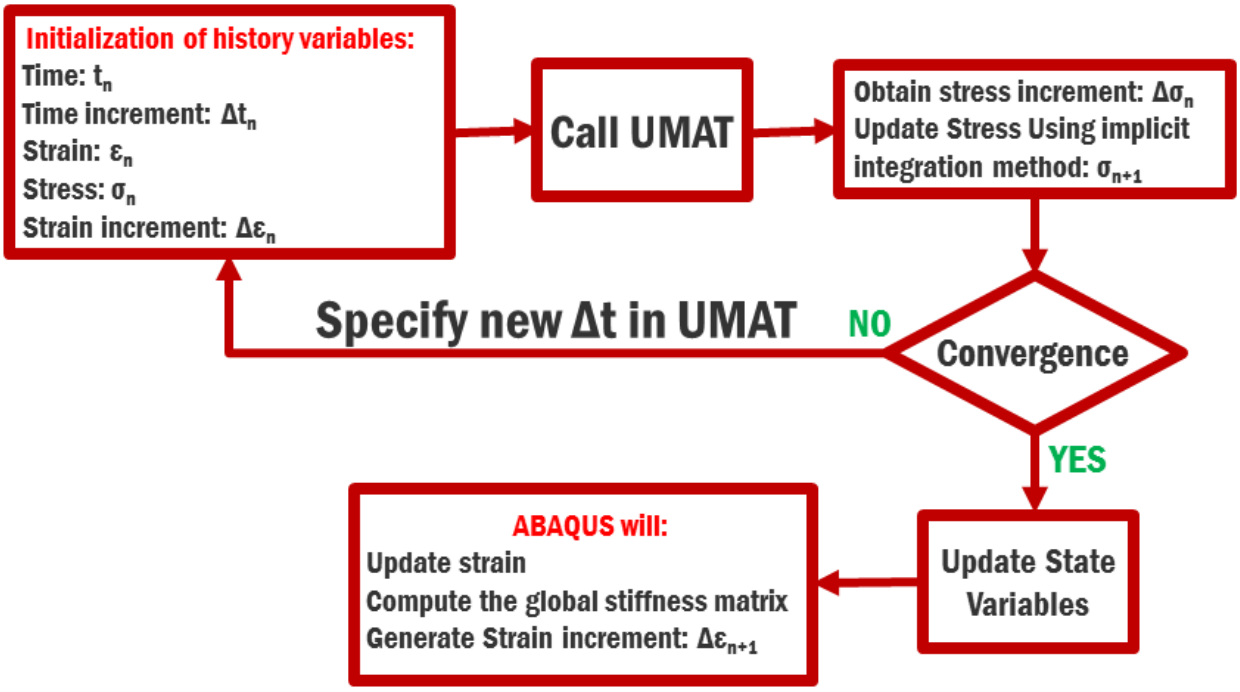

Figure 26: Flow-chart of the computational process

Mastic Scale

Contrary to common simplifications in many models in which the filler particles are considered to be of a uniform size smaller than the 0.075 mm sieve size, particle sizes can vary significantly at this scale (as shown in Figure 27), thus affecting the accuracy of the results. The "Laser

Diffraction" technique was used to experimentally determine the gradation of the filler particles in this study. In this technique a group of dispersed particles is irradiated by a laser beam, and the particle size distribution is calculated by measuring the intensity of light scattered from that group of particles. This method is widely used in many industries as a particle sizing technique for materials ranging in size from hundreds of nanometers up to several millimeters (Cyr, et al., 2001). The gradation of the granite stone filler is shown in Figure 27(a). In addition to the gradation, the realistic shape and geometry of the filler particles is captured through microscopic imaging and a database of 230 different filler particle shapes and geometries was developed. Figure 27(b) shows an example of the microscopic images used for development of the database.

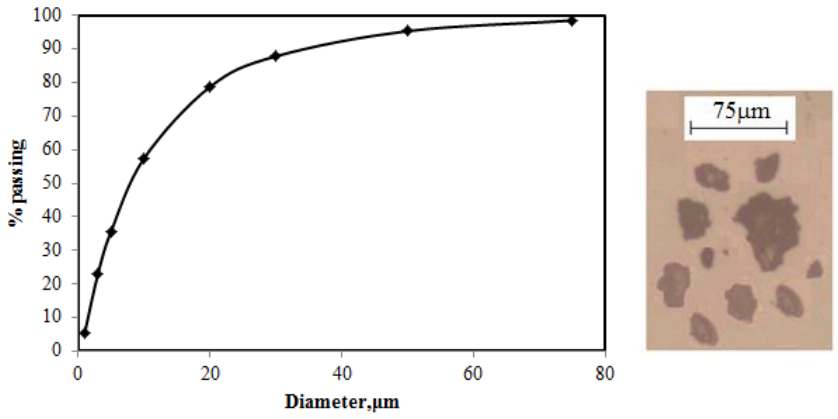

(a) (b)

Figure 27: (a) Gradation of the granite stone filler measured by laser diffraction methodology (b) Scanned microscopic image of granite stone filler

To study the mechanical behavior of the mixture in its mastic scale, the 2-dimensional images of the scale were generated based on the gradation and shape of the mineral fillers (Granite Stone labeled as GS) and the filler volume fraction of the mixture using a MATLAB based code. As it is explained earlier, granite filler gradation curve was measured by Laser Diffraction methodology and electron microscope images were used to obtain the filler particle

shapes. The code written for generating the sample images at lower scales can be found in Appendix A. Different steps of the code for generating the mastic (or mortar) images are summarized below:

1. Making the database of the particle shapes and separating the particles of each size.
2. Generating a fully black image with the size of the RVE.
3. Determination of the number of particles of each specific particle size (Nu_i) based on the particle gradation, particle size, particle volume fraction, and RVE size.
4. Placement of the particles in the RVE image based on their size and particle numbers determined from the last step. The particles will be selected from the database and placed in a random location in the RVE image with a random orientation.

The examples of artificially generated mastic images with four different filler volume fractions (φ), 0.1, 0.2, 0.3 and 0.4, are shown in Figure 28.

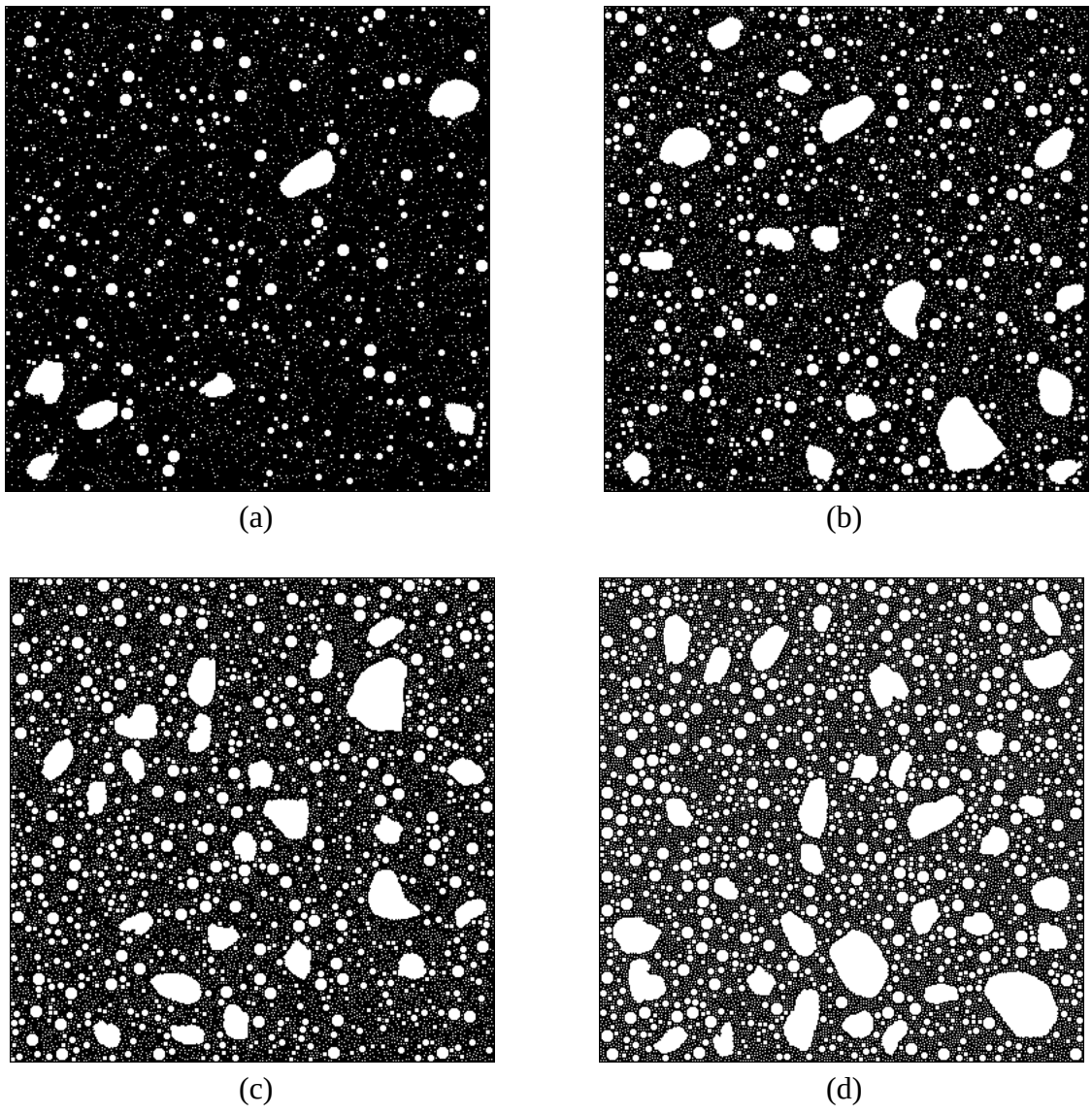

Figure 28: Examples of generated mastics with: (a) φ=0.1 (b) φ=0.2 (c) φ=0.3 (d) φ=0.4

To determine the optimum RVE, four mastic areas were modeled and analyzed using a filler volume fraction of 0.4, as the largest and most critical volume fraction considered in this study. The largest area was selected as 750 μm × 750 μm, 10 times larger than the maximum filler particle size. Three smaller subset areas (450 μm × 450 μm, 225 μm × 225 μm and 150 μm × 150 μm) were also obtained from the original image for RVE analysis, as shown in Figure 29. Finite element analysis was used to obtain the creep compliance curve for each image through

bulk strain measurement under uniform compressive loading. The optimum RVE size was selected based on the convergence of the measured creep compliance curves of each of the modeled mastic areas to that of the original large scale image. Figure 30 shows that as the size of the RVE increased the observed creep compliance curves quickly converged to the creep compliance of the original image. It also demonstrates that the square root of sum of squares sharply decreases for the 250 μm × 250 μm and gets close enough to zero. Based on the results, the optimum RVE size was determined to be a 225 μm × 225 μm area, which was used for all subsequent analysis at the mastic scale.

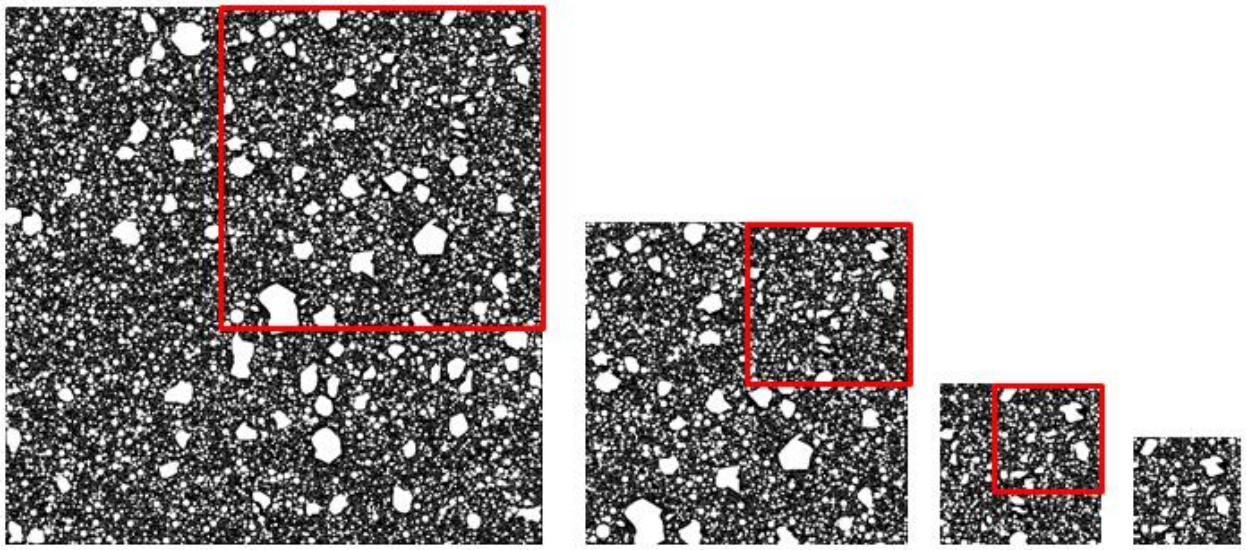

(a) (b) (c) (d)

Figure 29: Image analysis procedure for finding optimum RVE size of the GS mastic. (a) 750 μm × 750 μm (b) 450 μm × 450 μm (c) 225 μm × 225 μm (d) 150 μm × 150 μm

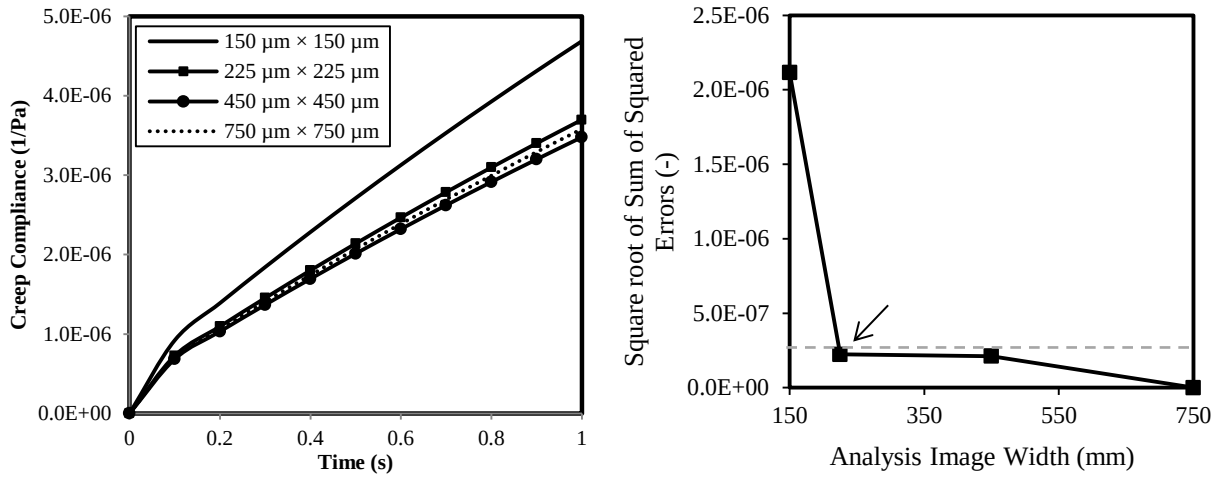

(a) (b)

Figure 30: (a) Creep Compliance of the generated GS mastic images (b) Square root of sum of squared error between reference image and reduced size images

Mortar Scale

The "mortar scale", the next higher level after the "mastic scale", consists of fine aggregates, larger than 0.075 mm (#200 sieve opening) and smaller than 1.18 mm (#16 sieve opening). The gradation of fine aggregates in the mortar scale is determined from the total aggregate gradation used for the mixture. The fine aggregate generation program developed as part of this study was used at the mortar scale to generate the mortar images based on the fine aggregate gradation and shape. The examples of artificially generated mortar images of two mixtures with fine and coarse aggregate gradations are shown in Figure 31.

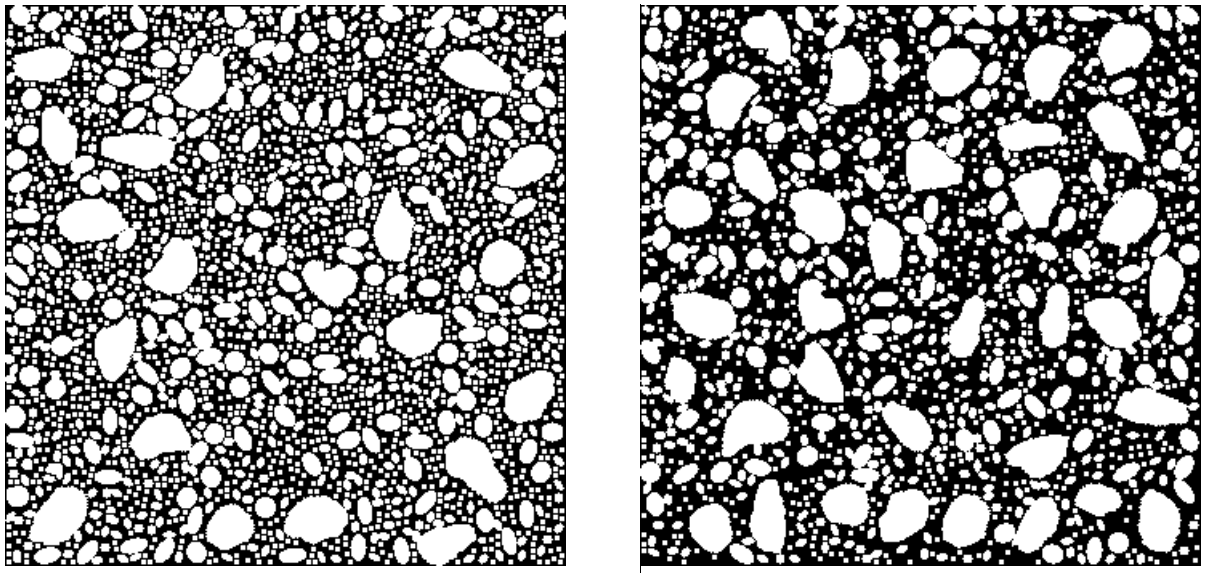

(a) (b)

Figure 31: Examples of generated mortars of mixtures with: (a) fine aggregate gradation (b) coarse aggregate gradation

For determination of the input properties for the mortar scale of the multi-scale model, the homogenized viscoelastic properties of the mastic scale assessed by performing a creep and recovery simulation and a creep loading simulation on the mastic RVE, and fitting the QLV model to the analysis results. These properties were used as material input values for the continuous matrix of mortar scale of the multi-scale simulations. The homogenization process assumes mastic isotropy and homogeneity, when inputted as the continuous phase in the mortar scale.

The fine aggregate volume fraction at the mortar scale was determined based on the mixture gradation and design volumetric properties. It was calculated that for regular asphalt mixture designs the volume fraction of the fine aggregates in mortar scale varies from 0.4 to 0.65 depending on the coarseness of overall gradation. In comparison, the volume fraction of fillers in the mastic scale ranged from 0.1 to 0.4. Coarser overall mixture aggregate gradations result in lower volume fraction of fines in the mortar and mastic scales. Based on convergence of the

creep compliance curves, an optimum RVE of 3.5 mm × 3.5 mm, approximately 3 times larger than the maximum size of fine aggregates in mortar scale was determined. Homogenized mortar scale mechanical properties were identified by performing the test procedure, explained earlier in chapter 3, on the mortar RVE. Results are inputted as material properties in the continuous matrix of the "macro scale", assuming an isotropic and homogeneous mortar matrix at this scale.

Asphalt Mixture Scale

The asphalt mixture scale is the highest level scale in the multi-scale analysis scheme used in the present study. A flatbed scanner was used to capture color images at a resolution of 20 μm/pixel of HMA cross sections. 2D digital image processing techniques were used to convert the color images to binary images. The continuous phase of the asphalt mixture scale images consist of the homogenized isotropic mortar scale. The imaging techniques used in this study cannot accurately capture aggregates smaller than 1.18 mm, mostly due to a portion of imaged particles smaller than 1.18 mm being lost during the application of filters when converting to binary. Therefore, a MATLAB code was used to eliminate the aggregates smaller than 1.18 mm from the images (Figure 32), and instead including this size range in the mortar and mastic scales.

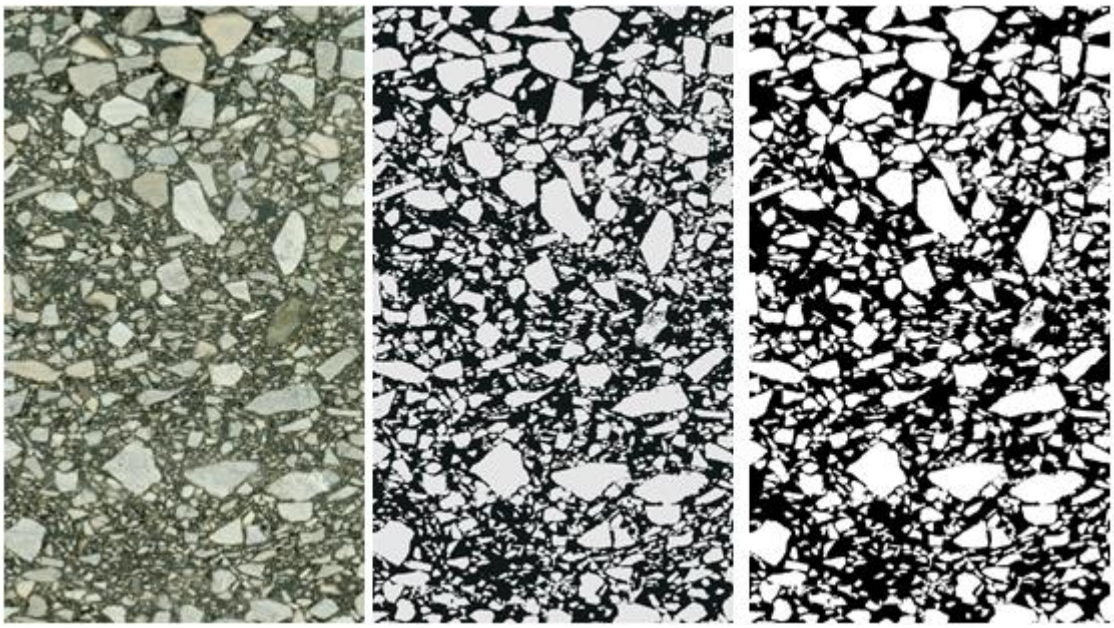

(a) (b) (c)

Figure 32: Images of the mixture. (a) Scanned image of HMA section (b) Scanned image after image filtering processes (c) Scanned image after elimination of aggregates smaller than 1.18 mm

Due to the lack of color contrast between air voids and the background asphalt, coupled with the unavoidable filling of most air voids on the cut surface due to binder smearing during the cutting process, air voids cannot be reliably captured using current 2D imaging techniques. In the present study it was decided to overcome this deficiency by introducing artificially generated circular air voids in the macro scale image. Masad et al. (2002) , studied the air void distribution in the asphalt mixtures, concluding that the air void distribution of gyratory compacted samples followed a bathtub shape distribution, such that larger air voids were located near the top and bottom of the specimens, with the air voids in central portion having a relatively consistent smaller size (Figure 33). The same distribution was used in this study to distribute the air voids at the asphalt mixture scale (Masad, et al., 2002). The air voids are considered as empty spaces in the FE simulation program.

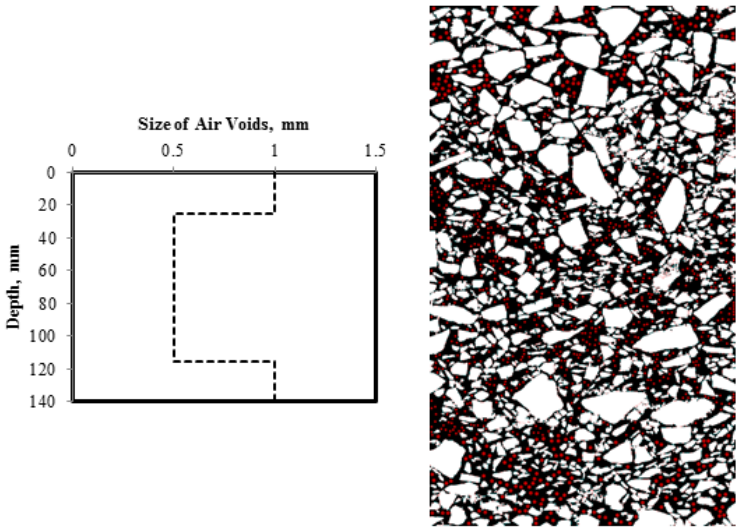

Figure 33: Distribution of air void sizes with depth

Optimized Finite Element Mesh Generation

Earlier studies on two dimensional FE simulation of asphalt mixtures were conducted by mapping each asphalt mixture scanned image pixel into a quadrilateral element in order to generate the meshed FE model (Kose, et al., 2000; Lakes, et al., 2002). Although it was a straightforward method to generate the FE mesh of the mixtures with any aggregate shapes and volume fractions; the simulation computational cost was extremely high due to the large number of elements. Therefore it was an inefficient method to mesh the asphalt mixture images with higher resolutions which represent the microstructure of the asphalt mixture more accurately. In latter studies image processing and ellipse fitting methods were used to simulate the microstructure with idealized elliptical aggregates in order to simplify the FE mesh generation of the asphalt mixture microstructure (Dai, 2004; Sadd, et al., 2004; Dai, et al., 2007). These models were promising in prediction of the asphalt mixture properties, however; irregular and angular aggregate shape was idealized as ellipse. Therefore, they were not successful to fully capture the micromechanical aggregate to aggregate contact mechanics (Dai, et al., 2007). Using

triangular elements in development of the FE model of asphalt mixture microstructure has gained considerable popularity in recent years (Dai, et al., 2007; Coleri, et al., 2012). Currently this easy to implement mesh generation method is mostly used by the researchers due to its accuracy in accounting for the microstructure of the mixture. Although one can model any geometry using triangular elements; it should be noted that these kinds of elements only represent a constant stress/ strain state while the quadrilateral elements represent a linearly varying stress/ strain across the diagonals (Reddy, 2006). Therefore a finer mesh and consequently higher computational cost is needed to converge to the exact solution for a FE model meshed with triangular elements in comparison with the one meshed with quadrilateral elements or a combination of the both elements.

In this study an algorithm was developed and used to generate the FE mesh by quadrilateral (CPE4) and triangular (CPE3) elements within aggregate particles and the matrix. The nodes on the particle boundary elements are shared with the matrix elements in order to ensure the deformation continuity. Although each matrix pixel is mapped to a CPE4 element; it is tried to apply a smart mesh generation algorithm to mesh the aggregate particles in all of the scales.

A MATLAB code was written to provide the input file (.inp) of each scale 2D image for ABAQUS. At the first step the aggregate particles are identified and labeled. Then, the FE mesh would be generated at each particle separately. The finer elements would be placed at the boundaries of the particle and the elements get coarser as it goes inside the element. The generation of particle mesh is taken place at different stages. At the first stage the CPE4 elements with the size of 1 pixel will be placed at the boundaries. Then, the size of the elements increases (2 pixels) and a combination of CPE3 and CPE4 elements will be placed inside the aggregate.

This process continues until the particle is meshed completely. The process of mesh generation of an aggregate particle is shown in Figure 34.

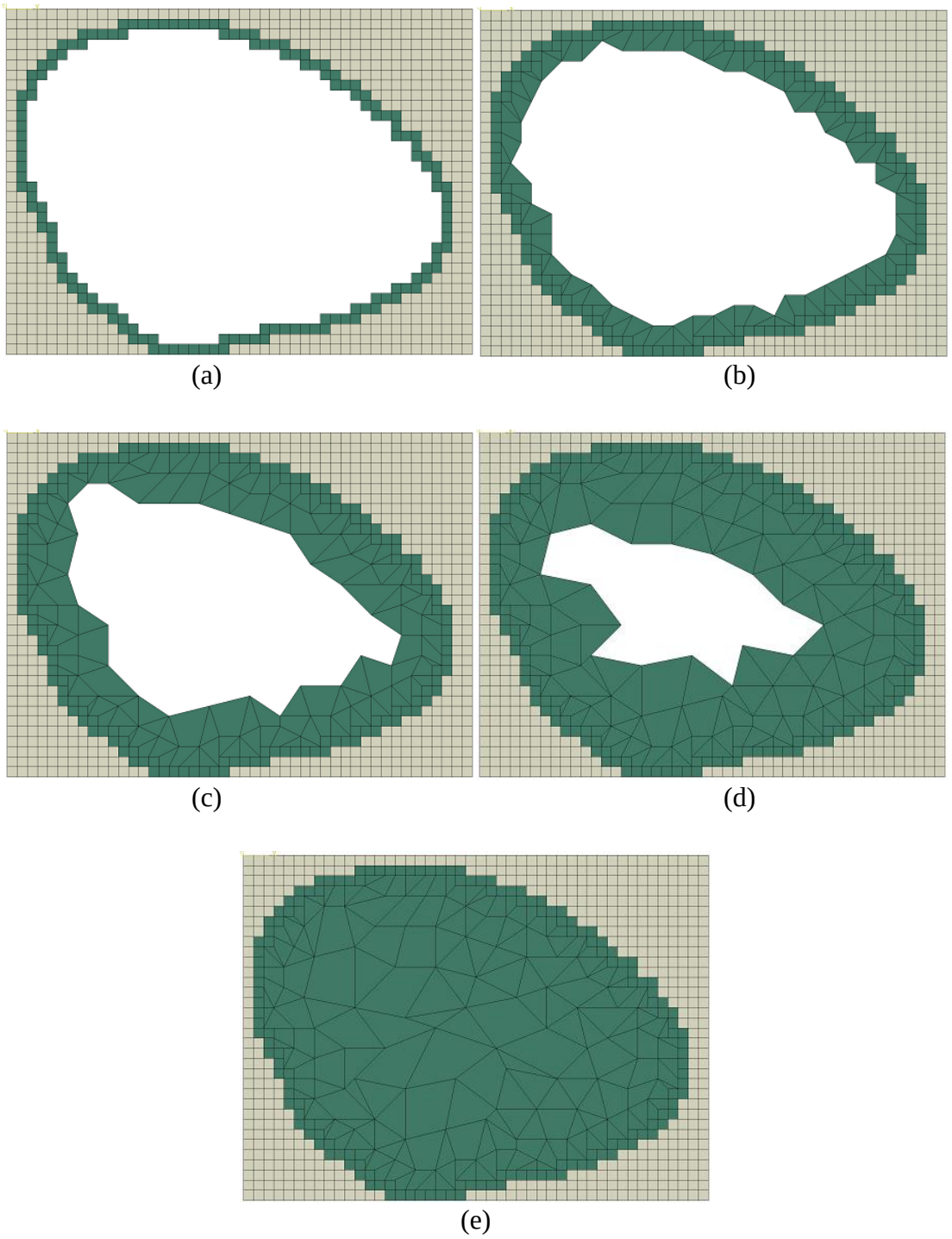

Figure 34: Different stages of FE mesh generation in an aggregate particle: (a) elements with size of 1 pixel (b) elements with size of 2 pixels (c) elements with size of 3 pixels (d) elements with size of 4 pixels (e) elements with size of 5 pixels

The abovementioned algorithm is used to generate the mesh at the mastic and mortar scales. However, at the asphalt mixture scale that the 2D scanned image of the mixture is used for the analysis; each image pixel is mapped to a CPE4 element. It is due to the existence of black pixels inside the white particles in binary images resulted from IPAS2 which makes the abovementioned algorithm inapplicable. The code written for generating the ABAQUS input files can be found in Appendix B.

Micro-Mechanical Modeling of Aggregate-Aggregate Contact

As mentioned earlier, one of the most important shortcomings of the micro-mechanical models presented by the researchers is the lack of an efficient contact law for the inter-particle behavior of two particles connected by a binder layer at lower scale levels. In order to simulate the binder behavior at the proximity zones, a simple contact law is defined based on the binder layer film thickness (Figure 35). In this approach the binder film elements are stiffened as stiff as an aggregate element when the binder film thickness tends to zero. In other words, the stiffening happens when the binder element compressive strain tends to unity. Figure 35 depicts the contact law used in the simulation. As shown, the stiffness of the binder element at the aggregate proximity zones is assumed as a function of particles distance which increases as the particles come into eventual contact.

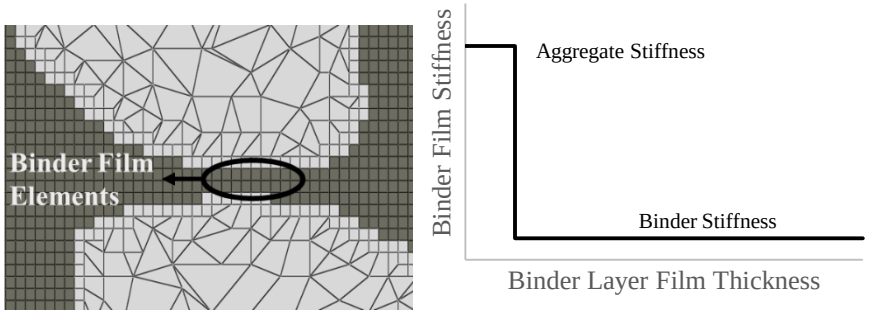

Figure 35: Depiction of the contact law applied to the binder film elements

The above mentioned contact law was defined in the ABAQUS user material subroutine and used in all simulations. This novel approach of using proximity to represent contact is not a perfect assumption as there could be still relative slip (movement) between aggregates. Figure 36 shows that implementation of the particle-to-particle contact law into FE model can significantly affect the response of a mastic with 40% filler volume fraction under 10 kPa uniaxial creep loading. Results shown demonstrate that after a certain loading time, the results from the simulation considering contacts between filler particles begin to deviate significantly from the results of the simulation with no contact consideration. This behavior is due to the evolution of the particle contact structure as a result of mastic deformation. In other words as binder in mastic deforms, filler particles get in contact (or proximity), which artificially stiffens the binder in proximity zones, and reduce strain mastic scale strain.

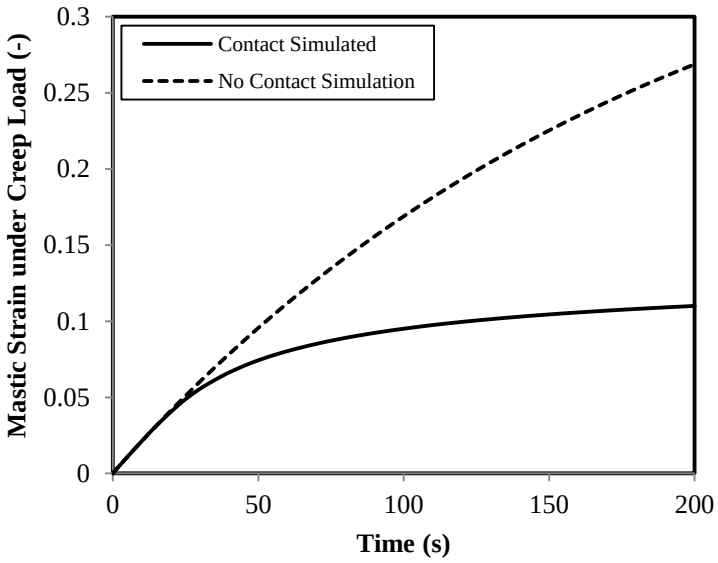

Figure 36: Creep deformation of a 40% filler volume fraction mastic

To address the effect of mastic scale particle contacts in the input properties of the mortar scale continuous phase, the nonlinear superposition, which allows the dependency of relaxation modulus to strain level, is used:

$$\boldsymbol{\sigma(t) = \int_0^t E(t-\tau, \epsilon(\tau)) \frac{d\epsilon(\tau)}{d\tau} d\tau.}$$ **Equation 14**

A separable Kernel was considered for the relaxation modulus, such as $E(t,\epsilon)=E(t).\Omega(\epsilon)$, in which the relaxation modulus is a product of a time-dependent part and a strain-dependent part. This method is called quasi-linear viscoelasticity (QLV), which is originally proposed by Fung (Fung, 1972). In order to determine the relaxation modulus components, two FE test simulations are performed on the desired scale: (a) determination of the scale complex modulus curve at a low strain amplitude level to make sure there is no effect of particle contact on the material response, and fitting a Prony series to the curve to quantify the time-dependent part of the mastic relaxation modulus, (b) creep loading test to determine the strain-dependent part of the relaxation modulus using Equation 14 while the time-dependent part is known from previous simulation.

The same FE test procedure is performed on the mortar scale to capture the particle contact effects on response of this scale. The obtained mortar scale relaxation modulus was used to provide the homogenized input parameters for the asphalt mixture scale.

Numerical Simulation and Model Validation

Two asphalt mixtures with significantly different gradations, categorized as fine and coarse were used in this study, as shown in Figure 37. An elastomer modified binder was used in both of the mixtures and the volumetric properties of the mixtures were kept constant for both of the gradations. Asphalt content was 5.1% by weight (12.0% by volume), and air void content was 6.5% by volume. Consequently almost 83% of the asphalt mixtures by volume would be constituted of aggregate. Figure 37 also shows the scanned images of the two mixtures used in this study, while Table 2 shows the volume fraction of the components at each scale.

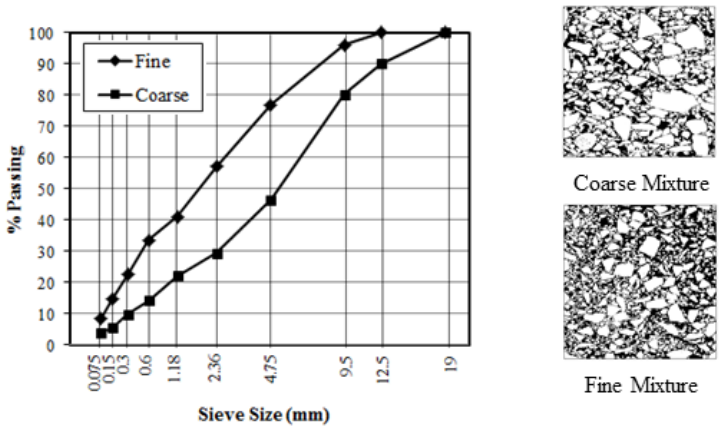

Figure 37: Aggregate Gradation and 2D scanned images of the Mixtures

Table 2: Volume fraction of components at each scale

Scale / Mixture	Asphalt Mixture Scale			Mortar Scale		Mastic Scale	
	Aggregates	Mortar	Air Void	Fine Aggregates	Mastic	Fillers	Binder
Coarse	0.645	0.290	0.065	0.49	0.51	0.20	0.80
Fine	0.484	0.451	0.065	0.59	0.41	0.40	0.60

In order to determine the prediction power of the multi-scale model, the total multi-scale response of the model from the binder through the macro scale was used to predict and simulate the mechanical response of the fine and coarse asphalt mixture samples, 100 mm in diameter and 150 mm high, placed under 345 kPa step stress and recovery periods. Each cycle consisted of 0.1 s of loading and 0.9 s recovery period. Results were compared to experimentally derived mixture testing results using a uniaxial testing machine at 46°C. The developed multi-scale approach is conducted at each scale and the results are presented in the following subsections.

Binder Experimentation and Mastic and Mortar Homogenization

The frequency sweep test was conducted to characterize the linear viscoelastic properties of the elastomer modified binder. The shifted complex modulus and fitted master curve at the reference

temperature 46℃ are shown in Figure 38. Table 3 summarizes the model parameters of the binder obtained from frequency sweep test results.

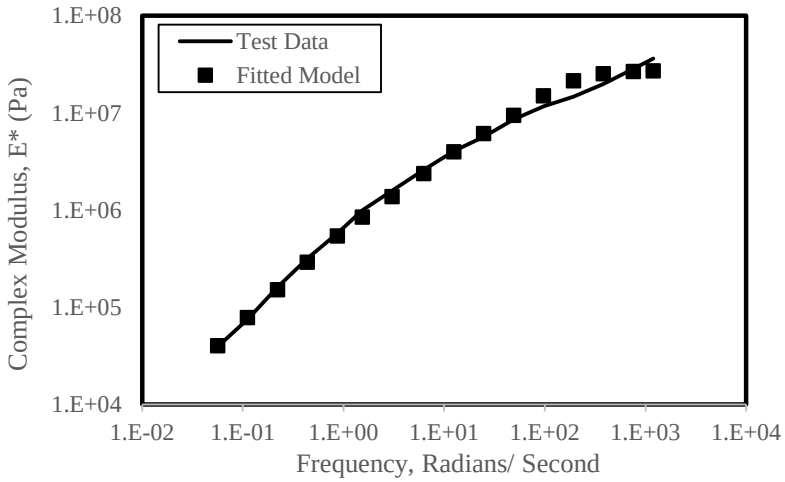

Figure 38: Shifted complex modulus and fitted master curve for elastomer modified binder

Table 3: Linear viscoelastic model parameters

Prony Series Parameters	
E_∞= 600.0 Pa	
E_1= 6963.4 Pa	τ_1= 1s
E_2= 505505.7 Pa	τ_2= 0.1 s
E_3= 3273660.7 Pa	τ_3= 0.01 s
E_4= 23478594.0 Pa	τ_4= 0.001 s

To validate and confirm the accuracy of the FE model's mechanical response prediction, the experimentally derived complex modulus master curve of the elastomer modified asphalt mastics with volume fractions of 0.2 and 0.4 were compared to those obtained using the FE Modeling. A constant Poisson's ratio of 0.49 was assumed for the binder material while linear elastic properties were used to model the aggregate phase, setting the Young's modulus and Poisson's ratio to 25 GPa and 0.25, respectively (Dessouky, et al., 2006). In the FE simulation,

uniaxial sinusoidal strain controlled loads with different loading frequencies, ranging from 0.01 to 100 Hz, were applied to the asphalt mastic samples and their complex modulus was calculated using the simulation results. The complex modulus diagrams of the mastics as well as the mastic models are shown in Figure 39.

The results indicate that there is a good agreement between experimental data and FE modeling results. The analysis shows that the mastic complex modulus does not increase proportionally to the increment of the filler content. It shows that adding 20% filler to the asphalt binder rather increases the complex modulus, however; adding another 20% filler to the asphalt mastic significantly increases the complex modulus. It should be noted that at lower filler volume fractions the distance between the filler particles is larger than the particle size; in such conditions the filler is effectively “diluted” in the viscoelastic binder matrix. Particle interactions are considered to be negligible in diluted blends. By increasing the volume fraction, particle interaction networks gradually form in the mastic. As the particle networks expands at higher volume fractions, the load transfer efficiency of the network increases, thus transferring a larger portion of the mastic load, effectively decreasing strain level in the binder matrix and consequently significantly increasing the mastic complex modulus.

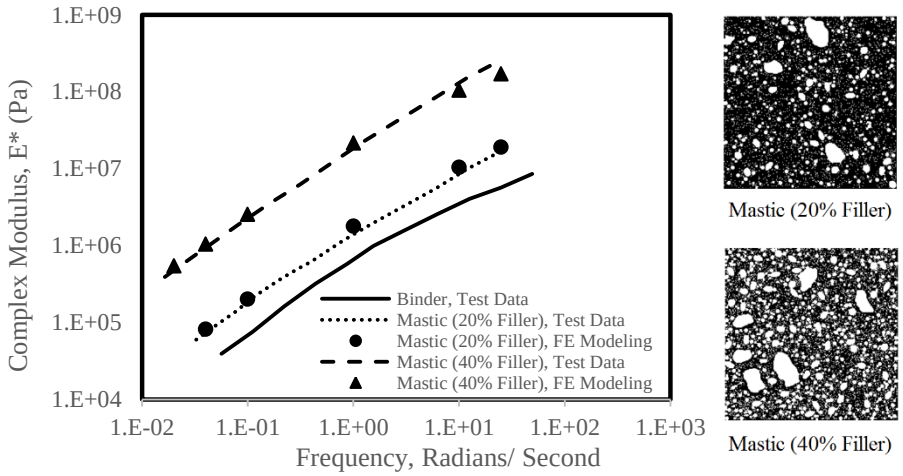

Figure 39: Complex modulus diagrams of elastomer modified binder and its mastics at 46°C

A Prony series model fitted to the complex modulus curve was used to provide the homogenized input parameters for the mortar scale. The Poisson's ratio of the mastic phase was calculated through the model response. It was found by taking the negative transverse strain and dividing it by the axial strain. Similar to the mastic scale, a Prony series fitted to the mortar simulated complex modulus curve of the mixtures was used to provide the homogenized input parameters of the continuous phase of the asphalt mixture scale which is the last scale in the multi-scale approach.

Table 4 summarizes the homogenized Prony series parameters as well as the Poisson's ratio of the mastic and mortar scale of both of the fine and coarse graded mixtures.

Table 4: Homogenized model parameters of lower scales of fine and coarse graded mixtures

Component	***Elastomer Modified Binder***	***Mastic of Coarse Mixture***	***Mastic of Fine Mixture***	***Mortar of Coarse Mixture***	***Mortar of Fine Mixture***
E_∞ *(MPa)*	0.0006	0.0017	0.0037	0.0077	0.0097
E_1 *(MPa)*	0.007	0.009	0.025	1.011	1.514
τ_1 *(s)*	1	1	1	1	1
E_2 *(MPa)*	0.51	1.43	23.93	29.14	167.84

τ_2 *(s)*	0.1	0.1	0.1	0.1	0.1
E_3 *(MPa)*	3.3	9.8	125.6	130.2	1080.2
τ_3 *(s)*	0.01	0.01	0.01	0.01	0.01
E_4 *(MPa)*	23.5	76.2	408.0	539.2	1572.4
τ_4 *(s)*	0.001	0.001	0.001	0.001	0.001
Poisson's Ratio	0.49	0.47	0.43	0.40	0.34

Mixture Scale Modeling

Aggregate volume fraction in asphalt mixture scale for coarse and fine graded mixtures was determined to be respectively 0.645 and 0.484 (Table 2). The RVE determination for the macro scale was carried out similar to that of the mastic and mortar scale, resulting in the selection of an optimum RVE of 60 mm × 60 mm for this scale.

Figure 40 and Figure 41 show the multi-scale simulation results of asphalt mixture permanent strain under the creep and recovery loading compared with test data for the fine and coarse graded mixtures. The comparisons indicate that the developed multi-scale model without consideration of particle contacts is only capable of predicting mixture mechanical properties with an acceptable accuracy at initial cycles of loading. The figures demonstrate that after the initial loading cycles, results begin to deviate from experimental measurements. This is believed to be due to evolving of the aggregate structure as a result of mixture consolidation and the increasing mechanical engagement of aggregate particles, thus increasing the importance of fully accounting for aggregate to aggregate contact mechanism. Figure 40 and Figure 41 also show that implementation of a contact law into the FE framework significantly improves the power prediction of the multi-scale model. As shown, the multi-scale model developed in this study predicts the deformation of asphalt mixture with an acceptable accuracy at primary and secondary zones of rutting. The analysis of the results showed that the FE model predicted

permanent strain after 70 cycles of loading is 30% and 16% higher than the experimentally obtained one for fine and coarse graded mixtures, respectively. The results indicate that the over-prediction is greater in the simulation of the fine graded mixture with higher number of particle contacts at lower scales, compared to that of coarse mixture, which had a lower particle volume fraction at mastic and mortar scale.

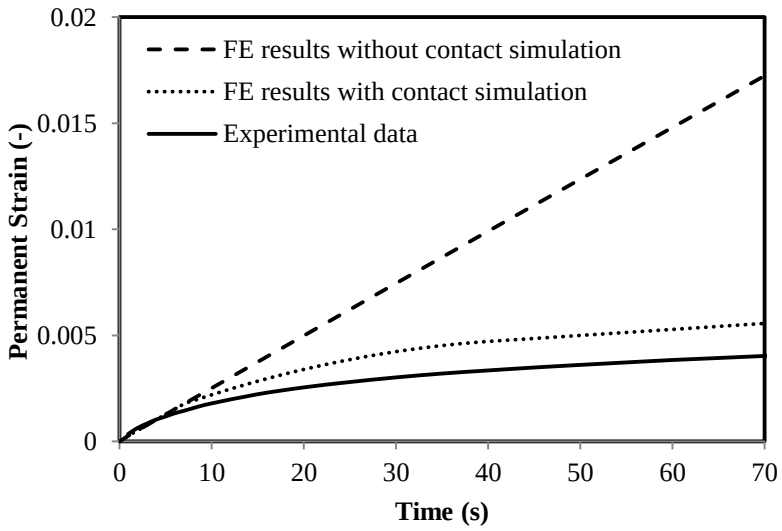

Figure 40: Fine mixture permanent strain under continued cyclic loading

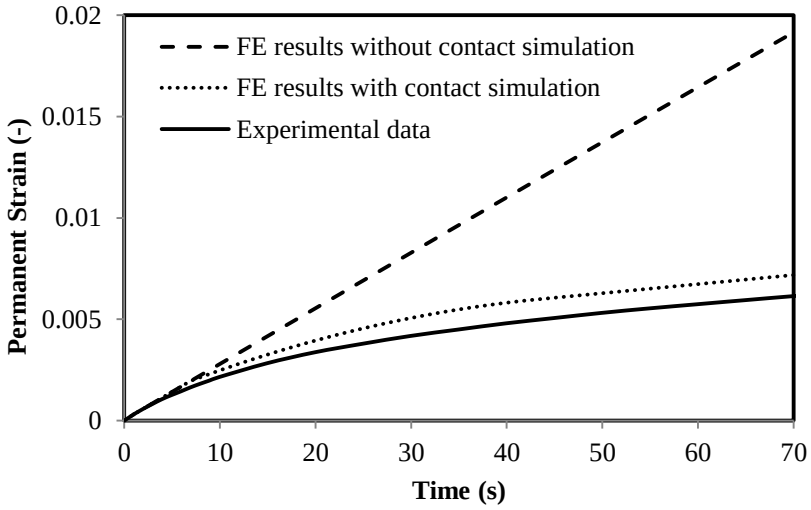

Figure 41: Coarse mixture permanent strain under continued cyclic loading

Asphalt mixture designers need to make decisions on selecting binder, filler or even aggregate gradations. This virtual simulation tool can cut down on experimental testing and on time required to make decisions. The developed model will be used in the following chapters to predict the fatigue cracking of asphalt mixtures.

CHAPTER 4: COUPLING OF VISCOELASTIC CONTINUUM DAMAGE MECHANICS AND FINITE ELEMENT MODELING

Viscoelastic Continuum Damage Analysis

Lee et al. used the Schapery's extended viscoelastic correspondence principle (Schapery, 1984) to develop a fatigue life model for asphalt concrete samples under uniaxial cyclic loading. This work was based on work potential theory and continuum damage mechanics (Lee, et al., 2000). Later Kim et al. (Kim, et al., 2006) presented an asphalt concrete fatigue life prediction model based on the work by Lee et al. (2000) but employed nonlinear dynamic modulus and the phase angle as the indicator of damage evolution instead of pseudo stiffness. Johnson (2010) applied the VECD framework developed by Kim et al. (2006) to asphalt binders tested in Dynamic Shear Rehometer (DSR). The binder test procedure proposed by Johnson, called LAS test, was recently modified by other researchers and is used in the present study to estimate the fatigue characteristics of asphalt binder (Hintz, et al., 2013; AASHTO, 2014).

The damage accumulation (D) in the asphalt binder sample under cyclic sinusoidal loading can be calculated using the following summation (AASHTO, 2014):

$$\boldsymbol{D(t_i) \cong \sum_{i=1}^{N} \left[\pi \gamma_i^2 (C_{i-1} - C_i)\right]^{\frac{\alpha}{1+\alpha}} (t_i - t_{i-1})^{\frac{1}{1+\alpha}}} \qquad \textbf{Equation 15}$$

where:

$C(t) \cong \frac{|G^*|(t)}{|G^*|_{initial}}$ which is complex shear modulus at time, t divided by its initial undamaged value. γ_i is the applied shear strain amplitude at each loading cycle and α is the exponent determining energy release rate. Researchers (Johnson, 2010; Hintz, et al., 2013; AASHTO,

2014) have shown that damaged and undamaged properties of binder can be related with a simple mathematical model as

$$\boldsymbol{C(t) = C_0 - C_1 D(t)^{C_2}} \quad \textbf{Equation 16}$$

where C_0, C_1, and C_2 are the model coefficients. The constant, α, and the model coefficients, C_0, C_1, and C_2, can be obtained from a single LAS test (Hintz, et al., 2013; AASHTO, 2014).

By assuming a constant loading frequency (f) and constant strain amplitude (γ_0) during the loading time, one can obtain the number of cycles, N_f, which yields to failure in the material as

$$\boldsymbol{N_f = \frac{f D_f^{1+(1-C_2)\alpha}}{1+(1-C_2)\alpha} \frac{1}{(\pi \gamma_0^2 C_1 C_2)^{\alpha}}} \quad \textbf{Equation 17}$$

The value of D_f is defined as the D(t) which corresponds to the reduction in initial |G*| at the peak shear stress. The above equation can be rewritten by grouping terms as follows

$$\boldsymbol{N_f = A\gamma^{-B}} \quad \textbf{Equation 18}$$

where

$$\boldsymbol{A = \frac{f D_f^{1+(1-C_2)\alpha}}{1+(1-C_2)\alpha} \frac{1}{(\pi C_1 C_2)^{\alpha}}} \quad \textbf{Equation 19}$$

$$\boldsymbol{B = 2\alpha} \quad \textbf{Equation 20}$$

In the following section the numerical implementation of VECD mechanics as well as viscoelastic behavior of asphalt binder into FE framework is discussed.

Finite Element Implementation

The one-dimensional linear constitutive behavior of the asphalt binder coupled with VECD, can be expressed by Boltzmann superposition integral as shown in Equation 21.

$$\sigma(t) = \int_0^t E(t-\tau, D)\frac{d\epsilon(\tau)}{d\tau}d\tau$$ **Equation 21**

The relaxation modulus is described using a Prony series form as shown in Equation 22. The initial parameters of the Prony series were determined by fitting a curve to the binder complex modulus master curve resulted from frequency sweep test.

$$E(t, D) = E_\infty(D) + \sum_{m=1}^{M} E_m(D).e^{\frac{-t}{\tau_m(D)}}$$ **Equation 22**

The formulation of three dimensional behavior of the asphalt binder is explained through Equation 7 to Equation 13.

Figure 42 shows the typical complex modulus and phase angle versus damage intensity curves obtained from LAS test. As the damage accumulates in the binder sample the complex modulus decreases significantly; however, the binder phase angle slightly increases by accumulation of damage. In order to simplify the calculation of Prony series parameters, it is assumed in this study that the variation of phase angle is negligible as the damage accumulates in the binder phase under loading with a constant frequency. This assumption means that the relaxation time components of Prony series are constant, however; the relaxation modulus components reduce with a same ratio as the reduction ratio of the dynamic modulus value. Knowing the incremental volumetric and deviatoric stresses, the incremental normal and shear stresses can be calculated using Equation 7.

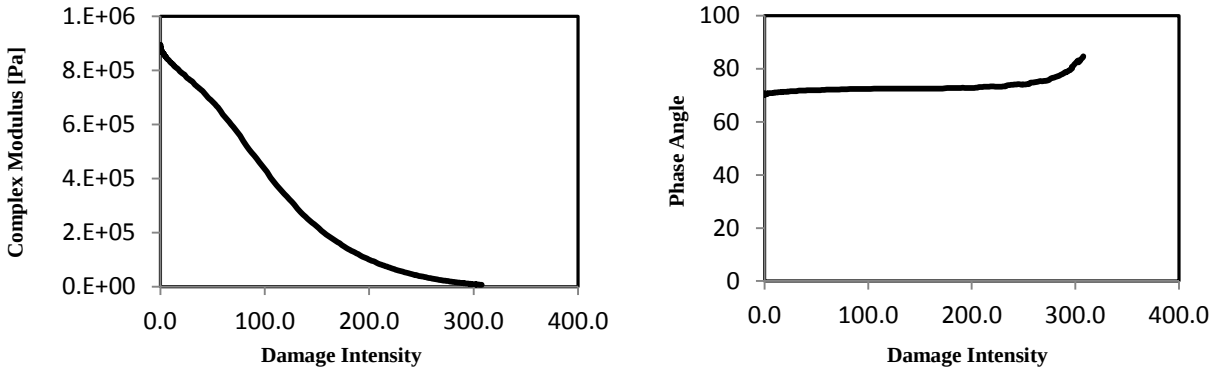

(a) (b)

Figure 42: Typical LAS test results. (a) Complex modulus vs. damage intensity (b) Phase angle vs. damage intensity

The procedure described above was implemented in the FE analysis software ABAQUS through a user-defined subroutine, UMAT, to obtain the incremental response of asphalt binder under cyclic loading (Appendix C).

Validation of the Finite Element Model

A PG 64-22 binder was used in this study to validate the FE approach. The frequency sweep test and LAS test was conducted on the short term (RTFO) aged binder sample to characterize the linear viscoelastic and fatigue properties of the binder, respectively. The shifted complex modulus and fitted master curve at the reference temperature 20℃ are shown in Figure 43. Table 5 summarizes the average model parameters of the binder resulted from the experiments.

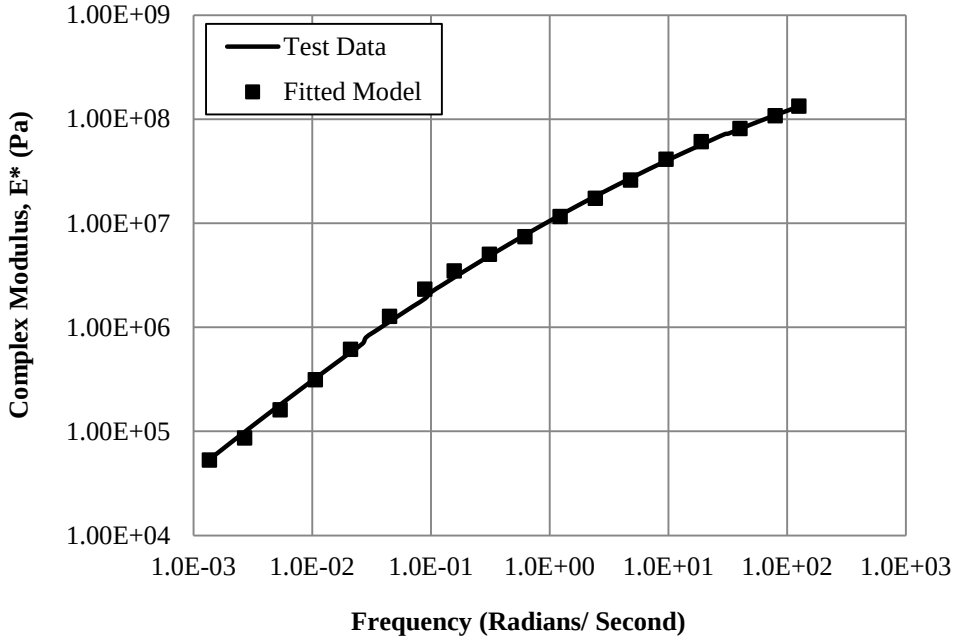

Figure 43: Shifted complex modulus and fitted master curve for PG 64-22 binder

Table 5: Model parameters

Prony Series Parameters			
E_∞= 56 kPa			
E_1= 2640 kPa	τ_1= 1s		
E_2= 10351 kPa	τ_2= 0.1 s		
E_3= 47751 kPa	τ_3= 0.01 s		
E_4= 140953 kPa	τ_4= 0.001 s		
VECD Model Parameters			
C_0	C_1	C_2	α
1.000	0.090	0.429	1.421

The binder model parameters were inputted into ABAQUS to simulate the binder damage response under strain controlled cyclic sinusoidal loading. The boundary condition used to simulate the behavior of asphalt binder is shown in Figure 44. A uniaxial sinusoidal loading with a constant frequency of 10 Hz and increasing strain amplitude was applied to the binder sample as shown in Figure 44. A 4-node bi-linear plane strain quadrilateral and full integration element

(i.e., CPE4) was used in the simulation. In this study a constant Poisson's ratio of 0.499 was assumed for the asphalt binder (Yin, et al., 2008).

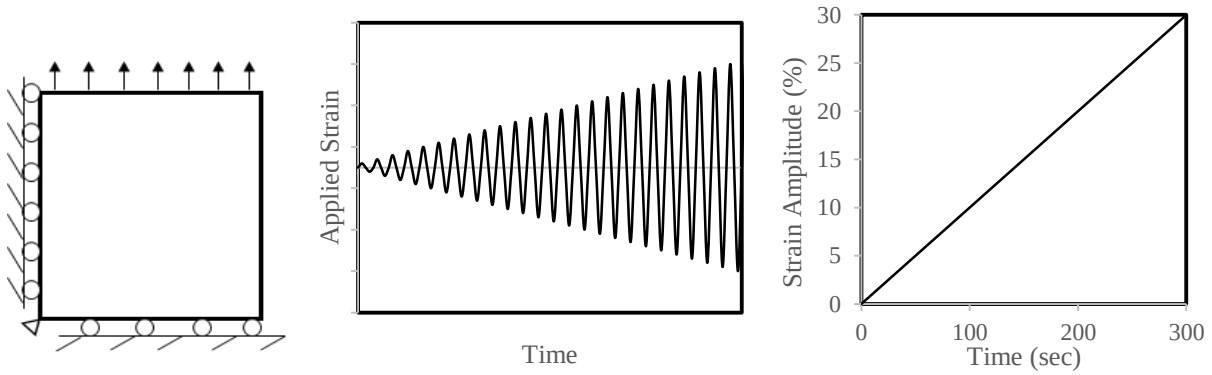

(a) (b) (c)

Figure 44: (a) Asphalt binder model showing boundary conditions (b) Depiction of strain applied to the binder sample (c) Strain amplitude vs. time

Figure 45 shows the comparisons between the FE simulation results and the test data for the PG 64-22 binder at the temperature of 20℃. In order to make the LAS test data comparable with the FE simulation results, the experimental data which are the binder shear stress and strain were converted into axial stress and strain with assumption of isotropy for the binder material. As shown, the FE simulation results without consideration of damage mechanics are in good agreement with the experimental data for the lower strains where the amount of damage of the binder is negligible. However, as the binder amount of damage increases the FE simulation results deviate from the measured results. The results in Figure 45 show that the FE modeling coupled with VECD mechanics can predict the damage response of binder with an acceptable accuracy. The binder maximum stress obtained from the experiment and the FE simulation is taken place at strain level of 10.1 and 9.9%, respectively. These results show that the failure strain estimated from the FE simulation is almost 2% higher than the experimentally obtained

result. The results also indicate that the binder maximum stress obtained from the FE simulation is 8.5% higher than the experimentally obtained maximum stress.

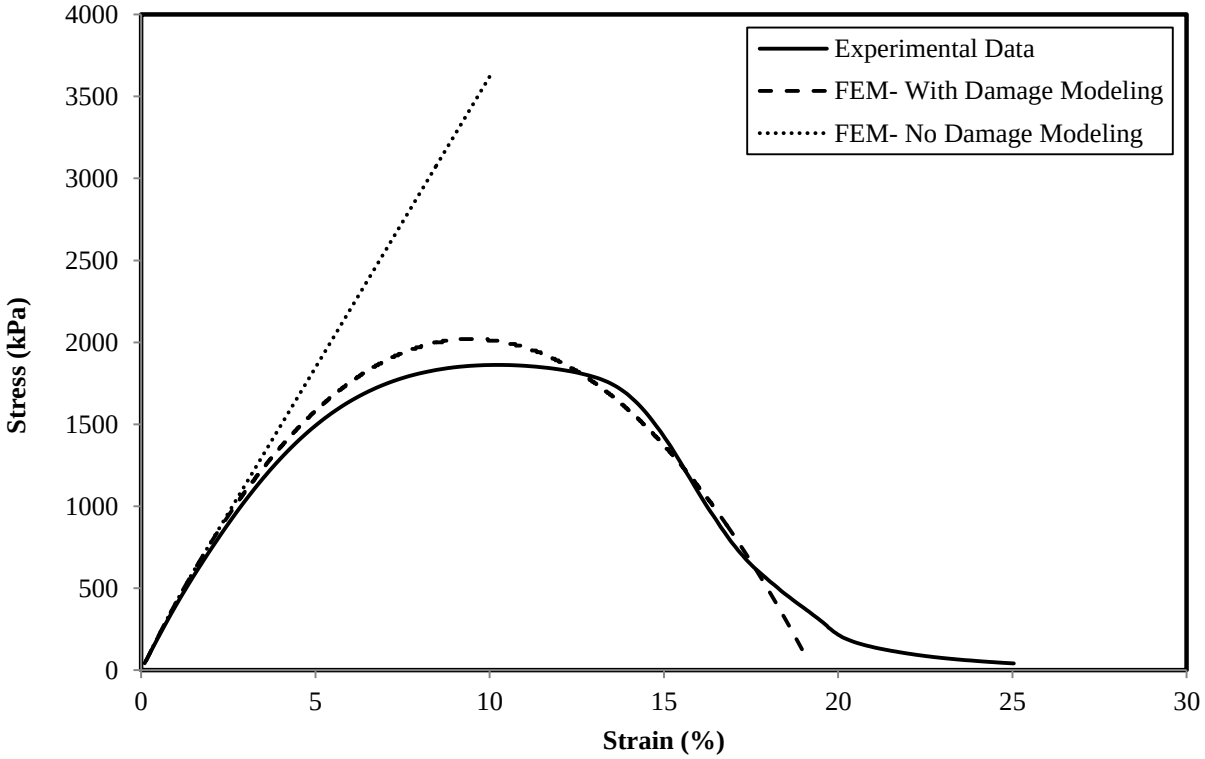

Figure 45: Comparison between FE simulation and experimental data

Since the results with damage modeling are promising the procedure can be used for mastics with various filler concentration. To study the prediction power of the developed FE model in the mastic scale, the LAS tests were performed on asphalt mastic samples with FVFs of 0.2 and 0.4 and the results were compared with the FE simulations. Figure 46 shows the shear stress versus shear strain plots of the asphalt binder and the mastics measured using the LAS test. The analysis shows that the applied stress to the mastic needed to cause a specific strain does not increase proportionally to the increment of the filler content. It shows that adding 20% filler to the asphalt binder rather increases the applied stress, however; adding another 20% filler to the

asphalt mastic significantly increases the needed applied stress. It should be noted that at lower filler volume fractions the distance between the filler particles is larger than the particle size; in such conditions the filler is effectively "diluted" in the viscoelastic binder matrix. Particle interactions are considered to be negligible in diluted blends. By increasing the volume fraction, particle interaction networks gradually form in the mastic. As the particle networks expands at higher volume fractions, the load transfer efficiency of the network increases, thus transferring a larger portion of the mastic load, effectively increasing the applied stress needed to cause a specific strain in the material. The results also indicate that the failure strain decreases as the filler concentration increases. Failure strains for the asphalt binder, mastic with 20% FVF, and mastic with 40% FVF, are 10.1, 7.2, and 5.5%, respectively. Table 6 summarizes the VECD parameters of the asphalt binder and the mastics estimated from LAS test.

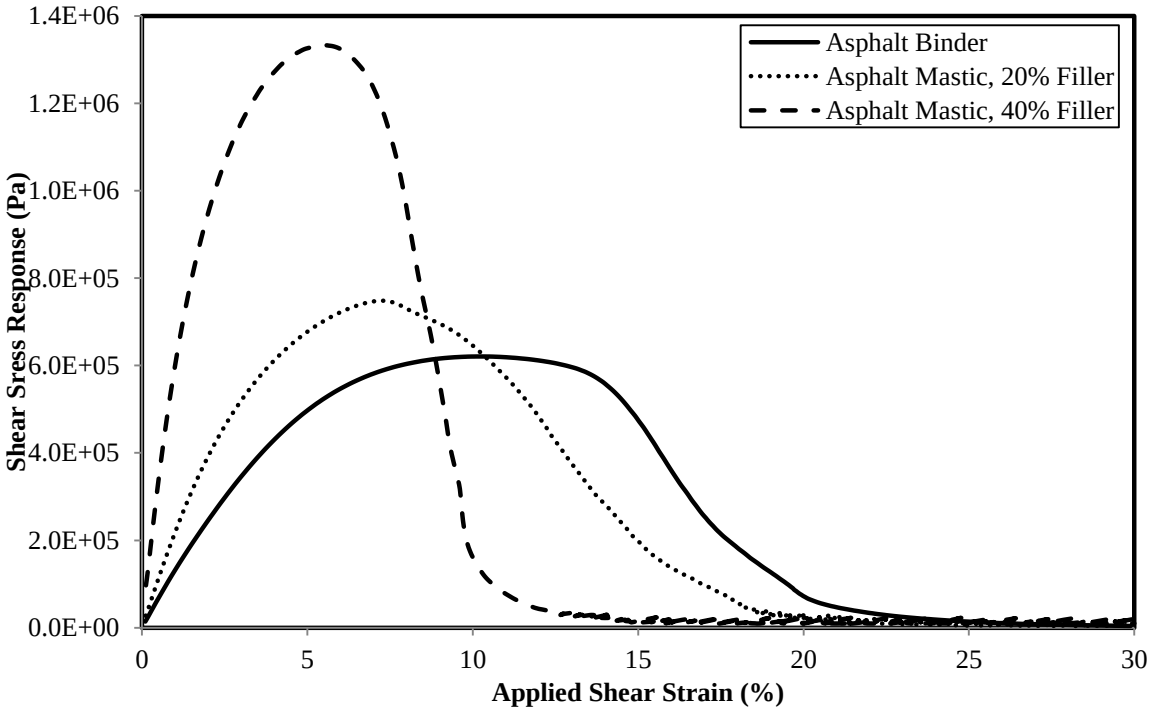

Figure 46: LAS test results for the PG 64-22 asphalt binder and its mastics with filler volume fractions of 0.2 and 0.4 at 20℃

Table 6: Summary of VECD parameters

	PG 64-22 Binder	***Mastic, 20% Filler***	***Mastic, 40% Filler***
α	1.421	1.466	1.521
C_0	1.000	1.000	1.000
C_1	0.090	0.144	0.240
C_2	0.429	0.368	0.315

In order to conduct the FE simulations, the 2D images of the asphalt mastics were generated based on the gradation, shape of the mineral fillers, and the filler volume fraction using a MATLAB code which is described elsewhere (Arshadi and Bahia, 2015). Filler gradation curve was measured by Laser Diffraction methodology and electron microscope images were used to obtain the filler particle shapes. The FE mesh was generated within the filler particles and asphalt binder, along the subdomain boundaries, using a combination of quadrilateral and triangular elements as shown in Figure 47. The asphalt mastic models were placed under repeated sinusoidal loading with loading frequency of 1 Hz and strain amplitude of 5%. The loading frequency and strain amplitude were selected relatively high to cause the damage failure in lower loading cycles due to the computer power limitation. The similar boundary conditions shown in Figure 44 were used to simulate the behavior of the asphalt mastics. Linear elastic properties were used to model the aggregate phase, setting the Young's modulus and Poisson's ratio to 25 GPa and 0.25, respectively.

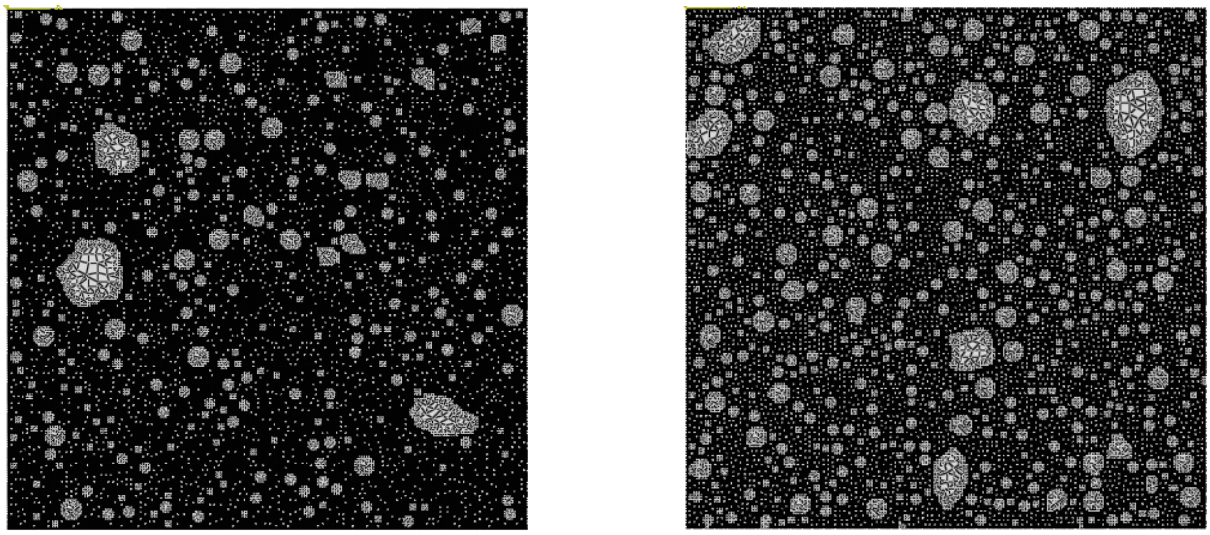

(a) (b)

Figure 47: The FE meshes of the asphalt mastic images with filler volume fraction of (a) 0.2 (b) 0.4

Figure 48 shows a comparison between the experiment and FE simulation. The number of cycles to failure was experimentally obtained at strain amplitude of 5% and loading frequency of 1 Hz, using Equation 18 for the asphalt binder and the mastics. The number of cycles to failure of the materials was determined through the FE simulation. As shown, there is a good agreement between experimentally obtained and FE simulated results. The analysis shows that the FE simulation error is less than 8, 10, and 19% for asphalt binder, mastic with 20% FVF, and mastic with 40% FVF, respectively. The results indicate that one can predict the fatigue life of the asphalt mastics through the developed finite element model knowing the binder and filler properties with a high accuracy.

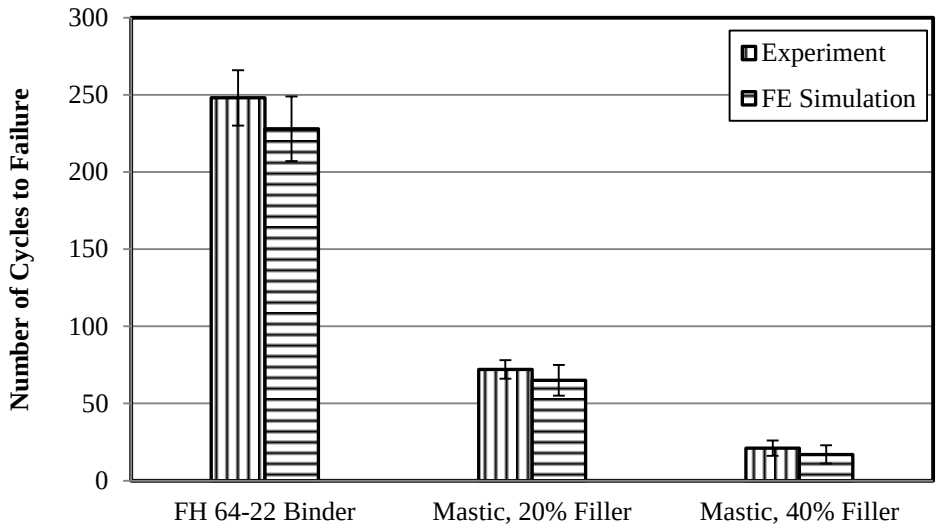

Figure 48: Number of cycles to failure at 5% strain amplitude

The prediction of fatigue life of asphalt mixture is a challenging task due to complicated behavior of the material under various loading and environmental conditions. The work presented in this chapter shows significant promise in that the damage behavior of binder can be modeled and used in the FE to predict the behavior of the next scale (mastic). It requires images of fillers and the binder damage testing results to construct virtual mastics and load them to estimate damage parameter. This approach gives significant flexibility in estimating effect of fillers and concentration of fillers. In the following chapter the developed FE procedure will be conducted on the asphalt mixture scale to numerically predict the fatigue life of the asphalt mixture using the properties of binder and aggregates.

CHAPTER 5: FE SIMULATION OF FATIGUE DAMAGE IN ASPHALT MIXTURES AND VALIDATION

Objectives

The purpose of this study is to evaluate the fatigue resistance of asphalt mixtures through finite element simulation. The fatigue damage properties of asphalt binder is characterized and imported into FE software and the fatigue damage resistance of asphalt mixture is evaluated through a scale by scale analysis explained in the previous chapters. IDT fatigue test is conducted on the asphalt mixture samples with 4±1% air voids and the results are compared with the FE simulation results.

Materials and Test Procedures

To study the accuracy of the developed multi-scale model in evaluating the fatigue resistance of asphalt mixtures, mixes were produced using two different aggregate gradations (i.e. a fine and a coarse gradation) and four different binder levels. Asphalt content was 5.1% by weight (12.0% by volume), and air void content was 4% by volume. Consequently almost 84% of the asphalt mixtures by volume would be constituted of aggregate. The gradations (Figure 49) have been designed for the purposes of this dissertation from aggregate sources commonly used for HMA production in Wisconsin. Table 7 shows the percentage of volume of the components at each scale.

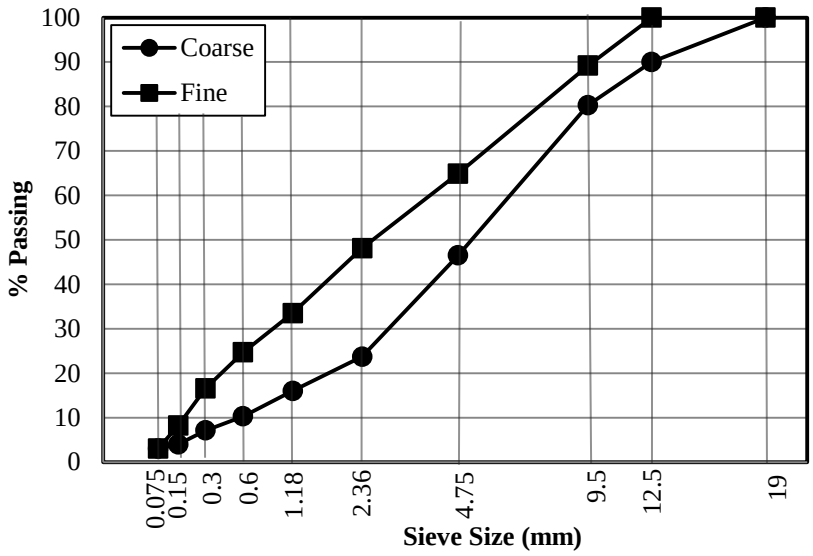

Figure 49: Aggregate Gradation

Table 7: Percentage of volume of components at each scale

Scale / Mixture	Asphalt Mixture Scale			Mortar Scale		Mastic Scale	
	Aggregates	Mortar	Air Voids	Fine Aggregates	Mastic	Fillers	Binder
Fine	55.8	40.2	4	57.9	42.1	20	80
Coarse	70.5	25.5	4	36.9	63.1	20	80

To cover a wide range of binder fatigue characteristics, four different binders were used in this dissertation: A neat binder (N) and three modified binders (i.e. a styrene butadiene styrene based elastomer modifier (E), a polyethylene based plastomer (P), and ground tire rubber (G)). The level of modification was selected to obtain high true grade of 78±0.5°C for all modified binders. The binders' designations, required percentage of each modifier, true grade, and performance grades (PG), are shown in Table 8.

Table 8: Asphalt binders used in the study

Designation	*% Modifier*	*True Grade*	*PG*
N	NA	NA	64-22
E	3.2	77.88	76-22
P	4.7	78.08	76-22
G	7.1	77.87	76-22

The reference mixing and compaction temperatures were selected as 150°C and 135°C, respectively based on the viscosity-temperature profile as explained in Superpave mix design procedure for the neat binder and was kept consistent for all mixes.

Binder Testing

Linear Amplitude Sweep test as explained in the previous chapter was conducted on all binders at 20°C. Two replicates were conducted for all the binders. Figure 50 shows the number of cycles to failure for frequency of 10 Hz at different strain levels for the binders. As shown, all types of binder modification improve the fatigue resistance of asphalt binder especially at strain levels lower than 7%. Plastomer modified binder improves the fatigue resistance slightly better than the elastomer modified one at strain levels lower than 1.5%, however; at higher strains the latter works better than the former.

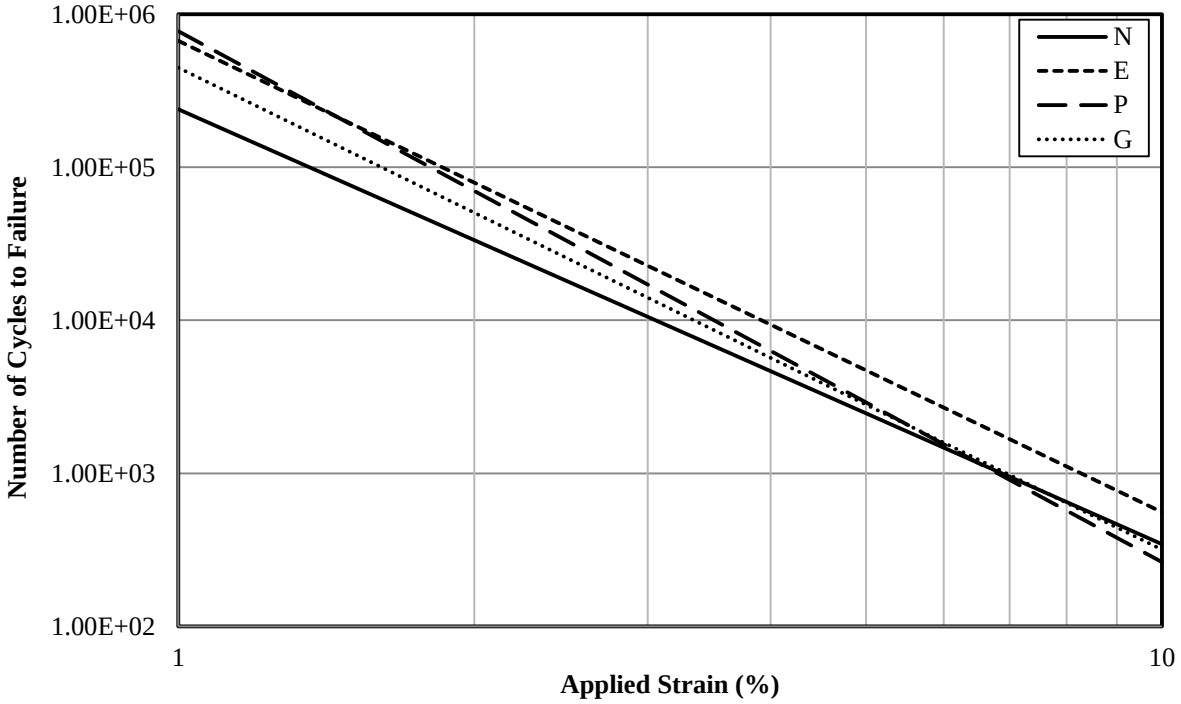

Figure 50: Number of cycles to failure versus applied strain

The viscoelastic continuum damage analysis was performed on the experimental data to obtain the fatigue damage parameters of the asphalt binders as shown in Table 9. The fatigue law parameters A and B are calculated at frequency of 10 Hz.

Table 9: Asphalt binders' fatigue parameters

	N	*E*	*P*	*G*
α	1.421	1.540	1.735	1.575
C_0	1	1	1	1
C_1	0.090	0.109	0.118	0.093
C_2	0.429	0.378	0.374	0.413
A	2.39E+05	6.72E+05	7.77E+05	4.47E+05
B	-2.84	-3.08	-3.47	-3.15

In addition to LAS test, frequency sweep test was conducted on the asphalt binders used in this study to characterize their linear viscoelastic properties. Figure 51 shows the shifted complex

modulus of all the binders at the reference temperature 20℃. As shown, although the stiffness of elastomer and rubber modified binders slightly differ from neat binder stiffness; the plastomer modification increases the binder stiffness significantly. Table 10 summarizes the average model parameters of the binders resulted from the experiments.

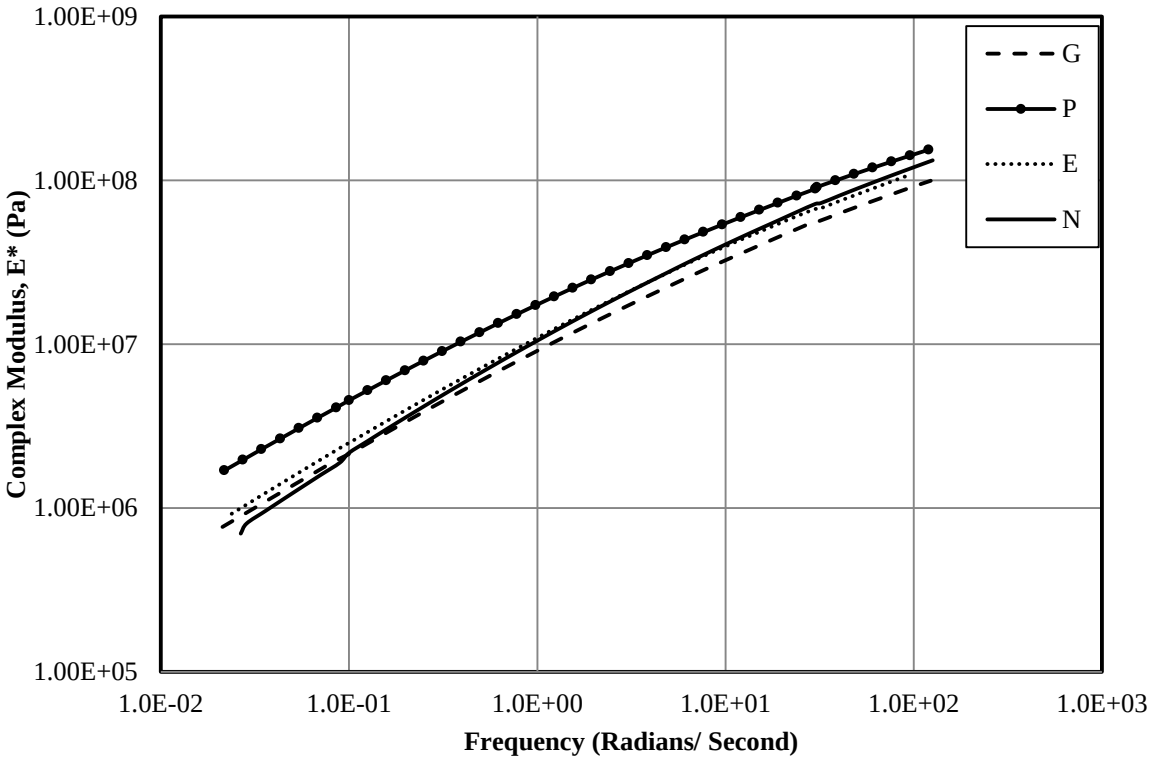

Figure 51: Shifted complex modulus at the reference temperature 20℃ for the binders used in the study

Table 10: Asphalt binders' model parameters

Component	*Neat Binder*	*Elastomer Modified Binder*	*Plastomer Modified Binder*	*Ground Rubber Modified Binder*
$E_\infty (Pa)$	1.62E+04	3.83E+04	5.51E+04	3.45E+04
$E_1 (Pa)$	2.64E+06	3.60E+06	6.72E+06	3.12E+06
$\tau_1 (s)$	1	1	1	1
$E_2 (Pa)$	1.04E+07	7.74E+06	1.21E+07	8.47E+06
$\tau_2 (s)$	0.1	0.1	0.1	0.1
$E_3 (Pa)$	4.78E+07	5.61E+07	7.27E+07	4.16E+07
$\tau_3 (s)$	0.01	0.01	0.01	0.01
$E_4 (Pa)$	1.41E+08	9.08E+07	8.0E+07	9.08E+07
$\tau_4 (s)$	0.001	0.001	0.001	0.001

Mixture Testing

As explained earlier, two gradations were used in this study to produce the asphalt mixtures. The mixtures were aged in the oven for 4 h before compaction. A Superpave gyratory compactor was used in this study to compact all the asphalt mixtures with target air void of 4% (Figure 52).

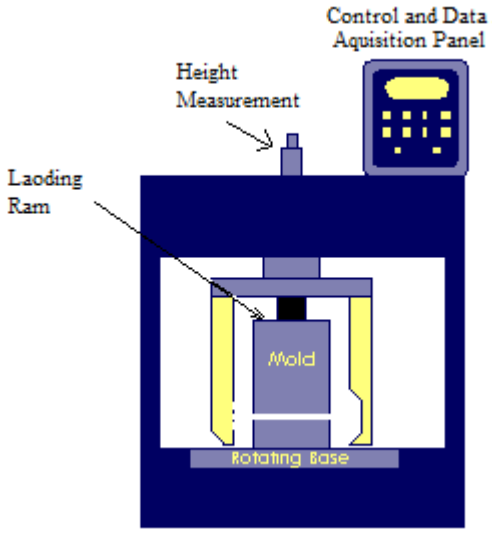

Figure 52: Schematic of Supeparve gyratory compactor

IDT Test

All the asphalt mixtures were cut into two disk-shaped specimens with the thickness and diameter of 50±5 mm and 150 mm, respectively (Figure 53). The IDT tests were conducted on the asphalt mixture specimens following AASHTO 322-07. To measure the horizontal deformation of the samples, two extensometers were attached on the front and back of the specimens with the gauge length of 25.4 mm (Figure 18).

Figure 53: IDT specimens

The IDT fatigue tests were conducted under stress-controlled mode of loading at 20°C. A constant amplitude (730 lbs.) sinusoidal cyclic load with no rest period was applied at frequency of 10 Hz until failure occurs in the specimen. The chosen frequency is approximately equivalent to a vehicle speed of 50 mph (Huang, 2004). The horizontal deformation of the sample was monitored and used to determine the failure of the mixtures. It is assumed that the failure occurs in the mixture when the constant rate of increase of the horizontal deformations is replaced by a higher rate as shown in Figure 54. After that point the existing micro-cracks in the specimen

combine into macro-cracks and the failure occurs. Figure 55 shows the number of cycles to failure for the fine and coarse mixtures produced in this study. As shown, the fine graded mixtures have better fatigue performance than coarse graded mixtures. It also can be seen that the elastomer modification of asphalt binder improves the asphalt mixture fatigue resistance better than plastomer modified and ground tire rubber modified binders. Plastomer binder modification improves the asphalt mixture fatigue resistance better than ground tire rubber modification.

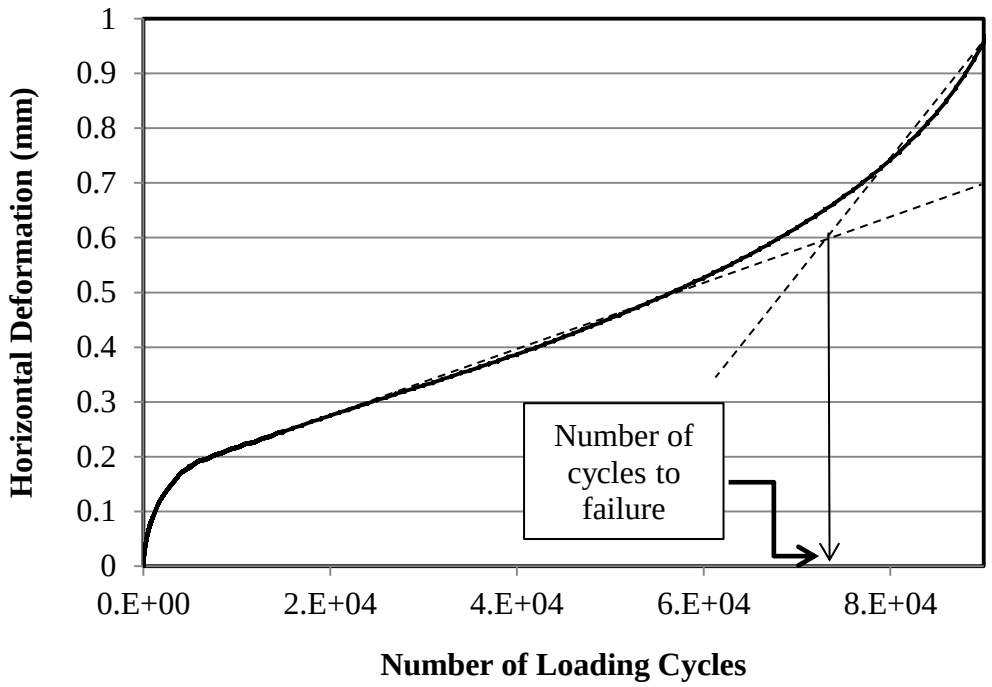

Figure 54: Fatigue failure criterion for controlled-force fatigue tests

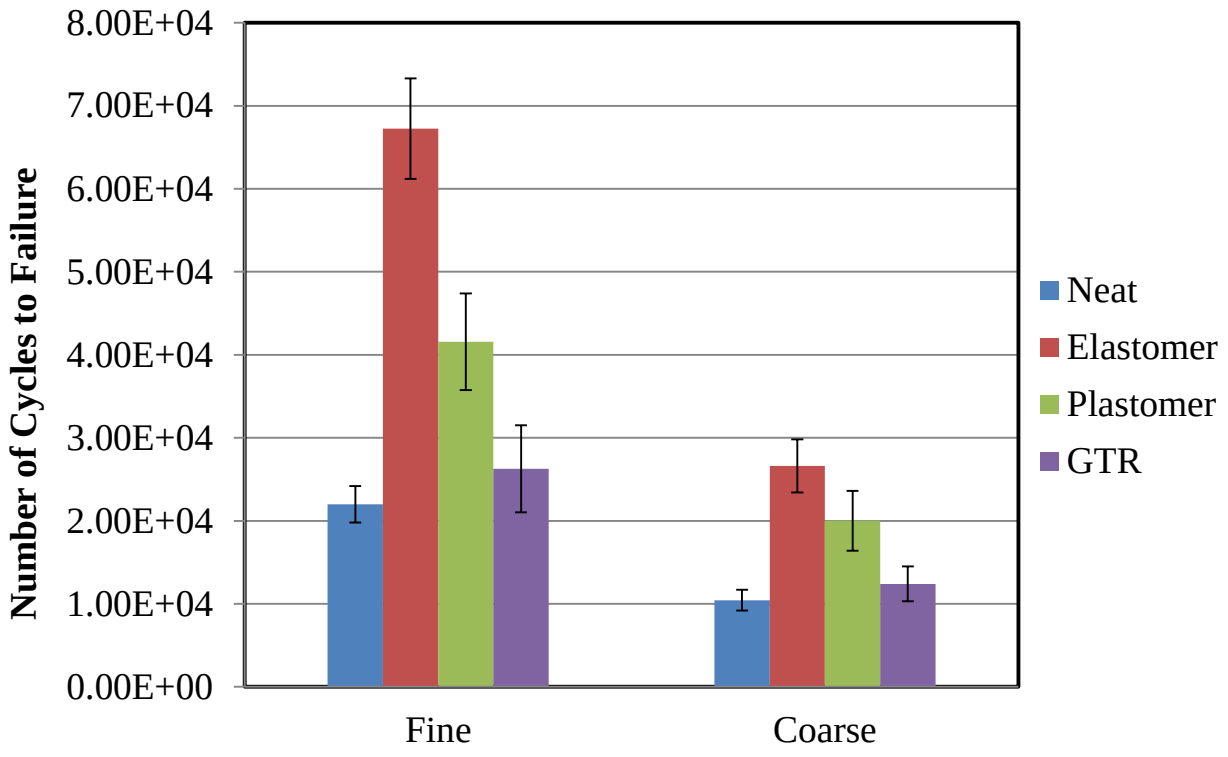

Figure 55: Number of cycles to failure for the fine and coarse mixtures

Kose et al (2000) indicated that the average binder strain level is 7.8 times higher than the asphalt mixture bulk strain. A rough analysis of the IDT test results indicated that the average tensile strain in the IDT test is almost 0.3% which corresponds to the average binder strain of 2.5%. It is interesting to note that the ranking of the asphalt mixtures is the same as asphalt binder ranking for the strain levels higher than 1.5% and smaller than 7%. Figure 56 shows the correlation between number of cycles to failure for the LAS at 2.5% strain and IDT mixture fatigue tests. A linear log-log relationship was calculated using the power law with an R^2 value of 0.94 and 0.92 for the fine and coarse HMA mixture designs, respectively. High correlations were measured at different LAS strain levels, but only 2.5% provided a high correlation on the same logarithmic decade as the mixture tests. Results validate that LAS can be used to measure

the fatigue performance of asphalt mixtures at the predicted strain levels in the asphalt binder cited by Kose et al.

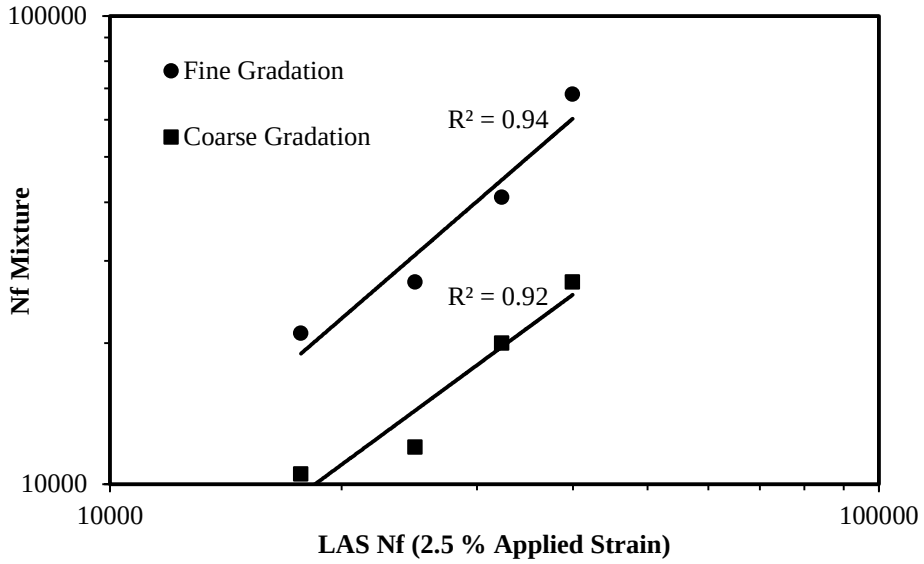

Figure 56: Comparison between number of cycles to failure from IDT fatigue testing and LAS fatigue results

Image Analysis

All the IDT samples were scanned using a flatbed scanner before testing. The image analysis and process system (IPAS2) was used to characterize the internal structure of asphalt mixtures. The results indicate that elastomer and plastomer modification improve the internal aggregate structure, however; the rubber modification slightly changes the aggregate microstructure. The comparison between the fine and coarse mixtures exhibits that the aggregate structure of fine mixtures is slightly better than that of coarse graded mixtures.

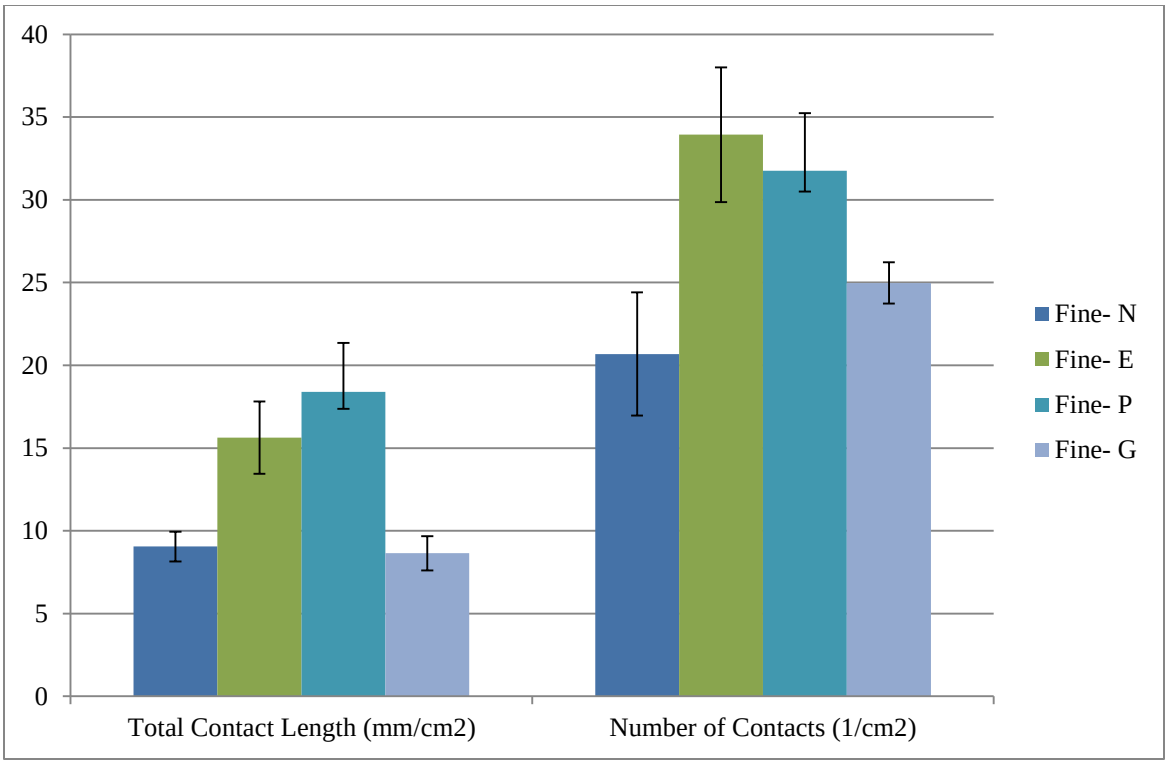

Figure 57: Internal aggregate structure of fine graded mixtures

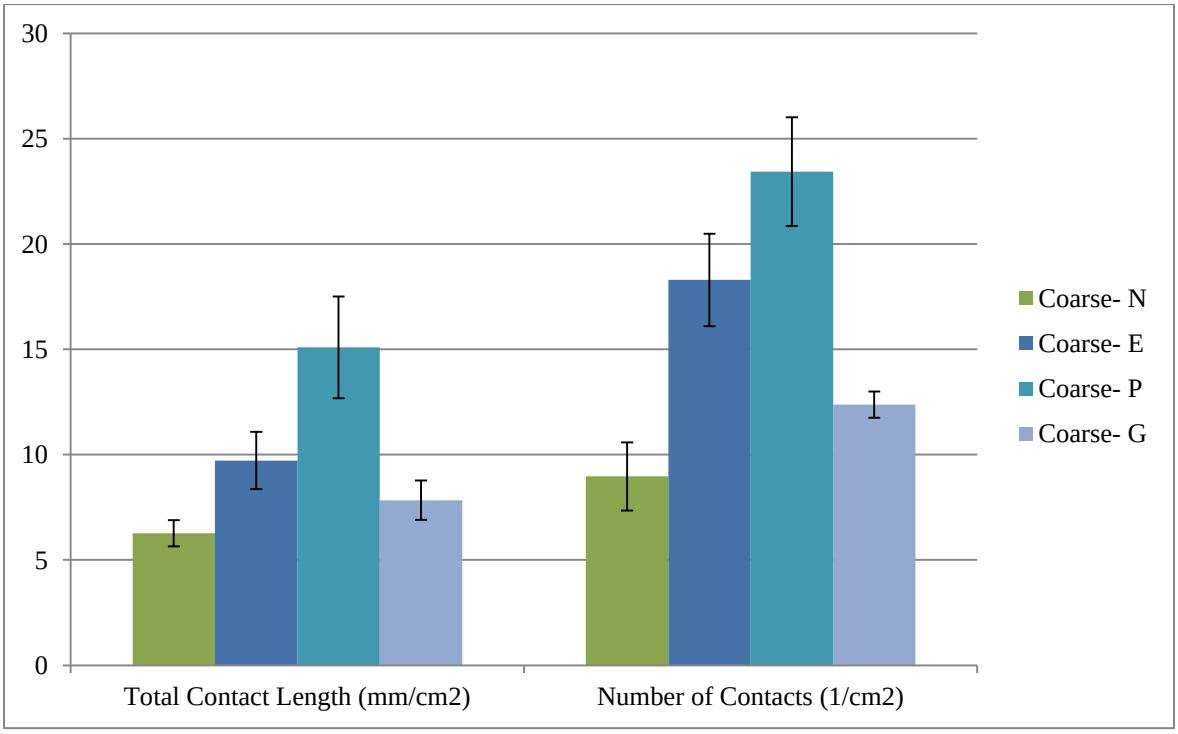

Figure 58: Internal aggregate structure of coarse graded mixtures

FE simulation of Fatigue Damage

As explained earlier in detail, the FE simulation is conducted at three interconnected scales: mastic, mortar, and asphalt mixture scale (Figure 24). The fatigue properties of the asphalt binder obtained from LAS test by application of VECD are used as the input properties of the homogeneous matrix of mastic scale. The FE simulation on mastic scale is conducted to obtain the mastic scale fatigue characteristics. The obtained mastic properties are used to characterize the mortar scale properties. Finally, the FE simulation is conducted on 2D images of asphalt mixtures to provide the fatigue behavior of asphalt mixtures under cyclic sinusoidal loading. In the following sub-sections the up-scaling process of the multi-scale model is described in detail.

Mastic Scale

A uniaxial sinusoidal load with a constant frequency of 1 Hz and increasing strain amplitude was applied to the artificially generated asphalt mastic image of fine and coarse graded mixtures to characterize the mastic scale fatigue properties (Figure 44). The loading frequency was selected relatively high in order to cause the damage failure in lower loading cycles due to the computer power limitation. Figure 59 shows the mastic strain-stress curve obtained from the FE analysis. As shown the peak stress in the FE simulation occurs at lower strain level, 4.4%, compared to LAS test, 7.2%, (Figure 46) due to higher load frequency used in FE analysis.

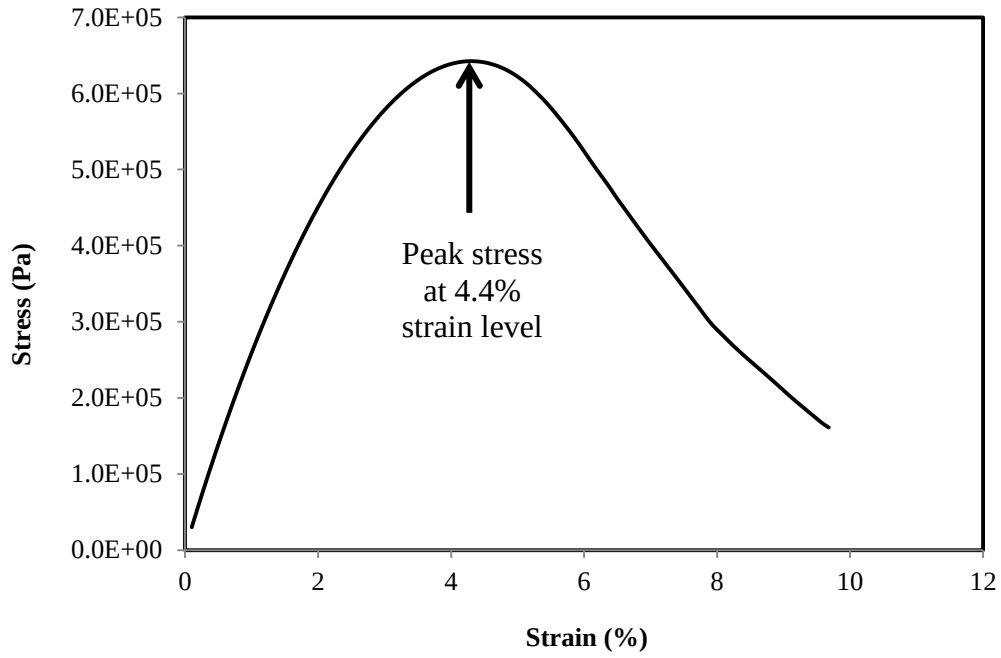

Figure 59: Asphalt mastic (neat binder+ 20% filler) stress-strain curve obtained from FE simulation

The VECD analysis is conducted on the FE simulation results to determine the fatigue parameters of the asphalt mastic. The LAS test was also conducted on the mastic sample to obtain the experimentally obtained fatigue parameters. Figure 60 shows that the FE analysis can predict the fatigue parameters with an acceptable accuracy. Comparisons with the experimental results indicate that the FE error in prediction of parameters α, C_1, and C_2 are 0.2, 11.8, and 4.6%, respectively.

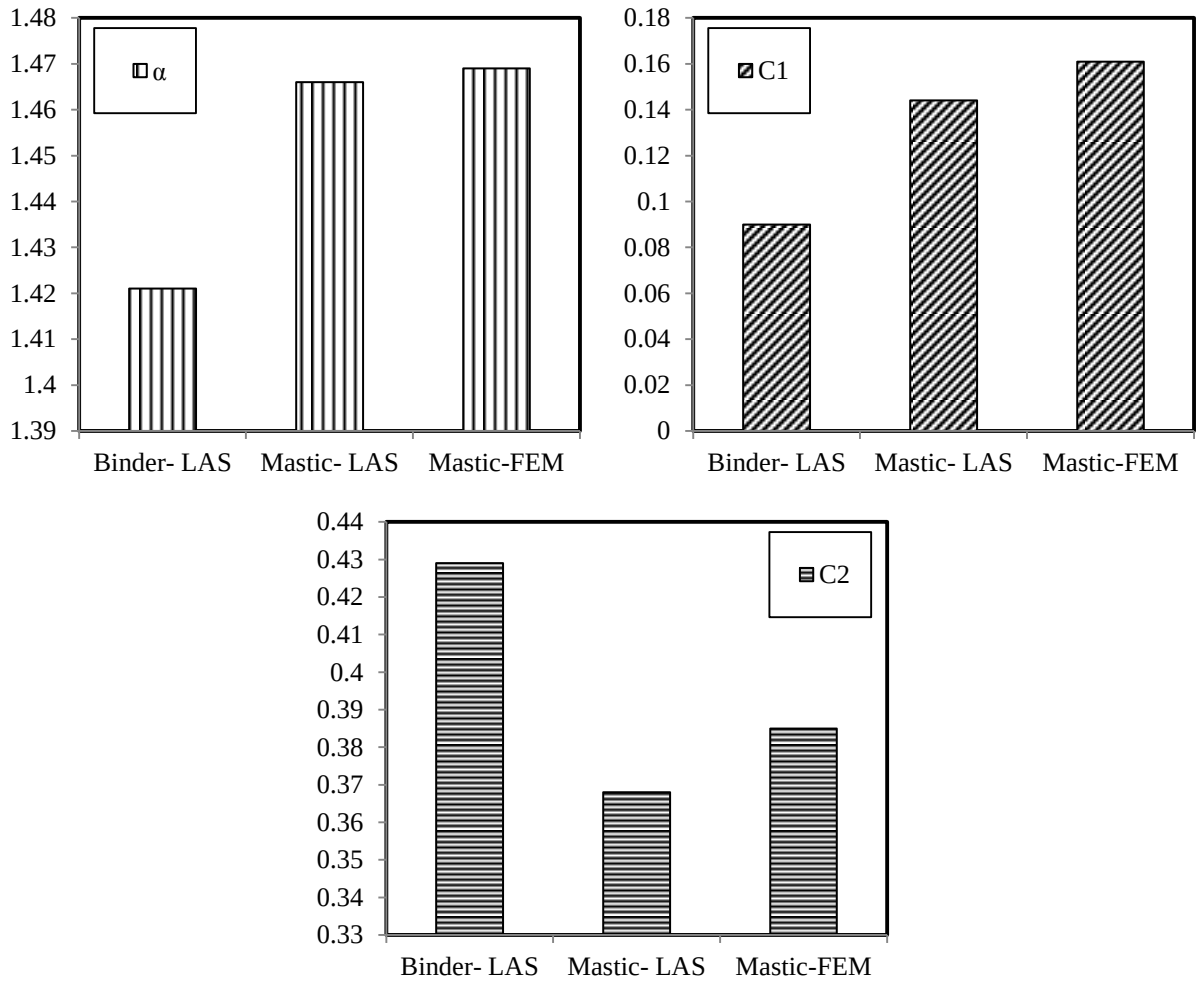

Figure 60: Comparison of fatigue parameters obtained from experiment and FE simulation

Same analysis was conducted on the rest of the mastic of the asphalt binders used in this study to determine their fatigue parameters. Table 11 shows the obtained fatigue parameters of the asphalt mastics by applying the VECD analysis on the FE simulated results.

Table 11: Fatigue parameters of the asphalt mastics with 20% volume fraction obtained from FE simulation

Component	Mastic (N)	Mastic (E)	Mastic (P)	Mastic (G)
α	1.469	1.602	1.775	1.601
C_0	1	1	1	1
C_1	0.161	0.185	0.202	0.169
C_2	0.385	0.336	0.330	0.379

The homogenized linear viscoelastic properties of the asphalt mastics were obtained by fitting a Prony series to the mastic complex modulus resulted from FE simulation. A strain-controlled axial repeated cyclic sinusoidal load is applied to each mastic model at 5 different frequencies, 0.04, 0.1, 1, 10, and 25 Hz, to obtain their complex modulus curve as shown in Figure 61. Table 12 shows the homogenized Prony series parameters of the mastics.

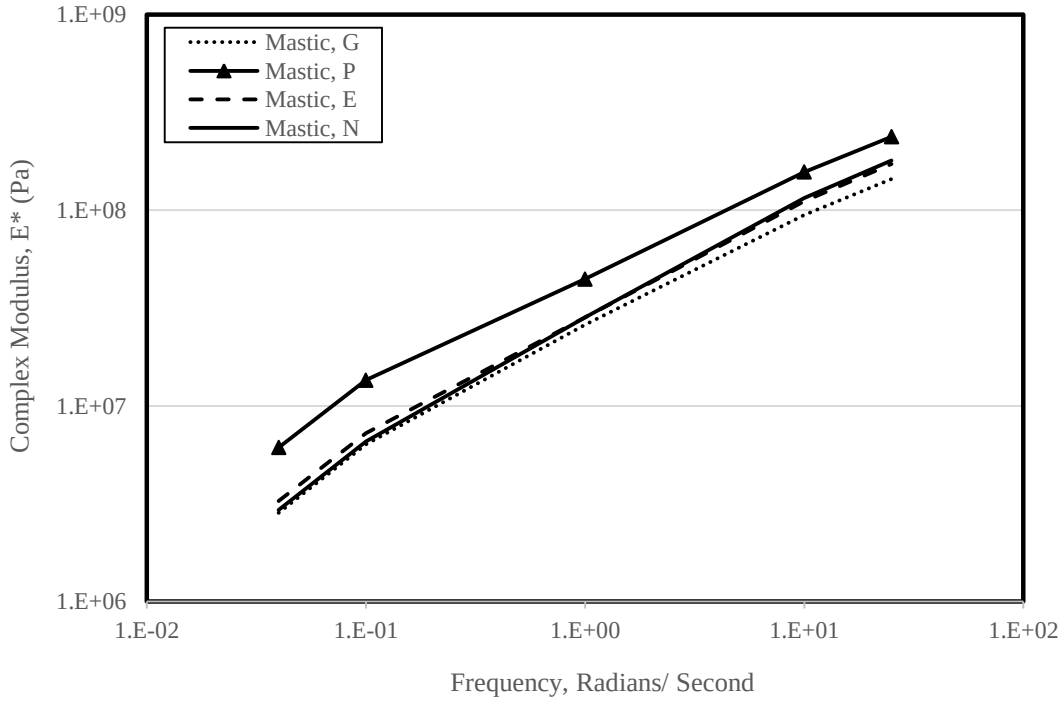

Figure 61: Complex modulus at the reference temperature 20℃ for the asphalt mastics resulted from FE simulation

Table 12: Homogenized Prony series parameters of the mastic scale

Component	*Mastic (N)*	*Mastic (E)*	*Mastic (P)*	*Mastic (G)*
E_∞ *(MPa)*	0.035	0.056	0.056	0.055
E_1 *(MPa)*	7.625	9.145	19.213	7.692
τ_1 *(s)*	1	1	1	1
E_2 *(MPa)*	25.96	24.95	35.86	25.49
τ_2 *(s)*	0.1	0.1	0.1	0.1
E_3 *(MPa)*	153.12	144.97	210.17	120.99
τ_3 *(s)*	0.01	0.01	0.01	0.01
E_4 *(MPa)*	205.28	198.68	113.43	126.73
τ_4 *(s)*	0.001	0.001	0.001	0.001

Mortar Scale

As shown in Table 7 the fine aggregate volume fraction in the mortar of fine and coarse graded mixtures is 0.58 and 0.37 respectively. The MATLAB image generator code was used to artificially generate the mortar images based on the particles' shape and gradation (Figure 62). Based on convergence of the creep compliance curves, an optimum RVE of 3.5 mm × 3.5 mm, approximately 3 times larger than the maximum size of fine aggregates in mortar scale was determined.

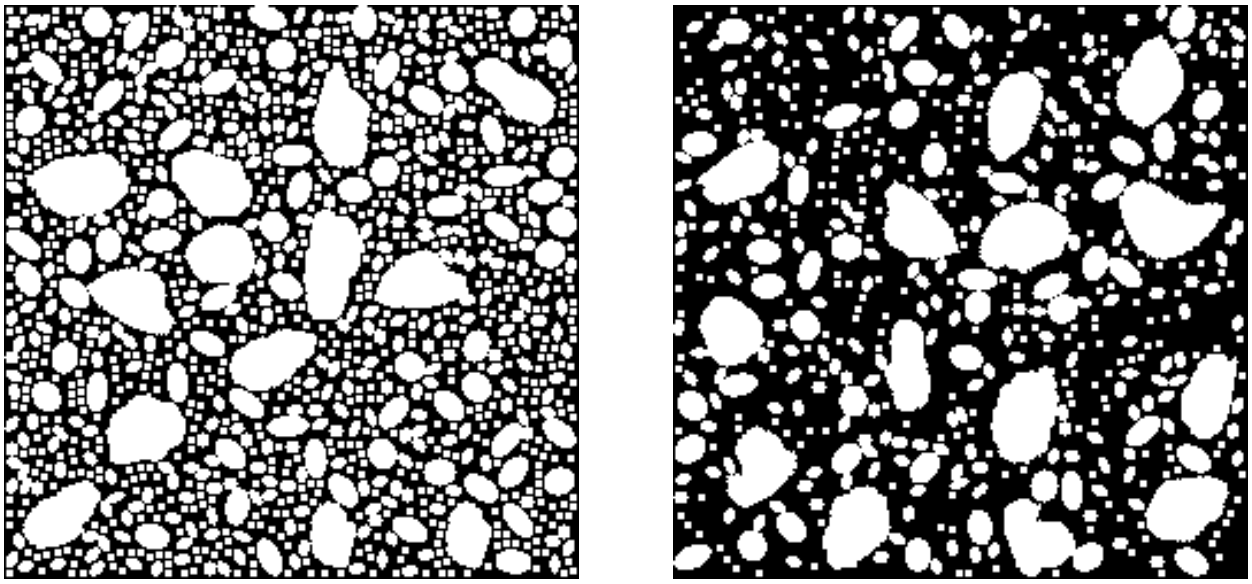

(a) (b)

Figure 62: Artificially generated asphalt mortar images of asphalt mixtures: (a) Fine graded mixture (b) Coarse graded mixture

The obtained viscoelastic and fatigue properties of the asphalt mastic was used as the input properties of the matrix of the mortar scale to simulate the behavior of mortar phase under loading. A total number of 8 mortar images with two levels of fine aggregate gradation (fine and coarse) and 4 levels of mastic type (N, E, P, and G) were numerically simulated in this study. Similar to the mastic scale the fatigue and viscoelastic properties of mortar scale were obtained through FE simulation.

A strain-controlled sinusoidal load is applied to the mortar scale to determine the complex modulus of the mortar scale. Very low strain amplitude, 0.5%, was used to apply the load in order to characterize the undamaged properties of the material. The load frequencies were selected to be 0.04, 0.1, 1, 10, and 25 Hz. Figure 63 indicates the complex modulus of all the 8 mortars. As shown the mortar of fine graded mixtures have higher complex modulus than those of coarse graded mixtures. It is due to the higher fine aggregate volume fraction of fine mixtures in comparison with coarse one. In order to characterize the linear viscoelastic properties of the

mortars, a Prony series is fitted to the complex modulus curve of each mortar. The Prony series parameters of the mortar samples are summarized in Table 13.

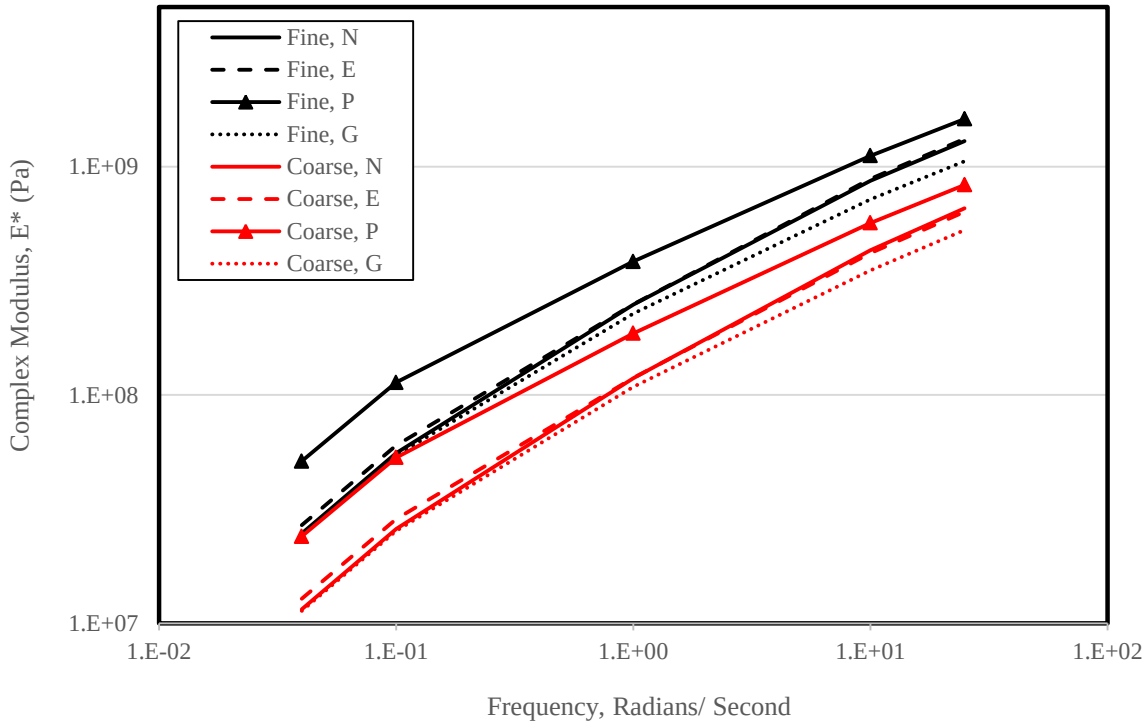

Figure 63: Complex modulus at the reference temperature 20℃ for the mortar of fine and coarse graded mixtures resulted from FE simulation

Table 13: Linear viscoelastic parameters of mortar phases of fine and coarse graded asphalt mixtures

Component	*Mortar (Fine, N)*	*Mortar (Fine, E)*	*Mortar (Fine, P)*	*Mortar (Fine, G)*	*Mortar (Coarse, N)*	*Mortar (Coarse, E)*	*Mortar (Coarse, P)*	*Mortar (Coarse, G)*
E_∞ *(MPa)*	0.055	0.058	0.058	0.058	0.055	0.058	0.058	0.058
E_1 *(MPa)*	62.351	72.576	158.995	65.178	28.385	34.353	72.920	29.740
τ_1 *(s)*	1	1	1	1	1	1	1	1
E_2 *(MPa)*	269.03	252.50	374.28	252.61	125.24	121.29	182.04	120.00
τ_2 *(s)*	0.1	0.1	0.1	0.1	0.1	0.1	0.1	0.1
E_3 *(MPa)*	1103.59	1154.43	1272.45	841.24	538.17	518.42	661.01	388.75
τ_3 *(s)*	0.01	0.01	0.01	0.01	0.01	0.01	0.01	0.01
E_4 *(MPa)*	699.34	630.31	696.34	637.14	670.05	594.70	500.13	669.97
τ_4 *(s)*	0.001	0.001	0.001	0.001	0.001	0.001	0.001	0.001
Poisson's Ratio	0.39	0.39	0.39	0.39	0.43	0.43	0.43	0.43

A uniaxial sinusoidal load with a constant frequency of 1 Hz and increasing strain amplitude was applied to the artificially generated mortar image of fine and coarse graded mixtures to characterize the mortar scale fatigue properties. The strain amplitude starts from 0.05% and increases with a constant rate to 8% during 300 seconds. The loading frequency was selected relatively high in order to cause the damage failure in lower loading cycles due to the computer power limitation. Figure 64 and Figure 65 show the strain-stress curves of mortars of fine and coarse graded mixtures obtained by conducting FE simulations on artificially generated 2D mortar images. As shown, between the N, E, and G binders which have same level of complex modulus, the mortar of E binder shows a better fatigue performance and its peak stress occurs at the highest strain level among all the other binders. The peak stress of mortar of P binder occurs at the lowest strain level in comparison with other mortars. However, it should be noted that a higher stress level has to be applied to P mortar in order to cause a specific strain in comparison with N, E, and G mortars. Comparison between fine and coarse mixtures indicates that mortars of fine graded mixtures fail at lower strain levels than those of coarse graded mixtures. It is due to higher particle volume fraction in mortars of fine mixtures which makes them stiffer and more brittle.

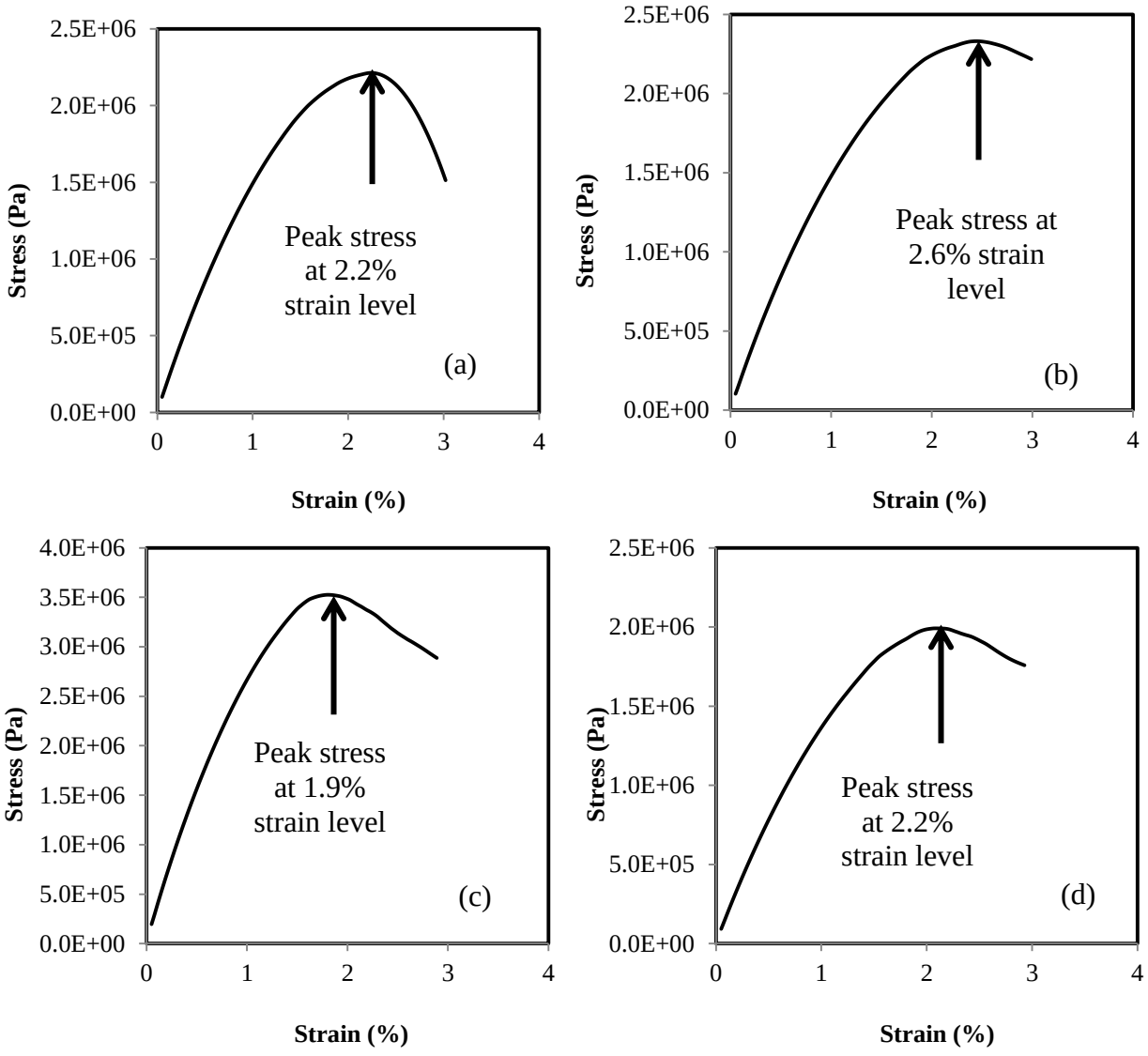

Figure 64: Stress-strain curve of the mortars of fine graded mixtures obtained from FE simulation (a) neat binder (b) elastomer modified binder (c) plastomer modified binder (d) ground rubber modified binder

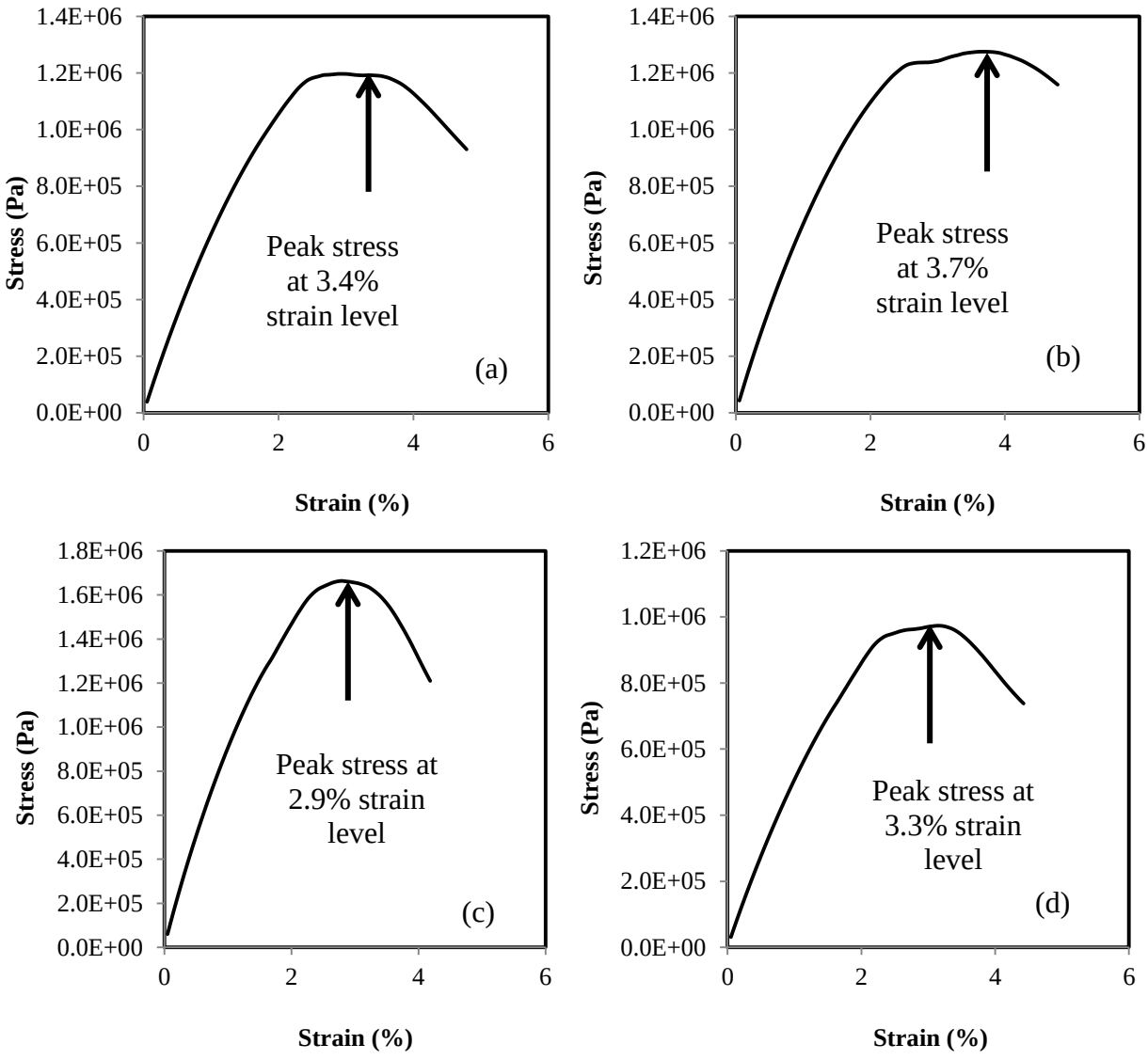

Figure 65: Stress-strain curve of the mortars of coarse graded mixtures obtained from FE simulation (a) neat binder (b) elastomer modified binder (c) plastomer modified binder (d) ground rubber modified binder

Table 14 and Table 15 show the obtained fatigue parameters of the asphalt mortars of all the fine and coarse graded mixtures by applying the VECD analysis on the FE simulated results.

Table 14: Fatigue parameters of mortars of fine graded mixtures

Component	Mortar (N)	Mortar (E)	Mortar (P)	Mortar (G)
α	1.661	1.672	1.851	1.759
C_0	1	1	1	1
C_1	0.167	0.174	0.189	0.17
C_2	0.411	0.379	0.386	0.401

Table 15: Fatigue parameters of mortars of coarse graded mixtures

Component	Mortar (N)	Mortar (E)	Mortar (P)	Mortar (G)
α	1.578	1.701	1.734	1.635
C_0	1	1	1	1
C_1	0.128	0.148	0.15	0.131
C_2	0.421	0.417	0.403	0.42

The homogenized viscoelastic properties of the mortar scale as well as the fatigue characteristics obtained from FE analysis are used as the input properties to simulate the fatigue behaviour of asphalt mixture scale.

Asphalt Mixture Scale

All the IDT samples were scanned using a flatbed scanner before testing. The IPAS2 software was used to convert the scanned images to binary images. For each type of mixtures 2 replicate images were used in the analysis at the asphalt mixture scale. Figure 66 shows the binary images of the two of the mixtures used in this study with fine and coarse aggregate gradations. As explained in the Chapter 3, air voids are distributed in the image, based on the air void content of the mixture following a bathtub shape (Figure 33).

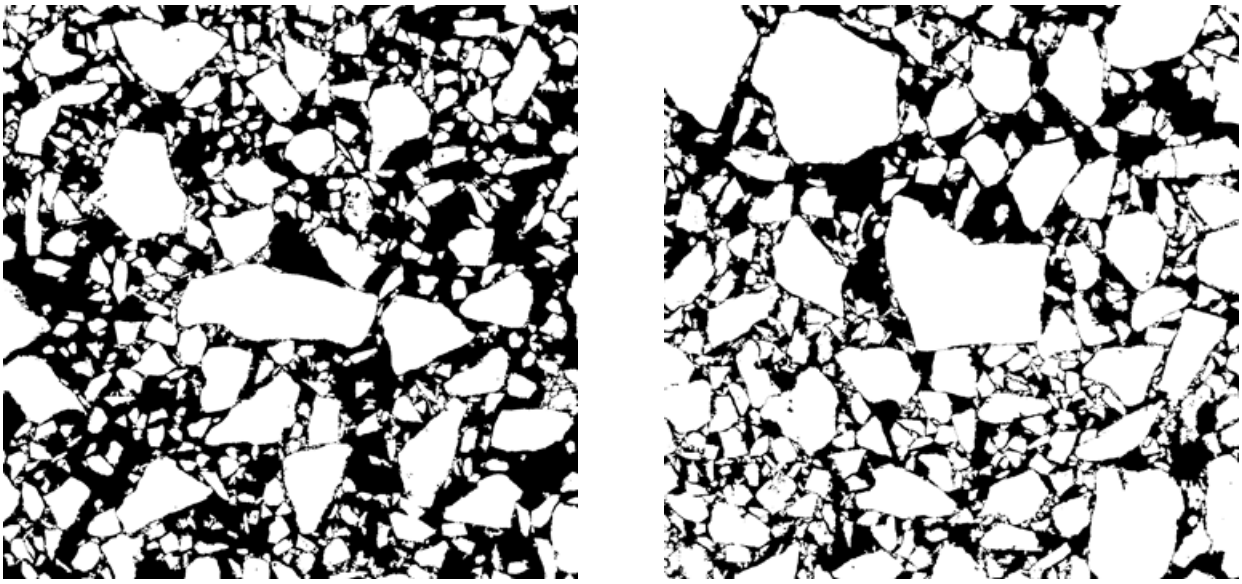

(a) (b)

Figure 66: 2D scanned images of the mixtures with neat binder tested with IDT test (a) fine graded mixture (b) coarse graded mixture

Two types of simulation are conducted at the asphalt mixture scale: force controlled and displacement controlled simulations. The results obtained from the force controlled simulation are compared with the IDT fatigue testing data and VECD concept is applied to the displacement controlled simulation results to obtain the fatigue life of the asphalt mixture at different strain levels.

Fatigue performance simulation: controlled-force mode

The asphalt mixture models were placed under a repeated cyclic load with a constant applied stress. The stress amplitude and loading frequency were selected to be 1375 kPa and 1 Hz, respectively. The stress applied is selected relatively high and frequency is chosen to be low in order to reduce the number of cycles to failure due to computer power limitations. Failure was defined as the number of load cycles to 50% reduction in initial stiffness. Figure 67 shows the number of cycles to failure for all the mixtures simulated in this study. Comparison between IDT fatigue test data and FE simulation results indicates that the developed multi-scale model is a

powerful tool in ranking the materials and can be used as the surrogate to time consuming and costly laboratory tests on asphalt mixtures. The mixtures with elastomer modified binder show the best fatigue performance among all the other types of binder. It is interesting to note that the elastomer modified binder is also the most fatigue resistant binder among the binders used in this study.

The results also show that the fine graded mixtures generally perform better than the coarse graded mixtures. Author believes that it is due to better internal aggregate structure of fine graded asphalt mixtures (Figure 57 and Figure 58). Better aggregate structure leads to lower stress level carried out by the asphalt binder resulting in better fatigue performance.

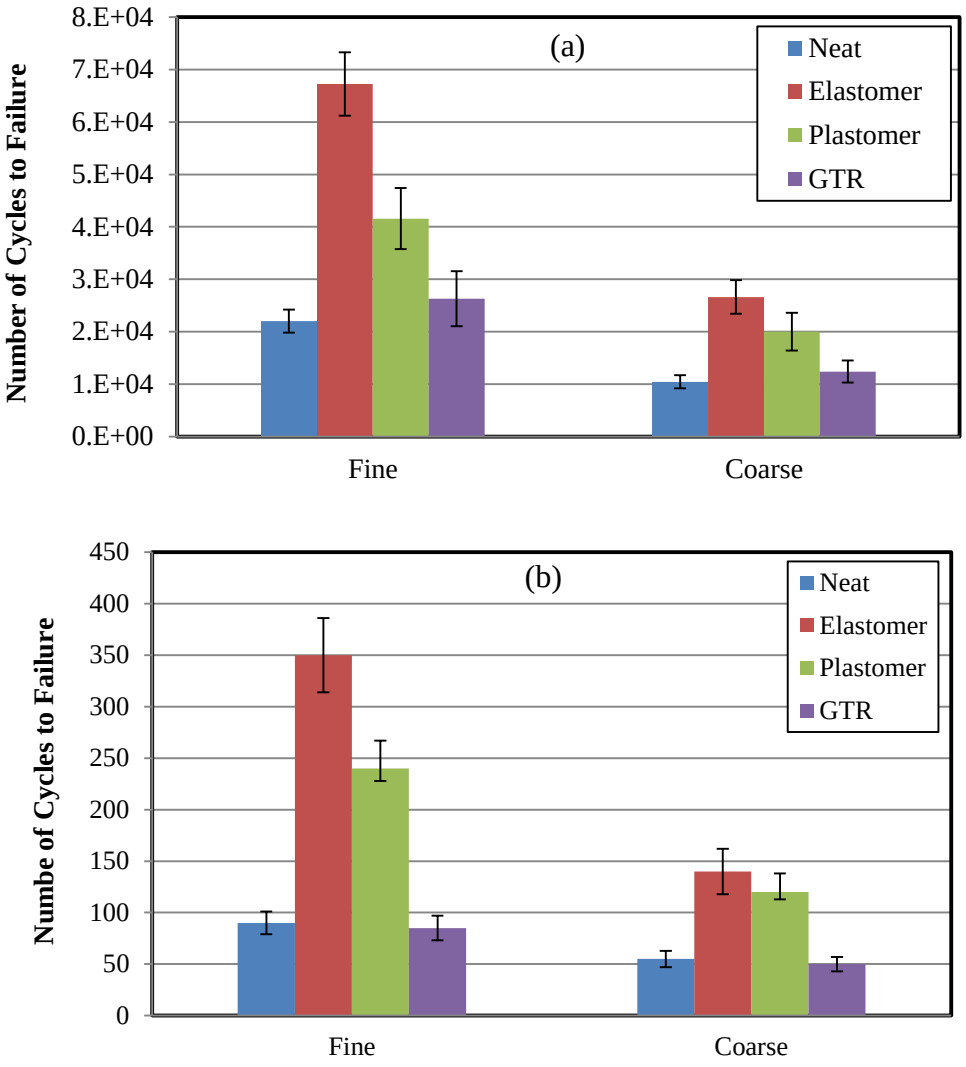

Figure 67: Number of cycles to failure for the fine and coarse mixtures obtained from (a) IDT fatigue testing (b) controlled-force FE simulation

Fatigue performance simulation: controlled-displacement mode

The asphalt mixture models were placed under a repeated cyclic load with an increasing applied strain. The applied strain starts from 0.005% and linearly increases to its maximum level of 2% is 300 seconds. Loading frequency of 1 Hz was selected in order to reduce the number of cycles to failure in comparison with frequency of 10 Hz due to computer power limitations. Figure 68 and Figure 69 show the FE simulation results for fine and coarse graded mixtures. As shown the mixture with elastomer modified binder fails at the highest strain level among all of the binders.

Figure 70 and Figure 71 indicate that the plastomer modified binder has the highest dynamic modulus among all the mixtures for both of gradations. It is interesting to note that although the modification of the asphalt binder with the elastomer slightly increases the dynamic modulus of the asphalt binder (Figure 51); the asphalt mixture with elastomer modified binder shows a significantly higher modulus than the mixture with neat binder. This phenomenon is due to the better internal aggregate structure of the mixture with elastomer modified binder.

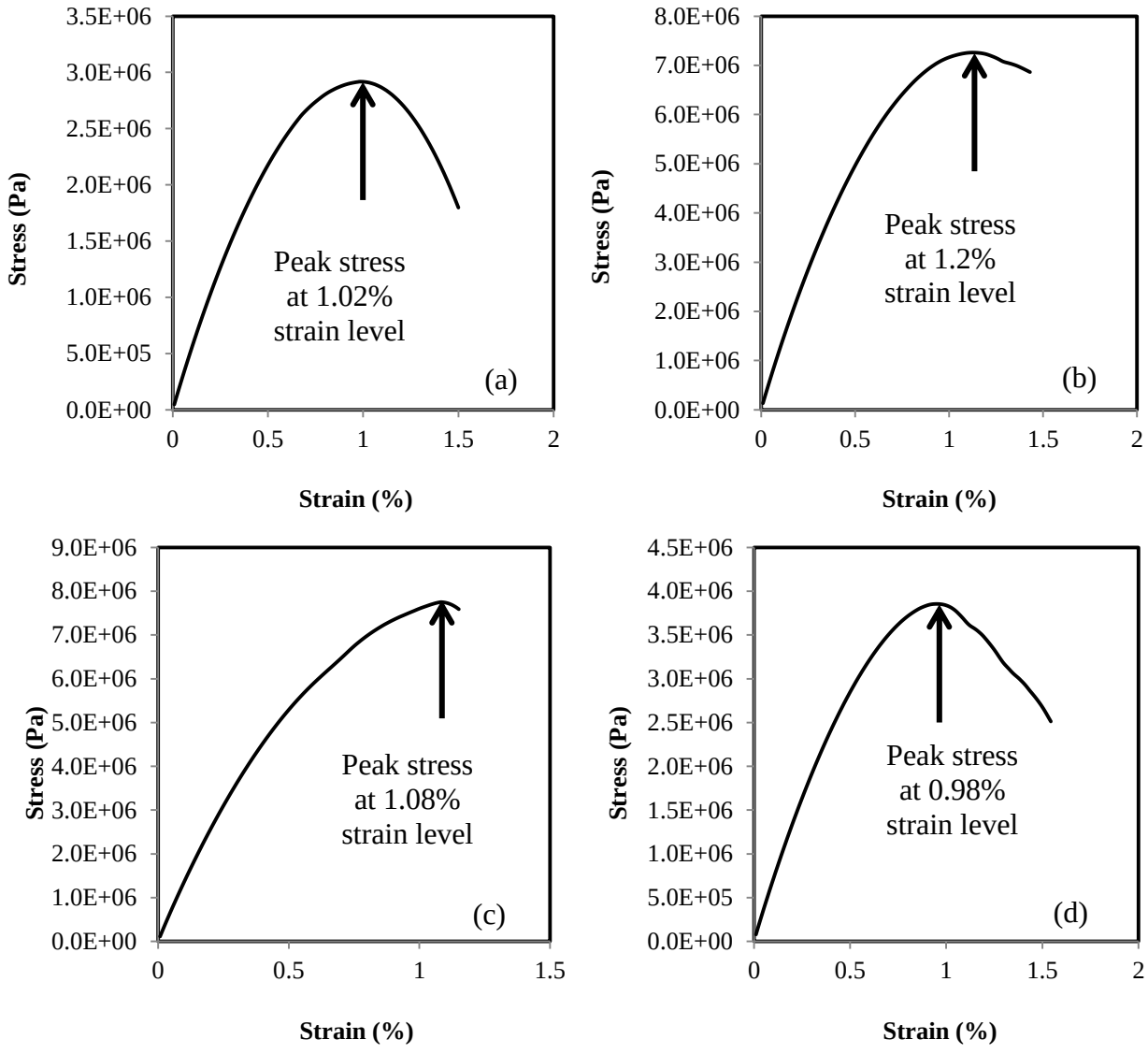

Figure 68: Stress-strain curve of the fine graded mixtures obtained from FE simulation (a) neat binder (b) elastomer modified binder (c) plastomer modified binder (d) ground rubber modified binder

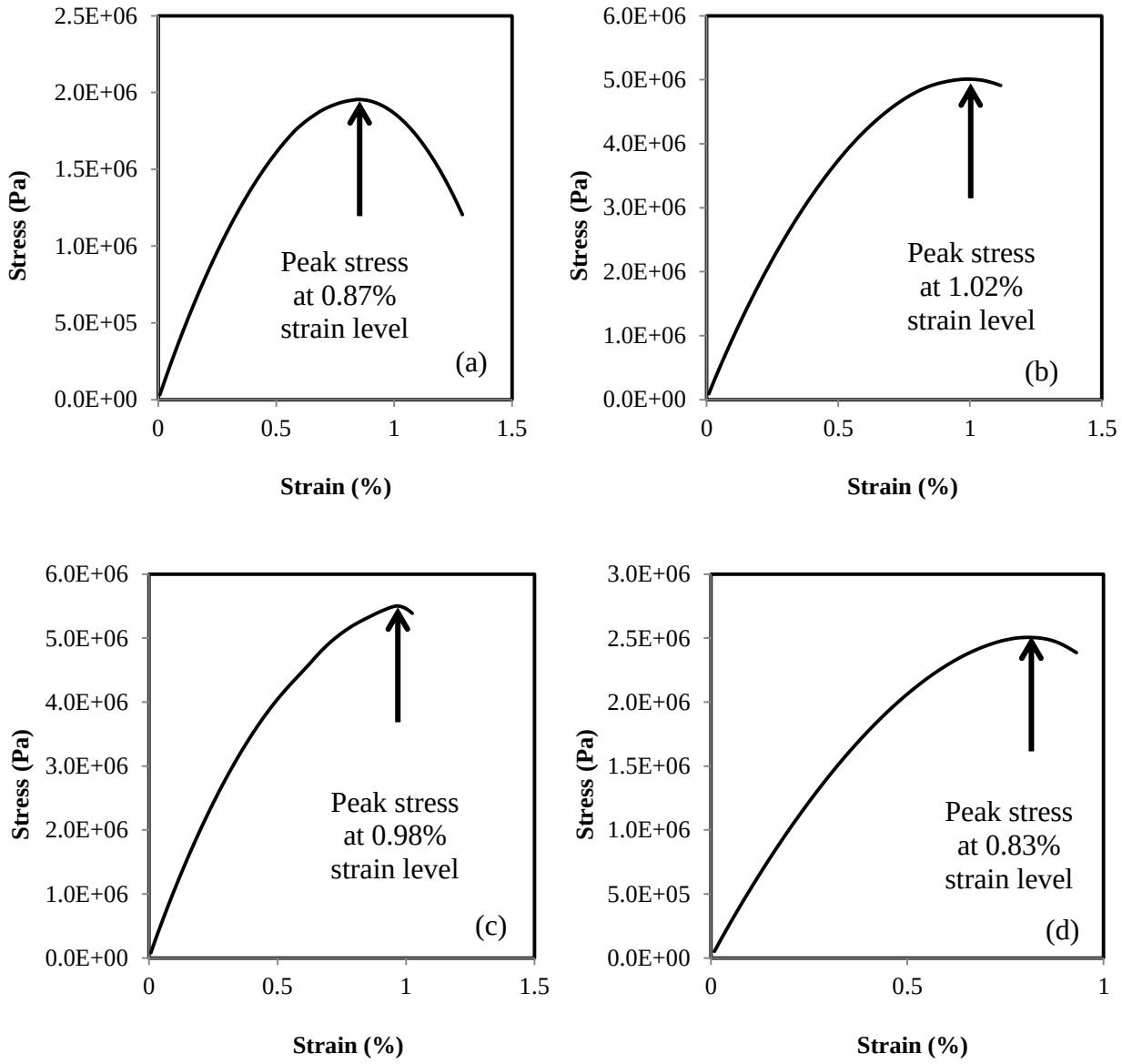

Figure 69: Stress-strain curve of the fine graded mixtures obtained from FE simulation (a) neat binder (b) elastomer modified binder (c) plastomer modified binder (d) ground rubber modified binder

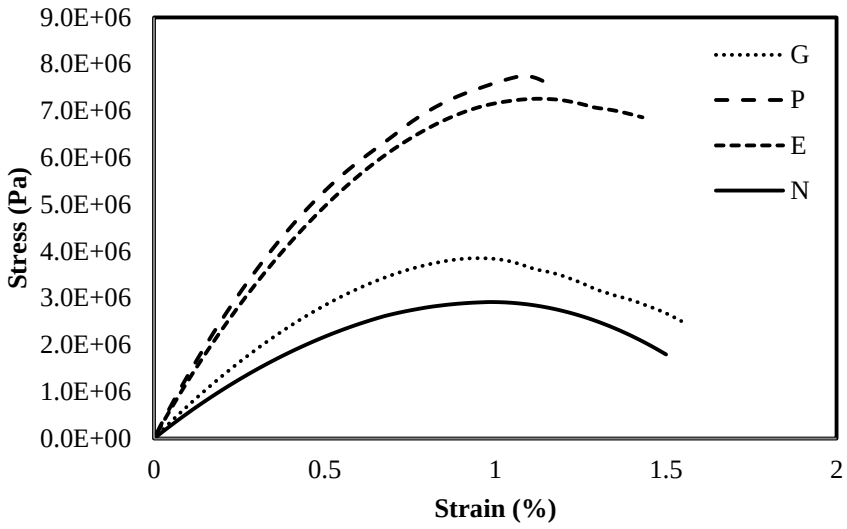

Figure 70: Comparison of stress-strain curves of fine graded mixtures

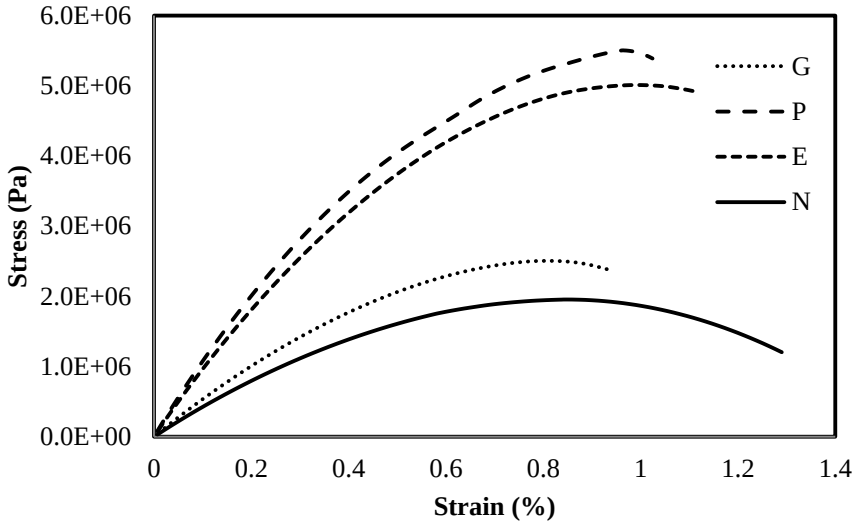

Figure 71: Comparison of stress-strain curves of coarse graded mixtures

The viscoelastic continuum damage analysis was performed on the FE simulation results of all the fine and coarse graded mixtures to obtain the fatigue parameters of the mixtures studied in this dissertation. Figure 72 shows the number of cycles to failure calculated using the fatigue law (Equation 18) for fine and coarse graded mixtures. As shown the fine graded mixtures show

a better performance in comparison with coarse mixtures. The results also indicate that elastomer and plastomer modification can be used to improve the fatigue resistance of asphalt mixtures.

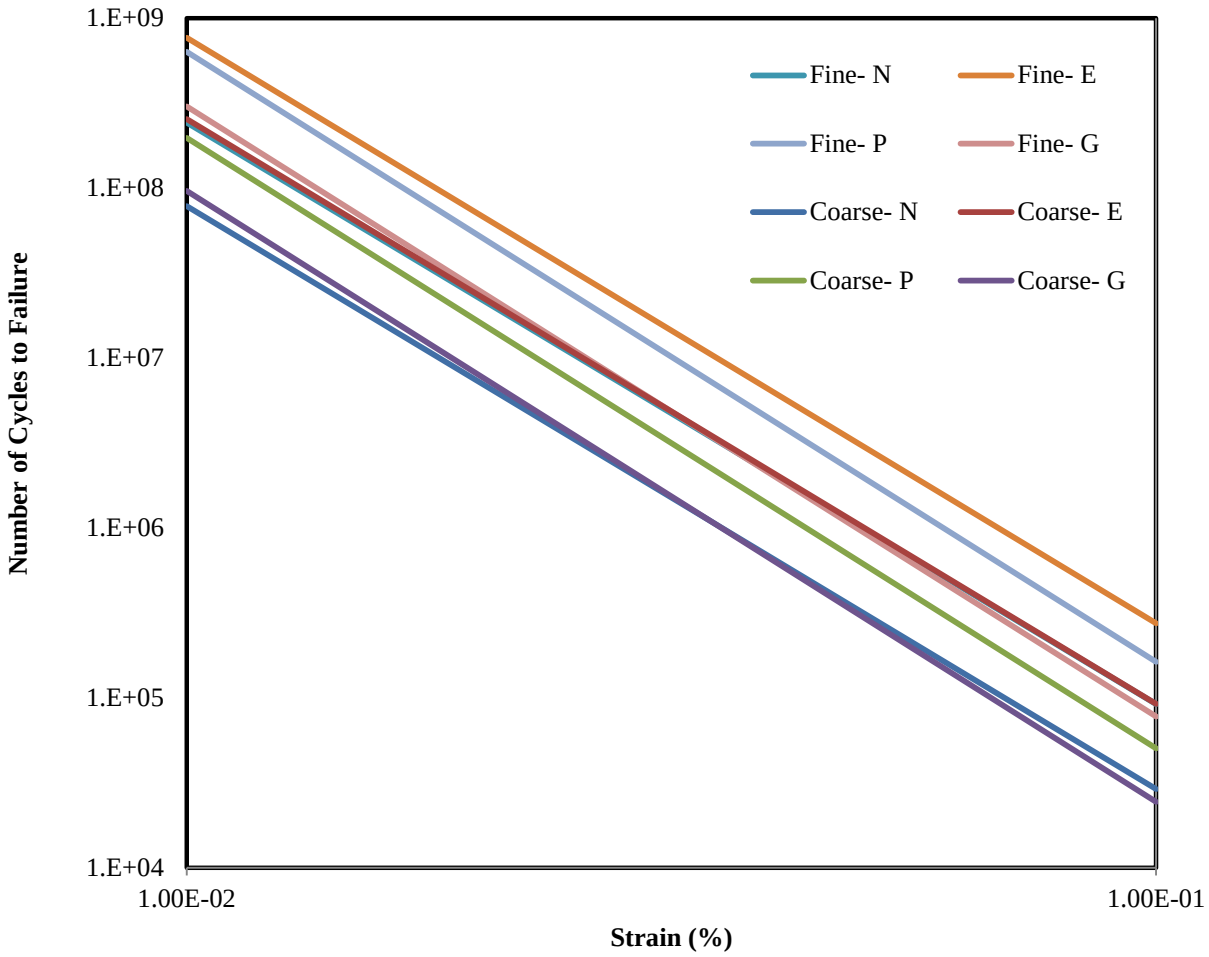

Figure 72: Traditional fatigue curve for asphalt mixtures used in this study

The FE simulation results indicated that the image-based multi-scale FE approach developed in this study can be used as a surrogate to costly and time consuming tests at the mixture level to predict the fatigue behavior of asphalt mixtures.

CHAPTER 6: SUMMARY OF FINDINGS

The physical properties of asphalt mixture are governed by the characteristics of its constituents such as aggregate properties (gradation, shape, structure, modulus, etc.) and binder properties (complex modulus, relaxation characteristic, etc.). Although experimental testing can provide the researchers with the macro-mechanical behavior of asphalt concrete, it is time consuming and costly to investigate the micro-mechanical response of the asphalt mixture in a laboratory due to difficulties in controlling the micro-structural features such as: aggregate shape, size, distribution, gradation, and volume fraction.

Asphalt mixture designers need to make decisions on selecting binder, filler or even aggregate gradations. Experimentation is a very time consuming and costly process to study the effect of asphalt mixture constituent properties on macro-behavior of asphalt mixture. This dissertation is an effort to present a virtual simulation tool which can cut down on experimental testing and on time required to make decisions.

In this study a novel multi-scale model of asphalt mixture containing the three main phases of binder, aggregate, and air voids was developed to predict mechanical behavior of asphalt mixture under loading. The up-scaling approach used includes virtual generation of asphalt mastic and mortars using a library of images of actual fillers and fine aggregate particles mixed with the asphalt binder. It also included a virtual generation of air voids in the mortar phase during the analysis of the mixture scale. The study focused on relating the macro-scale behavior of asphalt mixture to rheological properties of asphalt binder, particle gradation, particle shape, and particle volume fraction at the mastic and mortar scales. The laboratory experiments were conducted to validate the developed model at the mastic and asphalt mixture scale levels.

The main preliminary findings of this dissertation are:

- Multi-scale modeling is an effective method to simulate a complex material like asphalt mixture. It is shown that the accurate implementation of fine aggregate shape and gradation in the FE simulation increases the accuracy of the model. The multi-scale model developed and presented in this study is unique in terms of overcoming the challenge faced in current asphalt mixtures multi-scale models with regards to accurate implementation of fine aggregate geometry and shapes. In the present study the developed multi-scale aggregate geometries are significantly advanced for the finer scales through use of microscopic imaging and development of a fine mineral aggregate generator database and program. Furthermore, laser diffraction is used to generate accurate mineral aggregate gradation data for particles finer than 0.075 mm, thus resulting in mastic scale models of significantly higher accuracy than available in comparable models.

- The challenge of simulating particle contacts at lower scales is addressed by implementation of a simple contact law into ABAQUS through user material subroutine and transferred to the next higher scale by application of nonlinear superposition. The results indicate that evolution of the aggregate structure, as a result of mixture consolidation and distortion, significantly affect the asphalt mixture response under mechanical loading. A limited experimental verification of the accuracy of the developed methodology was presented and Comparison between experimental data and the simulation results shows that the finite element multi-scale model presented in this study has considerable promise for predicting the asphalt mixture mechanical properties.

- A single binder damage test is used to quantify the binder damage parameters through viscoelastic continuum damage (VECD) analysis. Based on the damage level of asphalt binder, calculated using the Chain rule, the Prony series parameters are determined during the loading and implemented into ABAQUS through UMAT. The simulation results indicated that the VECD analysis method makes the finite element simulation a powerful tool to predict the damage accumulation in the material due to cyclic loading.

- Experimental results indicated that binder modification can be used to improve the fatigue resistance of asphalt binders. Elastomer modified binder showed the best performance among all the binders used in this study at both of the binder and mixture levels.

- High correlations were measured between IDT fatigue tests and LAS results at different strain levels, but only 2.5% provided a high correlation on the same logarithmic decade as the mixture tests. Results validate that LAS can be used to measure the fatigue performance of asphalt mixtures at the predicted strain levels in the asphalt binder.

- The internal structure analysis of the asphalt mixtures indicated that the fine graded mixtures generally perform better than coarse graded mixtures due to their better aggregate structure and compaction.

- The developed multi-scale model is capable of studying and analysing the damage initiation and propagation in the asphalt mixtures. The controlled-force FE simulation ranks the asphalt mixtures in a same order that IDT fatigue test does. The controlled-displacement FE simulation was used to obtain the traditional fatigue curve of the asphalt mixtures. The FE simulation results indicated that the image-based multi-scale FE

approach developed in this study can be used as a surrogate to costly and time consuming tests at the mixture level to predict the fatigue behavior of asphalt mixtures.

Conclusions

The results of this study verified the hypothesis that using an improved micro-mechanical model, asphalt mixture physical properties can be obtained directly from the constituents. It was shown that in order to improve the simulation results a contact model has to be defined and incorporated into FE framework. It was also verified that viscoelastic continuum damage concept can be coupled with the FE simulation to predict the fatigue behavior of asphalt mixtures through a multi-scale approach.

REFERENCES

1. Standard, AASHTO Provisional. "Estimating Damage Tolerance of Asphalt Binders Using the Linear Amplitude Sweep." *AASHTO Designation: TP101-14* (2014).
2. Standard, AASHTO Provisional. "Determining the Creep Compliance and Strength of Hot Mix Asphalt (HMA) Using the Indirect Tensile Test Device." *AASHTO Designation: TP9-96* (2012).
3. ABAQUS: Version 6.12. - Providence, RI, 2012.
4. Al-Rub, Rashid K. Abu, Taesun You, Eyad A. Masad, and Dallas N. Little. "Mesomechanical modeling of the thermo-viscoelastic, thermo-viscoplastic, and thermo-viscodamage response of asphalt concrete." *International Journal of Advances in Engineering Sciences and Applied Mathematics* 3, no. 1-4 (2011): 14-33.
5. Adhikari, Sanjeev, and Zhan-Ping You. "3D microstructural models for asphalt mixtures using X-ray computed tomography images." *International Journal of Pavement Research and Technology* 1, no. 3 (2008): 94-99.
6. Ahmed, SaFRJ, and F. R. Jones. "A review of particulate reinforcement theories for polymer composites." *Journal of Materials Science 25*, no. 12 (1990): 4933-4942.
7. Aigner, Elisabeth, Roman Lackner, and Christian Pichler. "Multiscale prediction of viscoelastic properties of asphalt concrete." *Journal of Materials in Civil Engineering* 21, no. 12 (2009): 771-780.
8. Al-Rousan, Taleb, Eyad Masad, Erol Tutumluer, and Tongyan Pan. "Evaluation of image analysis techniques for quantifying aggregate shape characteristics."*Construction and Building Materials* 21, no. 5 (2007): 978-990.
9. Arshadi, Amir., and Hussain U. Bahia. " Development of an Image-based Multi-Scale Finite Element Approach to Predict Mechanical Response of Asphalt Mixtures." *Journal of Road Materials and Pavement Design* (2015).
10. Bahia, Hussain U., D. I. Hanson, M. Zeng, H. Zhai, M. A. Khatri, and R. M. Anderson. *Characterization of modified asphalt binders in superpave mix design*. No. Project 9-10 FY'96. 2001.
11. Bahia, Hussain U., Huachun Zhai, Menglan Zeng, Yuling Hu, and Pamela Turner. "Development of Binder Specification Parameters Based On Characterization Of Damage Behavior (With Discussion)." *Journal of the Association of Asphalt Paving Technologists* 70 (2001).
12. Buttlar, William G., and Zhanping You. "Discrete element modeling of asphalt concrete: microfabric approach." *Transportation Research Record: Journal of the Transportation Research Board* 1757, no. 1 (2001): 111-118.
13. Chang, C. S., and J. Gao. "Rheological modeling of randomly packed granules with visco-elastic binders of Maxwell type." *Computers and Geotechnics* 21, no. 1 (1997): 41-63.
14. Chang, George K., and Jay N. Meegoda. "Micromechanical model for temperature effects of hot-mix asphalt concrete." *Transportation Research Record: Journal of the Transportation Research Board* 1687, no. 1 (1999): 95-103.
15. Chen, Hsien H., Kurt M. Marshek, and C. L. Saraf. "Effects of truck tire contact pressure distribution on the design of flexible pavements: a three-dimensional finite element approach." *Transportation Research Record* 1095 (1986).

16. Cheung, C. Y., A. C. F. Cocks, and D. Cebon. "Isolated contact model of an idealized asphalt mix." *International Journal of Mechanical Sciences* 41, no. 7 (1999): 767-792.
17. Christensen Jr, D. W., T. Pellinen, and R. F. Bonaquist. "Hirsch model for estimating the modulus of asphalt concrete." *Journal of the Association of Asphalt Paving Technologists* 72 (2003).
18. Coenen, Aaron R., M. Emin Kutay, Nima Roohi Sefidmazgi, and Hussain U. Bahia. "Aggregate structure characterisation of asphalt mixtures using two-dimensional image analysis." *Road Materials and Pavement Design* 13, no. 3 (2012): 433-454.
19. Coleri, Erdem, John T. Harvey, Kai Yang, and John M. Boone. "Development of a micromechanical finite element model from computed tomography images for shear modulus simulation of asphalt mixtures." *Construction and Building Materials* 30 (2012): 783-793.
20. Cyr, M., and A. Tagnit-Hamou. "Particle size distribution of fine powders by LASER diffraction spectrometry. Case of cementitious materials." *Materials and Structures* 34, no. 6 (2001): 342-350.
21. Dai, Qingli, and Zhanping You. "Micromechanical finite element framework for predicting viscoelastic properties of asphalt mixtures." *Materials and Structures*41, no. 6 (2008): 1025-1037.
22. Dai, Qingli, and Zhanping You. "Prediction of creep stiffness of asphalt mixture with micromechanical finite-element and discrete-element models." *Journal of Engineering Mechanics* 133, no. 2 (2007): 163-173.
23. Dai, Qingli. "Micromechanical modeling of constitutive and damage behavior of heterogeneous asphalt materials." (2004).
24. Daniel, Jo Sias, and Y. Richard Kim. "Development of a simplified fatigue test and analysis procedure using a viscoelastic, continuum damage model (with discussion)." *Journal of the Association of Asphalt Paving Technologists* 71 (2002).
25. Darabi, Masoud K., Rashid K. Abu Al-Rub, Eyad A. Masad, Chien-Wei Huang, and Dallas N. Little. "A thermo-viscoelastic–viscoplastic–viscodamage constitutive model for asphaltic materials." *International Journal of Solids and Structures* 48, no. 1 (2011): 191-207.
26. Deacon, John A., John S. Coplantz, Aktarhusein A. Tayebali, and Carl L. Monismith. "Temperature considerations in asphalt-aggregate mixture analysis and design." *Transportation Research Record* 1454 (1994).
27. Dessouky, Samer, Eyad Masad, Dallas Little, and Hussein Zbib. "Finite-element analysis of hot mix asphalt microstructure using effective local material properties and strain gradient elasticity." *Journal of engineering mechanics* 132, no. 2 (2006): 158-171.
28. Dvorkin, Jack, and Hezhu Yin. "Contact laws for cemented grains: Implications for grain and cement failure." *International journal of solids and structures* 32, no. 17 (1995): 2497-2510.
29. Dvorkin, Jack, Gary Mavko, and Amos Nur. "The effect of cementation on the elastic properties of granular material." *Mechanics of Materials* 12, no. 3 (1991): 207-217.
30. Fung, Yuan-Cheng. "Stress-strain-history relations of soft tissues in simple elongation." *Biomechanics: Its foundations and objectives* 7 (1972): 181-208.
31. Gopalakrishnan, Kasthurirangan, Naga Shashidhar, and Xiaoxiong Zhong. "Study of compaction in hot-mix asphalt using computer simulations."*International Journal of Computer Science* 1, no. 4 (2008).

32. GRABOWSKI, Wojciech, Mieczysław S. KUCZMA, and Mieczysław SŁOWIK. "Mathematical modelling of rheological properties of polymer modified bitumens." *Foundations of Civil and Environmental Engineering* 2 (2002): 27-42.
33. Guddati, Murthy N., Zhen Feng, and Y. Richard Kim. "Toward a micromechanics-based procedure to characterize fatigue performance of asphalt concrete." *Transportation Research Record: Journal of the Transportation Research Board* 1789, no. 1 (2002): 121-128.
34. Guddati, Murthy N., Zhen Feng, and Y. Richard Kim. "Toward a micromechanics-based procedure to characterize fatigue performance of asphalt concrete." *Transportation Research Record: Journal of the Transportation Research Board* 1789, no. 1 (2002): 121-128.
35. Halstead, W. J., and J. Y. Welborn. "History of the development of asphalt testing apparatus and asphalt specifications." In *Association of Asphalt Paving Technologists Proc*, vol. 43. 1974.
36. Harrigan, Edward T., Rita B. Leahy, and Jack S. Youtcheff. *The SUPERPAVE Mix design system manual of specifications, test methods, and practices*. Vol. 379. Treetop Pub, 1994.
37. Hashin, Zvi, and S. Shtrikman. "A variational approach to the theory of the elastic behaviour of multiphase materials." *Journal of the Mechanics and Physics of Solids* 11, no. 2 (1963): 127-140.
38. Hua, Jianfeng. "Finite element modeling and analysis of accelerated pavement testing devices and rutting phenomenon." (2000).
39. Helwany, Sam, John Dyer, and Joe Leidy. "Finite-element analyses of flexible pavements." *Journal of Transportation Engineering* 124, no. 5 (1998): 491-499.
40. Hintz, Cassie, and Hussain Bahia. "Simplification of Linear Amplitude Sweep Test and Specification Parameter." *Transportation Research Record: Journal of the Transportation Research Board* 2370, no. 1 (2013): 10-16.
41. Hintz, Cassie. "Understanding Mechanisms Leading to Asphalt Binder Fatigue." PhD diss., THE UNIVERSITY OF WISCONSIN-MADISON, 2012.
42. Chi, J. M., R. Huang, C. C. Yang, and J. J. Chang. "Effect of aggregate properties on the strength and stiffness of lightweight concrete." *Cement and Concrete Composites* 25, no. 2 (2003): 197-205.
43. Huang, Baoshan, Xiang Shu, and Yongjing Tang. "Comparison of semi-circular bending and indirect tensile strength tests for HMA mixtures." *Advances in Pavement Engineering* 22, no. 8 (2005): 1-11.
44. Huang, Yang Hsien. *Pavement analysis and design*. 1993.
45. Huang, Baoshan, and Dragan Vukosavljevic. "Laboratory Study of Fatigue Characteristics of HMA Surface Mixtures Containing Recycled Asphalt Pavement (RAP)." (2009).
46. Johnson, Carl M. "Estimating asphalt binder fatigue resistance using an accelerated test method." PhD diss., UNIVERSITY OF WISCONSIN–MADISON, 2010.
47. Kim, Y. R., B. S. Underwood, S. Mun, and M. N. Guddati. "Perpetual pavement evaluation using the viscoelastic continuum damage finite element program." In*Proceedings of the 2006 International Conference on Perpetual Pavement, Columbus, Ohio*. 2006.

48. Kim, Yong-Rak, D. H. Allen, and D. N. Little. "Damage-induced modeling of asphalt mixtures through computational micromechanics and cohesive zone fracture." *Journal of Materials in Civil Engineering* 17, no. 5 (2005): 477-484.
49. Kim, Y. Richard, Hyon-Jong Lee, and Dallas N. Little. "Fatigue characterization of asphalt concrete using viscoelasticity and continuum damage theory (with discussion)." *Journal of the Association of Asphalt Paving Technologists* 66 (1997).
50. Kim, Yongrak, H. J. Lee, D. N. Little, and Y. Richard Kim. "A Simple Testing Method to Evaluate Fatigue Fracture and Damage Performance of Asphalt Mixtures (With Discussion)." *Journal of the Association of Asphalt Paving Technologists* 75 (2006).
51. Kose, Sadi, Murat Guler, Hussain U. Bahia, and Eyad Masad. "Distribution of strains within hot-mix asphalt binders: applying imaging and finite-element techniques." *Transportation Research Record: Journal of the Transportation Research Board* 1728, no. 1 (2000): 21-27.
52. Lakes, R. S., S. Kose, and H. Bahia. "Analysis of high volume fraction irregular particulate damping composites." *Journal of engineering materials and technology* 124, no. 2 (2002): 174-178.
53. Lee, Hyun-Jong, Jo Sias Daniel, and Y. Richard Kim. "Continuum damage mechanics-based fatigue model of asphalt concrete." *Journal of Materials in Civil Engineering* 12, no. 2 (2000): 105-112.
54. Lethersich, William. "The mechanical behaviour of bitumen." *Journal of the Society of Chemical Industry* 61, no. 7 (1942): 101-108.
55. Luo, Hui, Hong-ping Zhu, Yu Miao, and Chuan-yao Chen. "Simulation of top-down crack propagation in asphalt pavements." *Journal of Zhejiang University SCIENCE A* 11, no. 3 (2010): 223-230.
56. Lutif, Jamilla. "Computational micromechanics modeling of damage-dependent bituminous composites based on two-way coupled multiscale approach." (2011).
57. Lutif, Jamilla ES, Flavio V. Souza, Yongrak Kim, Jorge B. Soares, and David H. Allen. "Multiscale modeling to predict mechanical behavior of asphalt mixtures." *Transportation Research Record: Journal of the Transportation Research Board* 2181, no. 1 (2010): 28-35.
58. Wang, L. B., J. D. Frost, and J. S. Lai. "Noninvasive measurement of permanent strain field resulting from rutting in asphalt concrete." *Transportation Research Record: Journal of the Transportation Research Board* 1687, no. 1 (1999): 85-94.
59. Masad, E., V. K. Jandhyala, N. Dasgupta, N. Somadevan, and N. Shashidhar. "Characterization of air void distribution in asphalt mixes using X-ray computed tomography." *Journal of materials in civil engineering* 14, no. 2 (2002): 122-129.
60. Matthews, James M., Carl L. Monismith, and J. Craus. "Investigation of laboratory fatigue testing procedures for asphalt aggregate mixtures." *Journal of Transportation Engineering* 119, no. 4 (1993): 634-654.
61. Mehta, Yusuf A., Beena Sukumaran, John Liddle, and Jeremy Stevenson.*Investigation of New Devices for Use in Determining Mechanistic Properties and Performance*. No. WHRP 06-10. 2005.
62. Molenaar, A. A. A., A. Scarpas, X. Liu, and S. M. J. G. Erkens. "Semi-circular bending test; simple but useful?." *Journal of the Association of Asphalt Paving Technologists* 71 (2002).

63. Mori, T., and K. Tanaka. "Average stress in matrix and average elastic energy of materials with misfitting inclusions." *Acta metallurgica* 21, no. 5 (1973): 571-574.
64. Mun, Sungho, Murthy N. Guddati, and Y. Richard Kim. "Continuum damage finite element modeling of asphalt concrete." *KSCE Journal of Civil Engineering*9, no. 3 (2005): 205-211.
65. Papagiannakis, A. T., A. Abbas, and Eyad Masad. "Micromechanical analysis of viscoelastic properties of asphalt concretes." *Transportation Research Record: Journal of the Transportation Research Board* 1789, no. 1 (2002): 113-120.
66. Park, Sun Woo, Y. Richard Kim, and Richard A. Schapery. "A viscoelastic continuum damage model and its application to uniaxial behavior of asphalt concrete." *Mechanics of Materials* 24, no. 4 (1996): 241-255.
67. Reddy, Junuthula Narasimha. *An introduction to the finite element method*. Vol. 2, no. 2.2. New York: McGraw-Hill, 1993.
68. Reuss, A. "Berechnung der Fließgrenze von Mischkristallen auf Grund der Plastizitätsbedingung für Einkristalle." *ZAMM-Journal of Applied Mathematics and Mechanics/Zeitschrift für Angewandte Mathematik und Mechanik* 9, no. 1 (1929): 49-58.
69. *Hot mix asphalt materials, mixture design, and construction*. NAPA Research and Education Foundation, 2009.
70. Romberg, J. W., and R. N. Traxler. "Rheology of asphalt." *Journal of colloid science* 2, no. 1 (1947): 33-47.
71. Sefidmazgi, Nima Roohi, Laith Tashman, and Hussain Bahia. "Internal structure characterization of asphalt mixtures for rutting performance using imaging analysis." *Road materials and pavement design* 13, no. sup1 (2012): 21-37.
72. Sefidmazgi, Nima Roohi, Pouya Teymourpour, and Hussain U. Bahia. "Effect of particle mobility on aggregate structure formation in asphalt mixtures." *Road Materials and Pavement Design* 14, no. sup2 (2013): 16-34.
73. Saal, R. N. J., and J. W. A. Labout. "Rheological properties of asphalts."*Rheology: Theory and applications* 2 (1958): 363-400.
74. Sadd, Martin H., Qingli Dai, Venkit Parameswaran, and Arun Shukla. "Simulation of asphalt materials using finite element micromechanical model with damage mechanics." *Transportation Research Record: Journal of the Transportation Research Board* 1832, no. 1 (2003): 86-95.
75. Schapery, R. A. "Correspondence principles and a generalizedJ integral for large deformation and fracture analysis of viscoelastic media." *International Journal of Fracture* 25, no. 3 (1984): 195-223.
76. de Souza, Flávio Vasconcelos, Jorge Barbosa Soares, David H. Allen, and Francisco Evangelista. "Model for predicting damage evolution in heterogeneous viscoelastic asphaltic mixtures." *Transportation Research Record: Journal of the Transportation Research Board* 1891, no. 1 (2004): 131-139.
77. Stankowski, T. "Numerical simulation of failure in particle composites."*Computers & structures* 44, no. 1 (1992): 459-468.
78. Tsai, Bor-Wen, and C. L. Monismith. "Influence of Asphalt Binder Properties on the Fatigue Performance of Asphalt Concrete Pavements (With Discussion)."*Journal of the Association of Asphalt Paving Technologists* 74 (2005).

79. Valenta, Richard, Michal Sejnoha, and Jan Zeman. "Macroscopic constitutive law for mastic asphalt mixtures from multiscale modeling." *International Journal for Multiscale Computational Engineering* 8, no. 1 (2010).
80. Voigt, Woldemar. "Ueber die Beziehung zwischen den beiden Elasticitätsconstanten isotroper Körper." *Annalen der Physik* 274, no. 12 (1889): 573-587.
81. Walubita, Lubinda F., Fred Hugo, and Amy L. Epps Martin. "Indirect tensile fatigue performance of asphalt after MMLS3 trafficking under different environmental conditions: technical paper." *Journal of the South African Institution of Civil Engineering= Joernaal van die Suid-Afrikaanse Instituut van Siviele Ingenieurswese* 44, no. 3 (2002): p-2.
82. Wen, Haifang, and Hussain Bahia. "Characterizing fatigue of asphalt binders with viscoelastic continuum damage mechanics." *Transportation Research Record: Journal of the Transportation Research Board* 2126, no. 1 (2009): 55-62.
83. Yin, Anyi, Xinhua Yang, Shengfeng Yang, and Wen Jiang. "Multiscale fracture simulation of three-point bending asphalt mixture beam considering material heterogeneity." *Engineering Fracture Mechanics* 78, no. 12 (2011): 2414-2428.
84. Yin, H. M., W. G. Buttlar, Glaucio H. Paulino, and H. Di Benedetto. "Assessment of existing micro-mechanical models for asphalt mastics considering viscoelastic effects." *Road Materials and Pavement Design* 9, no. 1 (2008): 31-57.
85. Ying, Hao. "Using X-Ray Computed Tomography to Quantify Damage of Hot-Mix Asphalt in the Dynamic Complex Modulus and Flow Number Tests." PhD diss., Faculty of the Louisiana State University and Agricultural and Mechanical College in partial fulfillment of the requirements for the degree of Master of Science in Civil Engineering in The Department of Civil and Environmental Engineering By Hao Ying BS, China University of Geosciences, China, 2008, 2010.
86. Yun, Taeyoung, and Y. Richard Kim. "Viscoelastoplastic modeling of the behavior of hot mix asphalt in compression." *KSCE Journal of Civil Engineering*17, no. 6 (2013): 1323-1332.
87. Zhu, Han, and Julie E. Nodes. "Contact based analysis of asphalt pavement with the effect of aggregate angularity." *Mechanics of Materials* 32, no. 3 (2000): 193-202.
88. Zhu, Han, Ching S. Chang, and Jeff W. Rish. "Normal and tangential compliance for conforming binder contact II: Visco-elastic binder." *International journal of solids and structures* 33, no. 29 (1996): 4351-4363.
89. Zienkiewicz, Olgierd Cecil, Robert Leroy Taylor, Olgierd Cecil Zienkiewicz, and Robert Lee Taylor. *The finite element method*. Vol. 3. London: McGraw-hill, 1977.
90. Zocher, M. A., S. E. Groves, and D. H. Allen. "A three-dimensional finite element formulation for thermoviscoelastic orthotropic media." *International Journal for Numerical Methods in Engineering* 40, no. 12 (1997): 2267-2288.

APPENDIX A: MASTIC AND MORTAR GENERATION CODES

Different steps of the code for generating the mastic (or mortar) images are summarized below:

1. Generating a fully black image with the size of the RVE.
2. Determination of the number of particles of each specific particle size (Nu_i) based on the particle gradation, particle size, particle volume fraction, and RVE size.
3. Placement of the particles in the RVE image based on their size and particle numbers determined from the last step. The particles will be selected from the database and placed in a random location in the RVE image with a random orientation.

The Main Code

```
function Mastic()
%MASTIC-----------------------------------------------
AP=30; %Aggregate Area Fraction in whole image
nas=7+1; %number of aggregate sizes
Size(1)=75;PP(1)=98.46;
Size(2)=50;PP(2)=80;
Size(3)=30;PP(3)=60;
Size(4)=20;PP(4)=45;
Size(5)=10;PP(5)=40;
Size(6)=5;PP(6)=35.6;
Size(7)=3;PP(7)=22.9;
Size(nas)=1;
%-----------------------------------------------
PSAS=zeros(1,nas); %Percent of specific aggregate size, between aggregates
Area=zeros(1,nas); %Area of each aggregate
Nu=zeros(1,nas); %Number of aggregates with this size which are needed in the
mixture
AW=zeros(1,nas); %Total Area of the aggregates with this size
%-----------------------------------------------
aggregate=0;
xsize=(Size(1)*5);
ysize=(Size(1)*5);
MaterialIdentifier = zeros(xsize,ysize);
%-----------------------------------------------
PSAS(1)=100-PP(1);
```

```
PSAS(nas)=PP(nas-1);
for i=2:nas-1
   PSAS(i)=(100-PP(i))-(100-PP(i-1));
end;
for i=1:nas
   Area(i)=(pi*Size(i)^2)/4;
   Nu(i)=floor((AP/100*(xsize*ysize)*PSAS(i)/100)/Area(i));
end;
Nu
%-----------------------------------------------
%For 75 Particles
%-----------------------------------------------
%For 50 Particles
for j=1:Nu(2)
    check=1;
    while (check~=0)
        PN=round(20*rand);     %PN=Particle Number
        if PN==0
            PN=1;
        end;
        filePN=['50_',int2str(PN),'.tif'];
        PNIdentifier = imread(filePN);
        PNR=PNIdentifier;
        theta=round(360*rand);
        PNIdentifier=imrotate(PNR(:,:,1),theta);
        imsizePN = size(PNIdentifier);
        xsizePN = imsizePN(1);
        ysizePN = imsizePN(2);

        m=floor(rand*xsize)+1;
        if m>xsize-xsizePN
            m=xsize-xsizePN;
        end;
        n=floor(rand*ysize)+1;
        if n>ysize-ysizePN
            n=ysize-ysizePN;
        end;
        if (MaterialIdentifier(m,n)==0)
            check=0;
            for ii=m:m+xsizePN-1
                for jj=n:n+ysizePN-1
                    check=check+MaterialIdentifier(ii,jj);
                end;
            end;
            if check==0
                for ii=m:m+xsizePN-1
                    for jj=n:n+ysizePN-1
                        MaterialIdentifier(ii,jj)=PNIdentifier(ii-m+1,jj-
n+1);
                    end;
                end;
            end;
        end;
    end;
end;
%-----------------------------------------------
%For 30 Particles
```

```
for j=1:Nu(3)
    check=1;
    while (check~=0)
        PN=round(20*rand);      %PN=Particle Number
        if PN==0
            PN=1;
        end;
        filePN=['30_',int2str(PN),'.tif'];
        PNIdentifier = imread(filePN);
        PNR=PNIdentifier;
        theta=round(360*rand);
        PNIdentifier=imrotate(PNR(:,:,1),theta);
        imsizePN = size(PNIdentifier);
        xsizePN = imsizePN(1);
        ysizePN = imsizePN(2);

        m=floor(rand*xsize)+1;
        if m>xsize-xsizePN
            m=xsize-xsizePN;
        end;
        n=floor(rand*ysize)+1;
        if n>ysize-ysizePN
            n=ysize-ysizePN;
        end;
        if (MaterialIdentifier(m,n)==0)
            check=0;
            for ii=m:m+xsizePN-1
                for jj=n:n+ysizePN-1
                    check=check+MaterialIdentifier(ii,jj);
                end;
            end;
            if check==0
                for ii=m:m+xsizePN-1
                    for jj=n:n+ysizePN-1
                        MaterialIdentifier(ii,jj)=PNIdentifier(ii-m+1,jj-
n+1);
                    end;
                end;
            end;
        end;
    end;
end;
%-----------------------------------------------
%For 20 Particles
for j=1:Nu(4)
    check=1;
    while (check~=0)
        PN=round(20*rand);      %PN=Particle Number
        if PN==0
            PN=1;
        end;
        filePN=['20_',int2str(PN),'.tif'];
        PNIdentifier = imread(filePN);
        PNR=PNIdentifier;
        theta=round(360*rand);
        PNIdentifier=imrotate(PNR(:,:,1),theta);
        imsizePN = size(PNIdentifier);
```

```
        xsizePN = imsizePN(1);
        ysizePN = imsizePN(2);

        m=floor(rand*xsize)+1;
        if m>xsize-xsizePN
            m=xsize-xsizePN;
        end;
        n=floor(rand*ysize)+1;
        if n>ysize-ysizePN
            n=ysize-ysizePN;
        end;
        if (MaterialIdentifier(m,n)==0)
            check=0;
            for ii=m:m+xsizePN-1
                for jj=n:n+ysizePN-1
                    check=check+MaterialIdentifier(ii,jj);
                end;
            end;
            if check==0
                for ii=m:m+xsizePN-1
                    for jj=n:n+ysizePN-1
                        MaterialIdentifier(ii,jj)=PNIdentifier(ii-m+1,jj-
n+1);
                    end;
                end;
            end;
        end;
    end;
end;
%-----------------------------------------------
elipse=4;
for i=5:elipse
    for j=1:Nu(i)
        check=1;
        while (check~=0)
            theta=rand*pi;
            ratio=rand*1+1;
            re=Size(i)/2;
            a=re*ratio^(0.5);
            b=a/ratio;
            xmax=xelipse(a,b,theta);
            ymax=yelipse(a,b,theta);
            maxx=floor(xmax+0.5);
            maxy=floor(ymax+0.5);
            maxx=maxx+1;    %has to be checked
            maxy=maxy+1;    %has to be checked
            m=floor(rand*xsize);
            if m<maxy
                m=maxy;
            end;
            if m>xsize-maxy
                m=xsize-maxy;
            end;
            n=floor(rand*ysize);
            if n<maxx
                n=maxx;
            end;
```

```
            if n>ysize-maxx
                n=ysize-maxx;
            end;
            if (MaterialIdentifier(m,n)==0)
                check=0;
                for ii=m-maxy+1:m+maxy
                    for jj=n-maxx+1:n+maxx
                        c=cos(theta);
                        s=sin(theta);
                        distance=(((jj-n)*c+(ii-m)*s)^2)/a^2+((-(jj-n)*s+(ii-
m)*c)^2)/b^2;
                        if distance<=1
                            check=check+MaterialIdentifier(ii,jj);
                        end;
                    end;
                end;
                if check==0
                    for ii=m-maxy+1:m+maxy
                        for jj=n-maxx+1:n+maxx
                            c=cos(theta);
                            s=sin(theta);
                            distance=(((jj-n)*c+(ii-m)*s)^2)/a^2+((-(jj-
n)*s+(ii-m)*c)^2)/b^2;
                            if distance<=1
                                MaterialIdentifier(ii,jj)=255;
                            end;
                        end;
                    end;
                end;
            end;
        end;
    end;
end;
for i=elipse+1:nas
    for j=1:Nu(i)
        check=1;
        while (check~=0)
            m=floor(rand*xsize);
            if m<floor(Size(i)/2)+2
                m=floor(Size(i)/2)+2;
            end;
            if m>xsize-floor(Size(i)/2)-1
                m=xsize-floor(Size(i)/2)-1;
            end;
            n=floor(rand*xsize);
            if n<floor(Size(i)/2)+2
                n=floor(Size(i)/2)+2;
            end;
            if n>ysize-floor(Size(i)/2)-1
                n=ysize-floor(Size(i)/2)-1;
            end;
            if (MaterialIdentifier(m,n)==0)
                check=0;
                for ii=m-floor(Size(i)/2)-1:m+floor(Size(i)/2)+1
                    for jj=n-floor(Size(i)/2)-1:n+floor(Size(i)/2)+1
                        check=check+MaterialIdentifier(ii,jj);
                    end;
```

```
                end;
                if check==0
                    for ii=m-floor(Size(i)/2):m+floor(Size(i)/2)
                        for jj=n-floor(Size(i)/2):n+floor(Size(i)/2)
                            distance=sqrt((n-jj)^2+(m-ii)^2);
                            if distance<Size(i)/2
                                MaterialIdentifier(ii,jj)=255;
                            end;
                        end;
                    end;
                end;
            end;
        end;
    end;
end;
aggregate=0;
for i=1:xsize
    for j=1:ysize
        if MaterialIdentifier(i,j)==255
            aggregate=aggregate+1;
        end;
    end;
end;
aggregate/xsize/ysize*100
imshow(MaterialIdentifier)
imwrite(MaterialIdentifier,'Mastic30.tif');
```

Subroutines

```
function [xmax]=xelipse(a,b,theta);
c=cos(theta);
s=sin(theta);
co=(a^2-b^2)*s*c/(b^2*s^2+a^2*c^2);
coef=(c^2+co^2*s^2+2*c*s*co)/a^2+(s^2+co^2*c^2-2*c*s*co)/b^2;
xmax=(1/coef)^0.5;
```

```
function [ymax]=yelipse(a,b,theta);
c=cos(theta);
s=sin(theta);
co=(a^2-b^2)*s*c/(b^2*c^2+a^2*s^2);
coef=(s^2+co^2*c^2+2*c*s*co)/a^2+(c^2+co^2*s^2-2*c*s*co)/b^2;
ymax=(1/coef)^0.5;
```

APPENDIX B: MATLAB CODE FOR GENERATING ABAQUS INPUT FILES

The scanned image of the asphalt mixture is the input for this code. The output of the code is an input file for ABAQUS which has the mesh generated and the materials properties assigned to each individual element. The boundary condition and loading pattern is also generated in this code and can be modified inside the CAE environment.

```
function Input(filename)
MaterialIdentifier = imread(filename);
imsize = size(MaterialIdentifier);
xsize = imsize(1);
ysize = imsize(2);
aggregate=0;
binder=0;
air=0;
for i=1:xsize
    for j=1:ysize
        if MaterialIdentifier(i,j)<=127
            M(i,j)=0;
            binder=binder+1;
        else
            M(i,j)=255;
            aggregate=aggregate+1;
        end;
    end;
end;
BP=100*binder/xsize/ysize
AP=100*aggregate/xsize/ysize
%--------------------------------------------------------------------------
%Air Void Distribution
AP=4.0;
PSAS(1)=25;
PSAS(2)=30;
PSAS(3)=45;
Size(1)=5;
Size(2)=3;
Size(3)=1;
for i=1:3
   Area(i)=(pi*Size(i)^2)/4;
   Nu(i)=floor((AP/100*(xsize*ysize)*PSAS(i)/100)/Area(i));
end;
for i=1:3
    for j=1:Nu(i)
        check=1;
```

```
        while (check~=0)
            m=floor(rand*xsize);
            if m<floor(Size(i)/2)+2
                m=floor(Size(i)/2)+2;
            end;
            if m>xsize-floor(Size(i)/2)-1
                m=xsize-floor(Size(i)/2)-1;
            end;
            n=floor(rand*xsize);
            if n<floor(Size(i)/2)+2
                n=floor(Size(i)/2)+2;
            end;
            if n>ysize-floor(Size(i)/2)-1
                n=ysize-floor(Size(i)/2)-1;
            end;
            if (M(m,n)==0)
                check=0;
                for ii=m-floor(Size(i)/2)-1:m+floor(Size(i)/2)+1
                    for jj=n-floor(Size(i)/2)-1:n+floor(Size(i)/2)+1
                        check=check+M(ii,jj);
                    end;
                end;
                if check==0
                    for ii=m-floor(Size(i)/2):m+floor(Size(i)/2)
                        for jj=n-floor(Size(i)/2):n+floor(Size(i)/2)
                            distance=sqrt((n-jj)^2+(m-ii)^2);
                            if distance<Size(i)/2
                                M(ii,jj)=181;
                            end;
                        end;
                    end;
                end;
            end;
        end;
    end;
end;
%--------------------------------------------------------------------------
aggregate=0;
for i=1:xsize
    for j=1:ysize
        if M(i,j)==255
            aggregate=aggregate+1;
        end;
    end;
end;
aggregate/xsize/ysize*100
air=0;
for i=1:xsize
    for j=1:ysize
        if M(i,j)==237
            air=air+1;
        end;
    end;
end;
air/xsize/ysize*100
binder=0;
for i=1:xsize
```

```
    for j=1:ysize
        if M(i,j)==0
            binder=binder+1;
        end;
    end;
end;
%--------------------------------------------------------------------------
pixel=1;
Tfilename=strrep(filename,'.tif','');
newfilename=[Tfilename,'','.inp'];
file = fopen(newfilename,'w');
fprintf(file,'*Heading\n');
fprintf(file,'** Job name: MultiScale Model name: Student\n');
fprintf(file,'** Generated by: Abaqus/CAE Student Edition 6.8-2\n');
fprintf(file,'*Preprint, echo=NO, model=NO, history=NO, contact=NO\n');
fprintf(file,'**\n');
fprintf(file,'** PARTS\n');
fprintf(file,'**\n');
fprintf(file,'*Part, name=PART-1\n');
fprintf(file,'*Node\n');
NuNode=0;
for i=1:xsize+1
    for j=1:ysize+1
        NuNode=NuNode+1;
        fprintf(file,'%8.0f, %8.3f, %8.3f\n',NuNode,(j-1)*pixel,(1-i)*pixel);
    end;
end;
fprintf(file,'*Element, type=CPE4\n');
NuElement=0;
for i=1:xsize
    for j=1:ysize
        NuElement=NuElement+1;
        n1=i*(ysize+1)+j;
        n2=i*(ysize+1)+j+1;
        n3=(i-1)*(ysize+1)+j+1;
        n4=(i-1)*(ysize+1)+j;
        fprintf(file,'%8.0f, %8.0f, %8.0f, %8.0f,
%8.0f\n',NuElement,n1,n2,n3,n4);
    end;
end;
fprintf(file,'*Elset, elset=Bin, internal\n');
NuElement=0;
for i=1:xsize
    for j=1:ysize
        NuElement=NuElement+1;
        if M(i,j)==0
            fprintf(file,'%8.0f\n',NuElement);
        end;
    end;
end;
fprintf(file,'\n');
fprintf(file,'*Elset, elset=Agg, internal\n');
NuElement=0;
for i=1:xsize
    for j=1:ysize
        NuElement=NuElement+1;
        if M(i,j)==255
```

```
            fprintf(file,'%8.0f\n',NuElement);
        end;
    end;
end;
fprintf(file,'\n');
fprintf(file,'*Elset, elset=Air, internal\n');
NuElement=0;
for i=1:xsize
    for j=1:ysize
        NuElement=NuElement+1;
        if M(i,j)==237
            fprintf(file,'%8.0f\n',NuElement);
        end;
    end;
end;
%-----------------------------------------------------------
fprintf(file,'\n');
fprintf(file,'** Section: AggSec\n');
fprintf(file,'*Solid Section, elset=Agg, material=AGGREGATE\n');
fprintf(file,'');
fprintf(file,'** Section: BinSec\n');
fprintf(file,'*Solid Section, elset=Bin, material=BINDER\n');
fprintf(file,'');
fprintf(file,'** Section: AirSec\n');
fprintf(file,'*Solid Section, elset=Air, material=AIR\n');
fprintf(file,'');
fprintf(file,'*End Part\n');
%-------------------------------------------------------------
fprintf(file,'**\n');
fprintf(file,'**\n');
fprintf(file,'** ASSEMBLY\n');
fprintf(file,'**\n');
fprintf(file,'*Assembly, name=Assembly\n');
fprintf(file,'**\n');
fprintf(file,'*Instance, name=PART-1-1, part=PART-1\n');
fprintf(file,'*End Instance\n');
fprintf(file,'**\n');
fprintf(file,'*Nset, nset=U2, internal, instance=PART-1-1, generate\n');
fprintf(file,'%8.0f, %8.0f,
%8.0f\n',xsize*(ysize+1)+1,(xsize+1)*(ysize+1),1);
fprintf(file,'*Nset, nset=U1, internal, instance=PART-1-1, generate\n');
fprintf(file,'%8.0f, %8.0f, %8.0f\n',1,xsize*(ysize+1)+1,ysize+1);
fprintf(file,'*Elset, elset=Pressure, internal, instance=PART-1-1,
generate\n');
fprintf(file,'%8.0f, %8.0f, %8.0f\n',1,ysize,1);
fprintf(file,'*Surface, type=ELEMENT, name=Load, internal\n');
fprintf(file,'Pressure, S3\n');
fprintf(file,'*End Assembly\n');
%-------------------------------------------------------------
fprintf(file,'**\n');
fprintf(file,'** MATERIALS\n');
fprintf(file,'**\n');
fprintf(file,'*Material, name=AGGREGATE\n');
fprintf(file,'*Elastic\n');
fprintf(file,'2e+11, 0.3\n');
fprintf(file,'*Material, name=AIR\n');
fprintf(file,'*Elastic\n');
```

```
fprintf(file,'1e6, 0.3\n');
fprintf(file,'*Material, name=BINDER\n');
fprintf(file,'*Elastic, moduli=INSTANTANEOUS\n');
fprintf(file,'71591267.132473, 0.5\n');
fprintf(file,'*Viscoelastic, time=PRONY\n');
fprintf(file,'   0.9975,      0.9975, 0.0094\n');
fprintf(file,' 0.0024,    0.0024,   1.5164\n');
fprintf(file,'**\n');
fprintf(file,'** BOUNDARY CONDITIONS\n');
fprintf(file,'**\n');
fprintf(file,'** Name: Disp-BC-1 Type: Displacement/Rotation\n');
fprintf(file,'*Boundary\n');
fprintf(file,'U2, 2, 2\n');
fprintf(file,'** Name: Disp-BC-2 Type: Displacement/Rotation\n');
fprintf(file,'*Boundary\n');
fprintf(file,'U1, 1, 1\n');
fprintf(file,'*Boundary\n');
fprintf(file,'U1-1, 1, 1\n');
%----------------------------------------------------------------
NC=1;
for i=1:NC
    fprintf(file,'** ----------------------------------------------------------
--------\n');
    fprintf(file,'**\n');
    fprintf(file,'** STEP: L%0.0f\n',i);
    fprintf(file,'**\n');
    fprintf(file,'*Step, name=L%0.0f, inc=1000\n',i);
    fprintf(file,'*Visco, cetol=1e-05\n');
    fprintf(file,'0.01, 0.1, 0.001, 0.04\n');
    fprintf(file,'**\n');
    fprintf(file,'** LOADS\n');
    fprintf(file,'**\n');
    fprintf(file,'** Name: SURFFORCE-%0.0f   Type: Pressure\n',i);
    fprintf(file,'*Dsload, op=NEW\n');
    fprintf(file,'Load, P, 334000\n');
    fprintf(file,'**\n');
    fprintf(file,'** OUTPUT REQUESTS\n');
    fprintf(file,'**\n');
    fprintf(file,'*Restart, write, frequency=0\n');
    fprintf(file,'**\n');
    fprintf(file,'** FIELD OUTPUT: F-Output-%0.0f\n',2*(i-1)+1);
    fprintf(file,'**\n');
    fprintf(file,'*Output, field, variable=PRESELECT\n');
    fprintf(file,'**\n');
    fprintf(file,'** HISTORY OUTPUT: H-Output-%0.0f\n',2*(i-1)+1);
    fprintf(file,'**\n');
    fprintf(file,'*Output, history, variable=PRESELECT\n');
    fprintf(file,'*End Step\n');
    fprintf(file,'** ----------------------------------------------------------
--------\n');
    fprintf(file,'**\n');
    fprintf(file,'** STEP: U%0.0f\n',i);
    fprintf(file,'**\n');
    fprintf(file,'*Step, name=U%0.0f, inc=1000\n',i);
    fprintf(file,'*Visco, cetol=1e-05\n');
    fprintf(file,'0.09, 0.9, .001, 0.3\n');
    fprintf(file,'**\n');
```

```
    fprintf(file,'** LOADS\n');
    fprintf(file,'**\n');
    fprintf(file,'** Name: SURFFORCE-%0.0f   Type: Pressure\n',i);
    fprintf(file,'*Dsload, op=NEW\n');
    fprintf(file,'**\n');
    fprintf(file,'** OUTPUT REQUESTS\n');
    fprintf(file,'**\n');
    fprintf(file,'*Restart, write, frequency=0\n');
    fprintf(file,'**\n');
    fprintf(file,'** FIELD OUTPUT: F-Output-%0.0f\n',2*i);
    fprintf(file,'**\n');
    fprintf(file,'*Output, field, variable=PRESELECT\n');
    fprintf(file,'**\n');
    fprintf(file,'** HISTORY OUTPUT: H-Output-%0.0f\n',2*i);
    fprintf(file,'**\n');
    fprintf(file,'*Output, history, variable=PRESELECT\n');
    fprintf(file,'*End Step\n');
end;
fclose(file);
```

APPENDIX C: USER MATERIAL SUBROUTINE FOR MODELING VISCOELASTIC PROPERTIES OF THE MATRIX

The binder constitutive modelling is coded in this FORTAN written code, inclusing:

- Linear viscoelastic model of asphalt binder through Prony series.
- Contact modelling developed in the study.
- Coupling VECD with FE analysis.

```
      SUBROUTINE UMAT(STRESS,STATEV,DDSDDE,SSE,SPD,SCD,
     1 RPL,DDSDDT,DRPLDE,DRPLDT,
     2 STRAN,DSTRAN,TIME,DTIME,TEMP,DTEMP,PREDEF,DPRED,CMNAME,
     3 NDI,NSHR,NTENS,NSTATV,PROPS,NPROPS,COORDS,DROT,PNEWDT,
     4 CELENT,DFGRD0,DFGRD1,NOEL,NPT,LAYER,KSPT,KSTEP,KINC)
C
      INCLUDE 'ABA_PARAM.INC'
C

      CHARACTER*80 CMNAME
      real*8,dimension(128881,4,4)      :: Sn= 0d0
      real*8,dimension(128881,4,4)      :: Sm= 0d0
      real*8,dimension(128881,4)        :: DSKK= 0d0
      Integer,dimension(128881,4,4)     :: Hist=0
      real*8,dimension(128881,4)        :: I5= 0d0
      real*8,dimension(128881,4)        :: Avestr= 0d0
      real*8,dimension(128881,4,6,4)    :: SSn=0d0
      real*8,dimension(128881,4,6,4)    :: SSm=0d0
      Integer,dimension(128881,4,6,4)   :: Histn=0
      real*8,dimension(128881,4,6)      :: J5= 0d0
      real*8,dimension(128881,4)        :: NTIME=0d0
      real*8,dimension(128881,4)        :: Damage= 0d0
      real*8,dimension(128881,4)        :: Damagek= 0d0
      real*8,dimension(128881,4)        :: constant= 0d0
      real*8,dimension(128881,4)        :: Damco1= 1d0
      real*8,dimension(128881,4)        :: Damco2= 1d0
      !cycle strain history
      real*8,dimension(128881,4,2)      :: CyStHi= 0d0
      Integer,dimension(128881,4)       :: DHist=0
      INTEGER,dimension(128881,4)       :: StepNumber=1
      Integer                          :: check=1
      Integer                          :: NEL=1
      Integer                          :: NP=1
      real*8  :: Ax=0d0, Ay=0d0, EA1=0d0, EA2=0d0, EA12=0d0
      real*8  :: Bx=0d0, By=0d0, EB1=0d0, EB2=0d0, EB12=0d0
      real*8  :: Cx=0d0, Cy=0d0, EC1=0d0, EC2=0d0, EC12=0d0
```

```
      real*8  :: Dx=0d0, Dy=0d0, ED1=0d0, ED2=0d0, ED12=0d0, x=0d0
      Integer K1, K2, NPROPS
      real*8 I1, I3, J1, J3, DEkk
      real*8 nu, Einf, Kinf, Ginf, Km, rm, Gm
      real*8 C0, C1, C2, ALPAH
      DIMENSION STRESS(NTENS),STATEV(NSTATV),
     1 DDSDDE(NTENS,NTENS),
     2 DDSDDT(NTENS),DRPLDE(NTENS),
     3 STRAN(NTENS),DSTRAN(NTENS),TIME(2),PREDEF(1),DPRED(1),
     4 PROPS(NPROPS),COORDS(3),DROT(3,3),DFGRD0(3,3),DFGRD1(3,3)
      DIMENSION DSTRES(6),DDVS(6)
!-------------------------------------------------------
      if (NPROPS.gt.2) then
C     Restriction of the deformation of binder elements
          if (MOD(KSTEP,2).eq.1) then
              Einf=PROPS(1)
              if (NPT.eq.1) then
                EA1= STRAN(1)
                EA2= STRAN(2)
                EA12=STRAN(4)
              elseif (NPT.eq.2) then
                EB1= STRAN(1)
                EB2= STRAN(2)
                EB12=STRAN(4)
              elseif (NPT.eq.3) then
                EC1= STRAN(1)
                EC2= STRAN(2)
                EC12=STRAN(4)
              elseif (NPT.eq.4) then
                ED1= STRAN(1)
                ED2= STRAN(2)
                ED12=STRAN(4)
              endif
              if (NPT.eq.4) then
                    E1 =(EA1 +EB1 +EC1 +ED1 )/4d0
                E2 =(EA2 +EB2 +EC2 +ED2 )/4d0
                E12=(EA12+EB12+EC12+ED12)/4d0
                Bx=1+E1
                By=E12
                Cx=E12
                Cy=1+E2
                Dx=1+E1+E12
                Dy=1+E12+E2
                if (Ax+Cx.gt.(Bx+Dx)) then
                    Einf=PROPS(NPROPS)
                endif
                if (Ay+By.gt.(Cy+Dy)) then
                    Einf=PROPS(NPROPS)
                endif
              endif
          else
              Einf=PROPS(1)
          end if
          nu=PROPS(NPROPS-1)
!-------------------------------------------------------
          if (check.ne.KINC) then
c            print*, TIME(2)
```

```
            Hist= 0
            Histn=0
            I5=   0d0
            J5=   0d0
            if (MOD(KINC-1,8).eq.0) then
                Damco1=Damco2
                DHist=0
            endif
          endif
!-------------------------------------------------------
        if (MOD(KINC,8).eq.3) then
            CyStHi(NOEL,NPT,1)=STRAN(2)
        endif
        if (MOD(KINC,8).eq.7) then
            CyStHi(NOEL,NPT,2)=STRAN(2)
        endif
        if (MOD(KINC,8).eq.7) then
            st1=CyStHi(NOEL,NPT,1)
            st2=CyStHi(NOEL,NPT,2)
            if ((st1.gt.0).and.(st2.ge.0)) then
               ST=abs(50d0*(st1-st2))
            endif
           if ((st1.lt.0).and.(st2.gt.0)) then
               ST=abs(50d0*(st2-st1))
           endif
           if ((st1.gt.0).and.(st2.lt.0)) then
               ST=abs(50d0*(st1-st2))
           endif
           if ((st1.le.0).and.(st2.lt.0)) then
               ST=abs(50d0*(st1-st2))
           endif
            if (DHist(NOEL,NPT).eq.0) then
                if ((NOEL.eq.10).AND.(NPT.eq.1)) then
                    print*, TIME(2), Damco1(NOEL,NPT), ST
                endif
                constant(NOEL,NPT)=Damagek(NOEL,NPT)
                DHist(NOEL,NPT)=1
            endif
            C0=1.000d0
            C1=0.17d0
            C2=0.401d0
            ALPHA=1.759d0

            Damagek(NOEL,NPT)=constant(NOEL,NPT)+((1-C2)*ALPHA+1)*((3.14
     1  d0*C1*C2)**(ALPHA))*(ST**(2*ALPHA))*0.1d0
            Damage(NOEL,NPT)=Damagek(NOEL,NPT)**(1/((1-C2)*ALPHA+1))
            Damco2(NOEL,NPT) =C0-C1*(Damage(NOEL,NPT)**C2)
            if (Damco2(NOEL,NPT).lt.0.15d0) then
                Damco2(NOEL,NPT)=0.15d0
            endif
        endif

!-------------------------------------------------------
C     Calculation of defferentials of hydrostatic and deviatoric strains
          DEkk = 0d0
          DO K1=1,NDI
             DEkk = DEkk + DSTRAN(K1)
```

```
          END DO
          Do K1=1,NDI
            DDVS(K1)=DSTRAN(K1)-DEkk/3d0
          END DO
          DO K1=1,NSHR
            DDVS(K1+NDI)=DSTRAN(K1+NDI)
          END DO
          fstran=1d0
C     Calculation of I1 and J1
          Kinf=Damco1(NOEL,NPT)*fstran*Einf/(3d0*(1-2d0*nu))
          I1= 3d0*Kinf
          Ginf=Damco1(NOEL,NPT)*fstran*Einf/(2d0*(1+nu))
          J1= 2d0*Ginf
!-------------------------------------------------------
C     Calculation of I3 and J3
          I3=0d0
          J3=0d0
          do K1=1,NPROPS/2-1
            Km=Damco1(NOEL,NPT)*fstran*PROPS(2*K1)/(3d0*(1-2d0*nu))
            Gm=Damco1(NOEL,NPT)*fstran*PROPS(2*K1)/(2d0*(1+nu))
            rm=PROPS(2*K1+1)+0.0000000000000001d0
            I3= I3 +(3d0/DTIME)* ( Km*rm*(1d0-exp(-DTIME/rm)) )
            J3= J3 +(2d0/DTIME)* ( Gm*rm*(1d0-exp(-DTIME/rm)) )
          end do
!----------------------
          do K1=1,NPROPS/2-1
            Km=Damco1(NOEL,NPT)*fstran*PROPS(2*K1)/(3d0*(1-2d0*nu))
            rm=PROPS(2*K1+1)+0.0000000000000001d0
            if (Hist(NOEL,NPT,K1).eq.0) then
              I5(NOEL,NPT)= I5(NOEL,NPT) - 3d0*Km*
     1             (1d0-exp(-DTIME/rm)) * Sn(NOEL,NPT,K1)
              Hist(NOEL,NPT,K1)=1
              Sm(NOEL,NPT,K1)=Sn(NOEL,NPT,K1)
            endif
            Sn(NOEL,NPT,K1)=exp(-DTIME/rm)*Sm(NOEL,NPT,K1)+(DEkk/DTIME)*
     1                      rm*(1d0-exp(-DTIME/rm))
          end do
!----------------------
          DO K2=1,NTENS
            do K1=1,NPROPS/2-1
              Gm=Damco1(NOEL,NPT)*fstran*PROPS(2*K1)/(2d0*(1+nu))
              rm=PROPS(2*K1+1)+0.0000000000000001d0
              if (Histn(NOEL,NPT,K2,K1).eq.0) then
                J5(NOEL,NPT,K2)=J5(NOEL,NPT,K2)-2d0*Gm*
     1                          (1d0-exp(-DTIME/rm))*SSn(NOEL,NPT,K2,K1)
                Histn(NOEL,NPT,K2,K1)=1
                SSm(NOEL,NPT,K2,K1)=SSn(NOEL,NPT,K2,K1)
              endif
              SSn(NOEL,NPT,K2,K1)=exp(-DTIME/rm)*SSm(NOEL,NPT,K2,K1)+
     1                            (DDVS(K2)/DTIME)*rm*(1d0-exp(-DTIME/rm))
            enddo

            if (K2.lt.NDI+1) then
              DSTRES(K2)=((I1+I3)*DEkk+I5(NOEL,NPT))/3d0 +
     1                   ((J1+J3)*DDVS(K2)+J5(NOEL,NPT,K2))
              STRESS(K2)= STRESS(K2) + DSTRES(K2)
            else
```

```
                DSTRES(K2)= ((J1+J3)*DDVS(K2)+J5(NOEL,NPT,K2))
                STRESS(K2)= STRESS(K2) + DSTRES(K2)/2d0
              endif
            END dO

!-------------------------------------------------------
C     Calculation of Jacobian Matrix
      DO K1=1,NTENS
         DO K2=1,NTENS
            DDSDDE(K1,K2) = 0d0
         END DO
      END DO
      DO K1=1,NDI
         DDSDDE(K1,K1) = (I1+I3)/3d0 + (2d0/3d0)*(J1+J3)
      END DO
C
      DO K1=1,NDI-1
         DO K2=K1+1,NDI
            DDSDDE(K1,K2) = (I1+I3)/3d0 - (1d0/3d0)*(J1+J3)
            DDSDDE(K2,K1) = (I1+I3)/3d0 - (1d0/3d0)*(J1+J3)
         END DO
      END DO
      DO K1=1,NSHR
         DDSDDE(NDI+K1,NDI+K1) = (J1+J3)/2d0
      END DO
!-----------------------------------------------------------------
      else
c        if ((NOEL.eq.1).AND.(NPT.eq.1)) then
c            print*, KINC, check, Damco1(NOEL,NPT), 'agg'
c        endif
!-------------------------------------------------------
          if (check.ne.KINC) then
            print*, TIME(2), KINC, 'agg'
            Hist= 0
            Histn=0
            I5=   0d0
            J5=   0d0
            if (MOD(KINC-1,8).eq.0) then
                Damco1=Damco2
                DHist=0
            endif
          endif
!-------------------------------------------------------
          EMOD=25000000000d0
          ENU=0.25d0
          EBULK3=EMOD/(1d0-2d0*ENU)
          EG2=EMOD/(1d0+ENU)
          EG=EG2/2d0
          EG3=3d0*EG
          ELAM=(EBULK3-EG2)/3d0
C         ELASTIC STIFFNESS
          DO K1=1, NDI
            DO K2=1, NDI
              DDSDDE(K2, K1)=ELAM
            END DO
            DDSDDE(K1, K1)=EG2+ELAM
          END DO
```

```
            DO K1=NDI+1, NTENS
              DDSDDE(K1 ,K1)=EG
            END DO
C         CALCULATE STRESS
            DO K1=1, NTENS
              DO K2=1, NTENS
                STRESS(K2)=STRESS(K2)+DDSDDE(K2, K1)*DSTRAN(K1)
              END DO
            END DO
          end if
          check=KINC

          RETURN
          END)
```